UNIVERSITA' DEGLI STUDI DI VERONA
DIPARTIMENTO DI MEDICINA

SCUOLA DI DOTTORATO DI
SCIENZE DELLA VITA E DELLA SALUTE

DOTTORATO DI RICERCA IN
INFIAMMAZIONE IMMUNITA' E CANCRO
CICLO XXXIV/2018

Targeting immune dysregulation mediated by FLIP and putative FLIP-related pathways to develop new therapeutic approaches

MED/04

Coordinatore: Prof.ssa Gabriela Costantin

Tutor: Prof. Vincenzo Bronte

Dottorando: Dott.ssa Cristina Frusteri

INDEX

SOMMARIO 5

ABSTRACT 7

INTRODUCTION 9

1. Myeloid-derived suppressor cells 9

1.1. Mouse MDSCs 11

1.2. Human MDSCs 12

1.3. Immunologic functions of MDSCs 13

1.4. MDSCs differentiation, expansion, and recruitment 17

1.5. Role of MDSCs in tumor microenvironment and cancer progression 23

1.6. M-MDSCs and monocyte subpopulations in cancer 25

1.7. Strategies to target therapeutically MDSCs 27

2. Cellular FLICE (FADD-like IL-1β-converting enzyme)-inhibitory protein (c-FLIP) 33

2.1. c-FLIP structure and canonical biology 33

2.2. Non-canonical c-FLIP biology 36

2.3. c-FLIP regulation 39

2.4. c-FLIP in cancer and as therapeutic target for oncology treatment 40

2.5. c-FLIP in monocytic subset of MDSCs 42

3. Lung Cancer (LC), MDSCs and therapeutical treatments 44

3.1. Lung Cancer (LC) and staging 44

3.2. MDSCs and Lung Cancer (LC) 46

3.3. Immune Checkpoint Inhibitors (ICIs) in NSCLC 51

4. SARS-CoV-2 infection 56

4.1. SARS-CoV-2 infection: epidemiology, symptoms 57

4.2. Structure and viral transmission of SARS-CoV-2 virus 58

4.3. Viral replication cycle of SARS-CoV-2 and host immune responses 60

4.4. The immunopathological background 62

4.5. Cytokine storm disease (CSD) and COVID-19-associated cytokine storm.. 66
4.6. Immunosuppressive landscape in COVID-19 patients 70
4.7. Therapeutic intervention according to immune phases..... 71
AIM OF THE STUDY..... 75
MATERIALS AND METHODS..... 78
1. Mice..... 78
2. Generation of vFLIP chimera mice 78
3. Ethics and acquirement of human samples..... 79
4. Cell lines..... 82
5. Cytokines and synthetic peptides 83
6. STAT3 targeting..... 83
7. Detection of cytokines and serology 83
8. Preparation of cell suspensions from organs 84
9. PBMCs and $CD14^+$ cells isolation from human samples 84
10. Immunosuppression assay..... 85
11. Flow cytometry..... 86
12. Immunofluorescence (IF) and immunohistochemistry (IHC) 87
13. RNA synthesis..... 89
14. RNA transfection..... 89
15. Real-time qPCR..... 90
16. Lysate preparation and quantification 90
17. Immunoprecipitation 91
18. Western Blot analysis..... 91
19. Chromatin Immunoprecipitation sequencing (ChIP-seq)..... 92
20. Single-cell RNA sequencing (scRNA-seq) 93
21. Cell type identification 94
22. Mapping between human and mouse genes 95
23. Gene set analysis 95

24. Statistical analysis 96

RESULTS 97

1. The inhibition of STAT3 pathway modulates MDSCs immunosuppressive activity 97
2. FLIP-mediated immune dysregulation distinguished vFLIP chimera model .. 101
3. vFLIP chimera model promotes the activation of STAT3 pathway which distinguishes FLIP-over-expressing suppressive monocytes 106
4. STAT3 targeting restrains immunopathology and inflammatory conditions in vFLIP chimera mice 109
5. SARS-CoV-2 infection in COVID-19 patients induces c-FLIP over-expression and c-FLIP-correlated immunosuppressive properties in myeloid cells, and displays a dysregulated immunological landscape similar to vFLIP chimera model 112
6. pSTAT3 over-expression in both COVID-19 patients and virus-infected, HFH4-hACE2 transgenic mice and the efficacy of STAT3 targeting to mitigate the suppressive activity of COVID-19-derived monocytes..... 116
7. ICIs treatments restrain the normal c-FLIP expression levels and consequently mitigate the suppressive activity of NSCLC's cohort monocytes 120
8. c-FLIP as transcriptional regulator of immune responses-involved genes through p50 physical interaction in c-FLIP over-expressing monocytic cells..... 123

DISCUSSION 132

REFERENCES 137

SOMMARIO

Cellular FLICE (FADD-like IL-1β-converting enzyme)-inhibitory protein (c-FLIP) è una proteina con funzione anti-apoptotica che risulta altamente espressa in diversi contesti oncologici ed è indotta anche in malattie infettive con la funzione di bloccare la morte cellulare mediata dalle caspasi e promuovendo, inoltre, un'alterazione della normale mielopoiesi. Le cellule soppressorie di derivazione mieloide (MDSCs) rappresentano una popolazione mieloide eterogena comprendente sia progenitori mieloidi che cellule differenziate e sono in grado di alterare le risposte immunitarie in svariati contesti patologici. È stato riportato in diversi tipi di tumore con un elevato numero di MDSCs circolanti fosse associato ad una prognosi sfavorevole e ad una debole risposta ai trattamenti da parte dei pazienti oncologici. La via di trasduzione del traduttore di segnale e attivatore della trascrizione 3 (STAT3) rappresenta uno dei processi molecolari maggiormente indotti nei monociti dall'espressione aberrante della proteina c-FLIP, e costituisce pertanto un bersaglio ideale per controllare le funzioni associate alle MDSCs. Inoltre, la via di trasduzione regolata da STAT3 è fondamentale per stimolare la produzione di alcune citochine durante la sindrome della cascata citochinica (CRS). In questo studio, mediante l'utilizzato di un modello murino transgenico che esprime in modo non fisiologico la forma virale di FLIP (v-FLIP) a livello dei progenitori della linea mieloide, abbiamo dimostrato che i trattamenti diretti contro i processi molecolari regolati dall'attivazione di STAT3 fossero in grado di attenuare le caratteristiche funzionali indotti dalla proteina FLIP. Questi dati suggeriscono che strategie basate sull'utilizzo di STAT3 come bersaglio terapeutico potrebbero essere promettenti in una molteplicità di malattie in cui le MDSCs svolgono un ruolo patologico chiave. Per approfondire ulteriormente il ruolo molecolare svolto da c-FLIP durante i meccanismi di immuno-modulazione nel subset mieloide, noi abbiamo dimostrato la co-localizzazione nucleare di c-FLIP con la subunità p50 del complesso NF-kB. Questo ci ha suggerito che quando over-espresso, c-FLIP può essere in grado di traslocare nel comparto nucleare come unico complesso con la proteina p50 presupponendo l'acquisizione di funzioni trascrizionali da parte di c-FLIP. Abbiamo dimostrato una interazione fisica c-

FLIP-p50 in compartimenti cellulari, nucleare e citoplasmatico, e abbiamo rivelato, mediante analisi ChIP-seq, diverse sequenze di DNA legate a c-FLIP coinvolte in differenti processi immunologici. Infine, poiché l'espressione di FLIP risulta anche favorire la replicazione virale, abbiamo ipotizzato il coinvolgimento di FLIP nella progressione dell'infezione COVID-19 causata dal virus SARS-CoV-2. Infatti, abbiamo stabilito una diretta correlazione tra l'espressione di c-FLIP e l'attività immunosoppressoria dei monociti circolanti, come riportato dal nostro laboratorio anche nel contesto oncologico. Pertanto, il trattamento mirato nell'inibizione di STAT3 condotto nei monociti circolanti di pazienti con infezione da COVID-19, ci hanno permesso di confermare che l'immunosoppressione dei monociti possa essere regredita mediante uso di inibitori di STAT3. In conclusione, abbiamo investigato il ruolo di c-FLIP come potenziale biomarcatore predittivo delle risposte di soggetti oncologici alle immunoterapie. In una coorte di pazienti affetti da carcinoma polmonare non a piccole cellule (non-small-cell lung cancer, NSCLC) sottoposta ad immunoterapia con inibitori di checkpoint immunitari (ICIs), abbiamo dimostrato che l'analisi di c-FLIP sui monociti circolanti fosse in grado di predire l'esito della valutazione clinica dei pazienti sulle risposte alle immunoterapie.

Nel suo insieme, questo lavoro potrebbe contribuire ad approfondire le conoscenze riguardo la regolazione di processi immunitari ad opera di c-FLIP, e può aiutare a sviluppare inibitori selettivi per modulare l'attività immunoregolatrice delle MDSCs in differenti contesti patologici.

ABSTRACT

Cellular FLICE (FADD-like IL-1β-converting enzyme)-inhibitory protein (c-FLIP) is an anti-apoptotic protein that has been reported to be highly expressed in several cancer settings and induced in different infectious diseases to block caspase-mediated cell death. Myeloid derived suppressor cells (MDSCs) represent a heterogeneous myeloid cell population, comprising both myeloid-cell progenitors and fully differentiated cells, whose role in altering the immune responses was observed in various pathological contexts. In a variety of tumor settings, a high number of circulating MDSCs is associated with poorer prognosis and weaker response to treatment. Signal transducer and activator of transcription 3 (STAT3) pathway represents one those upregulated in immunosuppressive, c-FLIP-over-expressing monocytes and, therefore, it is an ideal target to control MDSC-associated functions. Moreover, STAT3 pathway is relevant to differentiate myeloid cells into a cytokine-producing source during the cytokine release syndrome (CRS). By availing of a transgenic (Tg) mouse model that over-expresses viral form of FLIP (v-FLIP) in the myeloid cell lineage, in this study we demonstrated that treatments to target STAT3 were able to mitigate the FLIP-mediated immune dysregulation. These data suggest that STAT3-targeting approaches might be promising in a variety of diseases in which MDSCs can play a pathogenic role. To investigate further the molecular role of c-FLIP behind the mechanisms of immunomodulation in myeloid cell subset we demonstrated the nuclear co-localization c-FLIP-p50 NF-kB subunit. When c-FLIP is over-expressed, it can translocate to the nucleus in a complex with p50 protein suggesting the acquisition of transcriptional functions. We demonstrated a physical interaction c-FLIP-p50 in both cytoplasmic and nuclear fractions, and revealed, through ChIP-seq analysis, several DNA sequences involved in immune system processes that were identified as c-FLIP-dependent. Since FLIP expression was linked to viral replication, we hypothesized its involvement in the progression of COVID-19 infection caused by SARS-CoV-2 virus. Indeed, we found a direct correlation between c-FLIP expression and immunosuppressive activity of monocytes circulating in the blood of COVID-19 patients, similarly to what previously

reported by our laboratory in oncology patients. Immunosuppression by COVID-19 patient monocytes could be indeed reverted by STAT3 inhibitors. Finally, we investigated c-FLIP as predictive biomarker of outcome following immunotherapy. In a non-small-cell lung cancer (NSCLC) cohort undergoing to immune-checkpoint inhibitors (ICIs) therapy, we demonstrated that c-FLIP assessment was able to predict the clinical response, indicating c-FLIP as promising predictive biomarker to optimize the current oncology treatments. Collectively, our results contribute to deepen the knowledge about c-FLIP regulation in immune cells, which can be used to develop selective inhibitors to restrain MDSC suppressive activity under different pathological conditions.

INTRODUCTION

1. Myeloid-derived suppressor cells

Myeloid cells are a highly heterogeneous population, composed by mononuclear myeloid cells (which includes monocytes, macrophages, and dendritic cells (DCs)) and granulocytic myeloid cells (polymorphonuclear neutrophils, eosinophils, basophils and mast cells). Myeloid cells are differentiated descendants from common progenitors derived from hematopoietic stem cells in the bone marrow (BM). Myeloid cell commitment is controlled by distinct transcription factors, followed by terminal differentiation in response to specific colony-stimulating factors (CSFs). Among transcriptional factors that play critical roles in myeloid development, Pu.1 is an essential factor for both early and late stages of lymphoid and myeloid differentiation[1]. Its target genes encode extracellular proteins or transmembrane proteins, most of which are involved in cellular communication. The loss of cellular communication caused by reduced Pu.1 levels can lead to leukemia[2]. CCAAT/enhancer-binding protein alpha, beta and gamma (CEBPα, β, ε) play major roles in commitment toward myeloid cells, primarily granulocytes, macrophages, and monocytes. This factor is essential for the transition from common myeloid progenitors (CMP) to granulocyte/monocyte progenitors (GMP). CEBP modifications are particularly associated with cytogenetically normal acute myeloid leukemia (CN-AML). Interferon regulatory factor (IRF) 8 is implicated in monocyte and dendritic cell lineages and it is highly expressed in plasmacytoid dendritic cells (pDCs)[1]. Mutations of this factor lead to abnormal differentiation of mononuclear phagocytes and play a critical role in anti-mycobacterial immunity. $IRF8^{-/-}$ mice lack pDCs, CD8α DCs, and $CD103^{+}$ DCs, and can develop a spontaneous myeloproliferative syndrome characterized by hyper-proliferation of granulocytes[1]. Upon pathogenic stimuli such as pathogen-associated molecular patterns (PAMPs) or danger-associated molecular patterns (DAMPs), neutrophils and monocytes are rapidly recruited by chemotaxis into local tissues, where they are activated for phagocytosis, respiratory burst as well as secretion of pro-inflammatory cytokines, thereby contributing to innate immunity. This emergency myelopoiesis and cell activation is quickly resolved, and the balance in myeloid cell

population is restored without negative consequences for the host. However, a number of conditions associated with chronic inflammation, autoimmune diseases and cancer results in aberrant, sustained myelopoiesis characterized by the accumulation of immature myeloid cells that deviate from the standard path of differentiation[3,4]. Indeed, tumor-derived factors (TDFs, i.e. cytokines, chemokines and metabolic soluble mediators) promote and sustain the expansion of a heterogeneous population of myeloid cells remarkably skewed towards an immunosuppressive phenotype and endowed with regulatory functions. The appearance of this tolerogenic population, called myeloid-derived-suppressor cells (MDSCs), represents a common trait of cancer and other diseases, such as sepsis, bacterial, viral and parasitical infection, autoimmune diseases and aging[5,6,7]. These cells have an activation programme (pathologic activation) which is different from that of mature (terminally differentiated) myeloid cells[8].

As shown in **figure 1**[9], under physiological conditions, hematopoietic progenitor cells (HPC) differentiate via common myeloid progenitor cells (CMP) into granulocyte/macrophage progenitor cells (GMP). These immature myeloid cells (IMC) differentiate further into monocytic/dendritic progenitor cells (MDP) or myeloblasts (MB) which develop further into DCs/macrophages or neutrophils, respectively. Under cancerous conditions, the tumor impairs general myelopoiesis leading to the accumulation of monocytic MDSCs (M-MDSCs) and polymorphonuclear MDSCs (PMN-MDSCs). These cells have different genomic, biochemical profiles and functional activity compared to neutrophils and monocytes, even though they are morphologically and phenotypically similar. Their main characteristic is the potent ability to suppress various types of immune responses, with a mechanism evolved to avoid a strong tissue damage caused by a continuous immune response during an unresolved inflammation[9].

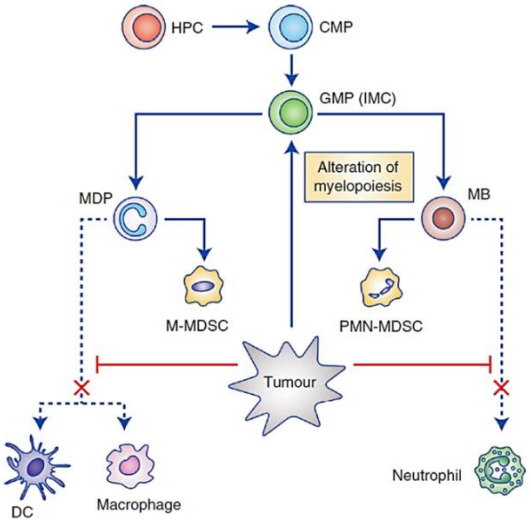

Figure 1. MDSC formation process in cancer. This image is adapted from[9]

1.1. Mouse MDSCs

In mice, MDSCs were defined as cells expressing Gr-1 and CD11b (also known as integrin αM) markers. Nevertheless, recent studies led to the identification of two main subsets with different phenotypic and biological properties: M-MDSCs and PMN-MDSCs. Both subpopulations share the CD11b myeloid marker but can be easily distinguished by the different expression of the two main Gr-1 epitopes, Ly6C and Ly6G. M-MDSCs (GR-$1^{lo/int}$CD11b^{+}Ly6C^{hi}Ly6G^{-}) display the highest immunosuppressive activity in an antigen-non-specific manner, whereas PMN-MDSCs (Gr-1^{hi}CD11b^{+}Ly6C^{lo}Ly6G^{+}) are less immunosuppressive and exert their function by antigen-specific mechanisms. M-MDSCs are side scatter low (SSC^{lo}), while PMN-MDSCs are side scatter high (SSC^{hi}). M-MDSCs usually express higher levels of F4/80 (macrophage marker), CD115 (also known as CSF-1R, colony stimulating factor 1 receptor), although these markers are not uniformly present in MDSCs induced by different tumors. Moreover, M-MDSCs but not PMN-MDSCs, when cultured with granulocyte macrophage colony-stimulating factor (GM-CSF), differentiate *in vitro* acquiring the expression of F4/80 and CD11c markers[10,11]. MDSCs express diverse markers on the surface membrane that are associated with early stages of myeloid differentiation (CD31 and ER-MP58), low levels of the major histocompatibility complex (MHC) class II and co-

stimulatory molecules (i.e., CD80), in line with their origin from immature myeloid-monocytic precursors[12], as well as the co-inhibitory molecule programmed death ligand-1 (PDL-1)[10], which con promote T cell impairment. M-MDSCs are plastic and can acquire phenotypic, morphological and functional features of PMN-MDSCs by a mechanism that involves the epigenetic down-regulation of the retinoblastoma protein (Rb1) by histone deacetylases[13]. Thus, M-MDSCs not only have the capacity to down-modulate strongly antitumor immunity but also serve as "precursors" that maintain the PMN-MDSC pool. M-MDSCs proliferate faster than either PMN-MDSCs or the normal monocytes, from colonies in agar, and can generate a wide range of myeloid cells when adoptively transferred to tumor-bearing host[14]. By preventing the extrinsic apoptotic death pathway and the activation of caspase-8, the cellular FLICE (FADD-like IL-1β-converting enzyme)-inhibitory protein (c-FLIP) is constitutively required for the development of M-MDSCs, whereas myeloid cell leukaemia 1 (MCL-1) protein, which controls the intrinsic mitochondrial death pathway, is essential for the development of PMN-MDSCs[15]. The plasticity of MDSCs relies on the ability of these myeloid cells to lose their lineage identity in response to specific environmental signals.

1.2. Human MDSCs

In cancer patients MDSCs were detected in both blood and tumours[16]. Due to the absence of really suitable phenotypical markers sufficient to identify MDSCs[8], it was necessary to define them by functional assays. Since human MDSCs do not express Gr-1 markers, their enumeration is complex requiring the detection of a combination of myeloid markers. Human M-MDSCs express monocytic markers such as of CD14 and lack of CD15 markers[17,18], and the low/absent expression of HLA-DR marker. Therefore, human M-MDSC are characterised as $CD11b^{+}CD14^{+}HLA\text{-}DR^{low/-}CD15^{-}$. PMN-MDSCs contain a cell population resembling granulocytes and are phenotypically characterized by CD15 and CD66b expression and the absence of CD14[19,20,21]. Therefore, they can be characterised as $CD11b^{+}CD14^{-}CD15^{+}$ (or $CD66b^{+}$) cells[3]. Lectin-type oxidised LDL receptor-1 (LOX-1) has also been proposed as a new marker to distinguish human PMN-MDSCs from non-immunosuppressive neutrophils[22,23]. Recently, CD84 was also

identified to be a robust MDSC-specific cell surface marker[24,25,26]. A useful marker for the identification of immunosuppressive MDSCs is the CD124; indeed, its expression on MDSCs of colon cancer and melanoma patients correlated with a more immunosuppressive phenotype[27]. In addition, a subset of more immature human MDSCs defined as early-stage, or immature, MDSCs (eMDSCs or iMDSCs) lacks the expression of mature blood cell markers (including CD3, CD14, CD15, CD19, CD56) and are therefore characterised as $Lin^{-}HLA\text{-}DR^{-}CD33^{+}$ [22,28], which mouse counterpart is yet to be identified[29,30] . The MDSC phenotyping can be summarized as: **total MDSC**: $CD11b^{+}HLA\text{-}DR^{-/low}CD33^{+}$; **PMN-MDSC**: $CD11b^{+}HLA\text{-}DR^{-/low}CD33^{+}$ $CD14^{-}CD15^{+}$; **M-MDSC**: $CD11b^{+}HLA\text{-}DR^{-/low}CD33^{+}$ $CD14^{+}CD15^{-}$; **e-MDSC**: $CD11b^{+}HLA\text{-}DR^{-/low}CD33^{+}$ $CD14^{-}CD15^{-}$[29,30]**.**

1.3. Immunologic functions of MDSCs

MDSCs display potent immunosuppressive driven by different mechanisms including induction of immunosuppressive immune elements, blocking of lymphocyte homing, production of both reactive oxygen species (ROS) and nitrogen species (RNS), depletion of metabolites on the tumor microenvironment (TME) and the expression of negative immune checkpoint molecules[9]:

- *Induction of other immunosuppressive cells* –Transforming growth factor-β (TGF-β), produced in high amount by MDSCs, arrests T lymphocytes cell cycle, blocks the differentiation of $CD4^{+}$ T cells in T helper 1 (Th1) or 2 (Th2) cells and promotes the clonal expansion of antigen-specific natural Tregs inducing the conversion of naïve $CD4^{+}$ T cells into induced (i)Tregs in combination with other products, such as interferon (IFN)-γ and IL-10 or retinoic acid[31]. Moreover, by decreasing macrophage production of IL-12, MDSCs skew macrophages toward an M2 phenotype[27,32]. Thus, MDSCs are also able to promote indirectly immune suppression, favouring the generation of the expansion of other regulatory populations.
- *Blocking lymphocyte homing* – This function is related to the impairment of lymphocyte's adhesion to endothelial cells (ECs) that allows the T cells extravasation and tissue infiltration. The down-regulation of adhesion

molecules, CD162 (selectin P ligand) and CD44 (receptor for the extracellular matrix component hyaluronic acid HA), have been identified to impact negatively the T cells homing[9]. Moreover, it was reported that L-selectin (CD62L) expression on naïve T cells is inversely correlated to expression of metalloprotease ADAM 17 (TACE) on the MDSCs surface[9].

- *Production of reactive oxygen and nitrogen species* – Arginase 1 (ARG-1) and nitric oxide synthases (NOS) are two MDSCs enzymes that promote the depletion of essential metabolites. Their activities lead to an increased production of highly reactive radical compounds by MDSCs, such as ROS and RNS, all species that have a high reactivity for macromolecules like DNA, lipids and proteins. MDSCs produce a high amount of ROS, such as hydrogen peroxide (H_2O_2), which affects T cell fitness by down-regulating CD3 ζ-chain expression and reducing cytokine secretion, as observed in pancreatic cancer and in melanoma[19,33]. At high ROS concentration, radicals can directly react with macromolecules or combine with NO to generate more dangerous RNS, such as peroxynitrite and dinitrogen trioxide, which can avoid the detoxifying system and nitrate/nitrosylate tyrosine, cysteine, methionine and tryptophan in different proteins and enzymes, thus changing their biological functions. Under pathological conditions RNS may induce apoptosis and autophagy directing tumor evolution, and more importantly suppress T cell trafficking ad cytotoxic functions contributing in shaping an immune privileged environment that promotes tumor outgrowth. RNS indeed can prevent antigen-specific activation of $CD8^+$ T cells, altering the immunodominant peptide structure, the peptide loading process on MHC-I on target cells, the receptor of T cells (TCR) binding to peptide-MHC-I complex, or the TCR signaling ability[34]. RNS can alter both α and β chains of the TCR and modify leukocytes trafficking promoting homing to tumor of immune suppressive subsets other than T cells. This is in part mediated by tyrosine nitration of either chemokines (CCL2, CCL5, CCL21, CXCL12) or receptors (CXCR4)[35,36].

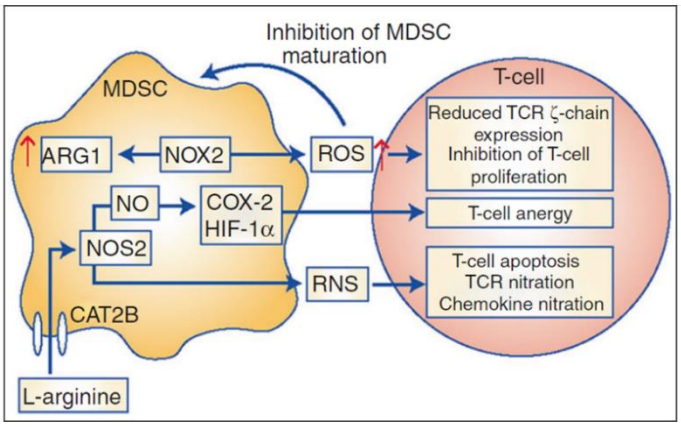

Figure 2. MDSCs immunosuppressive mechanisms: free radical production. This image is adapted from[9]

- *Depletion of metabolites critical for T cell functions* – MDSCs can induce the depletion of L-arginine, tryptophan and cysteine, essential amino acids for the function of the mammalian immune system[34]. L-arginine represents the common substrate for two enzymes: inducible NOS (iNOS) and ARG-1. iNOS generates NO, ARG-1 converts L-arginine to urea and L-ornithine. L-arginine depletion induces a translational blockade of the ζ chain of CD3, preventing T cells responses. L-arginine starvation blocks protein translation through the accumulation of empty aminoacyl tRNA that activates the kinase general control non-derepressible 2 (GCN2) and phosphorylates the translational of the eukaryotic initiation factor 2 α (eIF2 α) for the isoform β (eIF2 β), thus interfering with protein synthesis. MDSC regulate also the metabolism of L-Tryptophan. This amino acid degradation is catalysed by 2 isoenzymes of indoleamine-2,3-dioxygenase (IDO) enzyme, IDO1 and IDO2. These enzymes are expressed by tumor cells and specific leukocytes subsets such as TAMs, DCs, and MDSCs[37] and are involved in regulation of local inflammation. In particular, the 2 enzymes catalyse the degradation of the amino acid along the kynurenine pathway. L-tryptophan starvation activates GCN2 kinase, which in turns inhibits $CD8^+$ T cell proliferation, causing cell cycle arrest and inducing anergy and directs $CD4^+$ T cell differentiation towards a Treg phenotype by the FoxP3 transcription factor upregulation[38] (**Figure 3**[39]). Moreover, IDO1 and ARG-1 were reported to be linked by an entwined pathway in

immunometabolism. The ARG-1-dependent production of polyamines or their release by MDSCs, condition DCs toward an IDO1-dependent, immunosuppressive phenotype via activation of the Src kinase, which has IDO1-phosphorylating activity. The joint modulation of these two enzymes could represent an important target for effective immunotherapy in several disease settings[40]. Finally, MDSCs compete with antigen presenting cells (APC), such as macrophages and DCs, for cysteine import and limit the availability of cysteine in the microenvironment. T lymphocytes proliferation and fitness rely on the availability of L-cysteine, but they lack both the enzymes to import it, thus depending on APC, during the immunologic synapsis. Consequently, T cells display impaired activation and function in a MDSC-conditioned, poor cysteine environment[41].

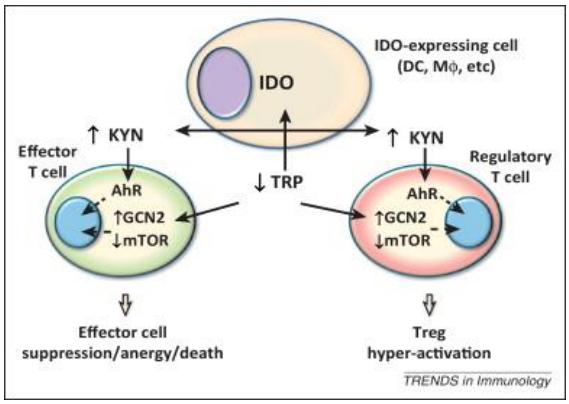

Figure 3. Metabolic control of T cell and Treg responses via IDO. This image is adapted from[39]

- *Expression of ectoenzymes regulating adenosine metabolism* - Another mechanism exploited by MDSCs to control T cell functions includes the generation of adenosine from ATP[42], through induction of the ectoenzymes CD39 (which converts ATP released into the extracellular space into AMP) and CD73 (which catalyses ATP dephosphorylation into adenosine) in a hypoxia-inducible factor 1- α (HIF-1α)-dependent manner. Increased adenosine concentration within the interstitial fluid of solid tumors inhibits priming of naïve T lymphocytes and reduces the expression of effector molecules on

activated T cells modifying their adhesion capability to tumor cells and their cytotoxic activity[43].

- *Expression of negative immune checkpoint molecules* – PD-L1 and cytotoxic T-lymphocyte antigen 4 (CTLA-4) immune checkpoints expression by MDSCs is another important mechanism exerted by these population for tumour cells immune evasion[44] . PD-L1 is known to be a prominent negative regulator of T cell functions and a mediator of immune evasion by tumour cells. Moreover, the inhibition of signaling by PD-L1 or CTLA-4 has proven to be beneficial for cancer patients' survival favouring a strong tumor infiltration with immune cells[45] . Indeed, PD-L1 exerts its effect by binding to its receptor PD-1 on T cells, inducing T cell anergy and apoptosis. The induction of PD-L1 on MDSCs has been recently shown to be mediated by soluble factors M-CSF and vascular-endothelial growth factor (VEGF)[46] .

1.4. MDSCs differentiation, expansion, and recruitment

The differentiation of MDSCs is a complex and still debated topic. It is generally demonstrated that it could be driven by various mediators including granulocyte-macrophage (GM) -CSF, granulocyte (G) -CSF, monocyte (M) -CSF, VEGF, stem cell factor (SCF), interleukin-6 (IL-6), and interleukin-13 (IL-13)[11,47]. and other cytokines such as tumour necrosis factor β (TNF-β), IL-1β, TGF-β, and IL-10 related to immunosurveillance[48,49]. Evidence suggested that MDSCs expansion can be separated into two processes governed by different signal transduction pathways, following the so-called "two-signal" model (**Figure 4**)[50]. Based on this model, one pathway is predominantly responsible for MDSCs expansion (**Figure 4A**) and the second one for driving MDSCs activation (**Figure 4B**)[50].

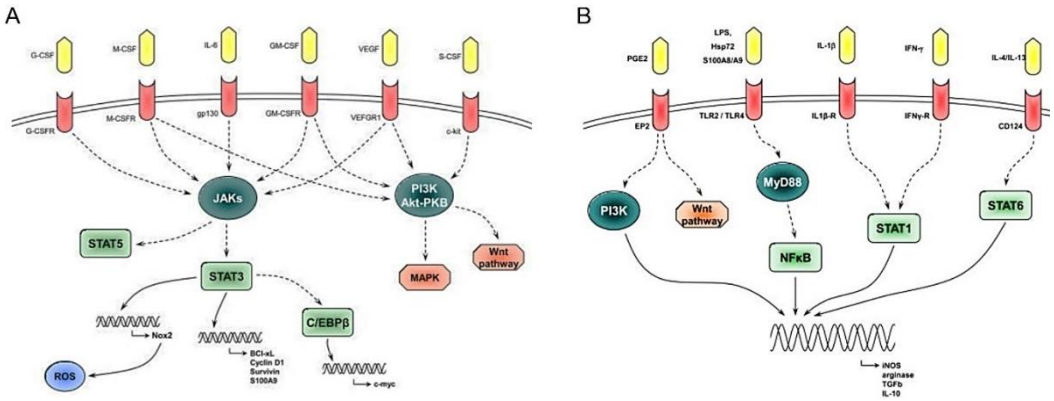

Figure 4. Schematics of possible signaling pathways involved in MDSC expansion and activation. This image is adapted from[50]

The first process is induced by various cytokines and growth factors produced by tumours or BM stroma in response to chronic stimulation. It involves factors including GM-CSF, M-CSF, G-CSF, IL-6, VEGF able to activate signal transducer and activator of transcription 3 (STAT3) and 5 (STAT5)-associated molecular pathways. STAT3 is one of the master transcriptional factors of MDSC expansion and its genetic ablation promotes a substantial MDSC contraction in tumor-bearing mice[51]. STAT3 signaling plays a pivotal role in the conversion of monocytes into functional MDSCs in cancer setting[52,53].

STAT3 not only promotes MDSC survival by regulating signaling of several anti-apoptotic proteins such as cyclin D1 and B-cell lymphoma XL (Bcl-xL), and by regulating c-Myc expression in a CCAAT-enhancer-binding protein β (CEBPβ)-dependent manner, but it also increases the MDSC production of ROS by phagocytic oxidase[53]. Indeed, this factor regulates transcription of subunits of NADPH oxidase 2 (Nox2), that results in increased production of ROS, and controls the expression of CEBPβ transcription factor, that plays a crucial role in regulating differentiation of myeloid precursors to functional MDSCs[50]. All together these factors contribute to proliferation and survival of immature myeloid cells and prevent their differentiation to mature cells (**Figure 5A**[50]). STAT3 is required to promote the suppressive activity of MDSCs. Vasquez-Duddel and co-authors reported that p-STAT3 is able to bind different sites on the ARG-1 promoter to favor its transcription[54]. A unique STAT3-dependent expression of ARG-1 in a

subset of pancreatic-derived monocytes, which exhibit immunosuppressive properties, was recently identified[55]. Moreover, STAT3-dependent over-expression of S100 calcium-binding proteins A8 and A9 (S100A8/A9), which are important mediators in cancer-induced inflammation, also prevents the normal differentiation of myeloid progenitor cells, promoting their conversion in functional MDSCs[56].
STAT5 is involved in the regulation of MDSCs survival. Ko JS *et al*. have reported STAT5 activation in MDSCs within both mice and human tumors[50].
However, this signaling context alone is not sufficient to generate accumulation of MDSCs. Indeed, it requires a second activating signal for MDSC activation, which manifests in up-regulation of arginase, NO, production of immune suppressive cytokines, etc. This type of signaling is provided by pro-inflammatory molecules such as IFNγ, IL-1β, IL-13 and TLR ligands and induces the activation of JAK-STAT signaling pathway (STAT1, STAT6), toll-like receptor (TLR) signaling, Cyclooxygenase-2 (COX-2) upregulation, and nuclear factor kappa-light-chain-enhancer of activated B cells (NF-κB) transcription factor (**Figure 5B**[50]). STAT1 and STAT6 act directly, while TLR signaling fulfils its role via myeloid differentiation primary response 88 (MyD88) and NF-κB activation favouring the up-regulation of genes involved in the immune suppressive activity of MDSCs such as iNOS, ARG1, IDO, TGF-β and IL-10. Although transcriptional factors STAT1 and STAT6 are activated by different stimuli, STAT1 is activated upon IFN-γ stimulation, whereas STAT6 can be activated through engagement of IL-4Rα (CD124) by IL-4 or IL-13, they are both implicated in the up-regulation of ARG1 expression. STAT1 can also be involved in the iNOS up-regulation, especially in M-MDSCs[57] . NF-κB is one of the most relevant transcription factors involved in MDSCs activation and, consequently, in triggering the immunosuppressive phenotype. Indeed, the role of NF-κB as a crucial link between inflammation and cancer has been well-established[58]. NF-κB can be activated through the canonical pathway, which is mediated by p50 and p65 subunits (RelA), or non-canonical pathway, mediated by p52, p100 and RelB subunits[59] (**Figure 5**[59]). Normally, NF-κB proteins exist as hetero- and homodimers in the cytoplasm and bind a class of inhibitory proteins called IκBs. In the canonical pathway, NF-κB activation depends on the IκB kinase complex (IKK), which contains two catalytic subunits,

IKKα and IKKβ, and a regulatory subunit, IKKγ. Upon stimulation, the subunit α of IκBs (κBα) is phosphorylated by IKK in a manner that requires IKKβ, resulting in the degradation of IκBα and the release and nuclear translocation of the p65/p50 dimer[60]. In the non-canonical pathway, RelB/p100 heterodimers are processed to RelB-p52 heterodimers by IKKα homodimer. In the nucleus, NF-κB dimer can activate genes involved in cell cycle regulation as cyclin D1, apoptosis as B-cell lymphoma 2 (Bcl-2) and Bcl-xL, and inflammation including cytokines encoding genes. Furthermore, NF-κB can interact with different kinases, such as glycogen synthase kinase 3 (GSK3)-β, p38, or phosphoinositide 3-kinases (PI3K), modulating the NF-κB transcriptional activity or affecting upstream signaling pathways[60].

NF-κB not only is a crucial player for the survival and proliferation of cancer cells, but its activation is also fundamental to confer immunosuppressive properties to MDSCs. In MDSCs, NF-κB pathway is normally activated by various factors, such as TLR ligands, IL-1β or TNF-α[61]. Different studies have shown that MyD88, a cytoplasmic adaptor molecule essential for integrating and transducing the signals generated by TLR family, acted upstream of NF-κB and could be involved in suppressive activities of MDSCs in the context of lung carcinoma in mice[62] . A recent study performed *in vitro* on mouse renal carcinoma cell line, demonstrated that NF-κB activation through MyD88 has been linked to the engagement of TLR2 by exosome heat shock protein 70 (HSP70)[63]. Exosomes enriched in tumor-derived HSP70 triggered a TLR2/MyD88-dependent STAT3 activation. Interestingly, STAT3 was shown to be an important transcription factor cooperating with NF-κB in MDSCs. STAT3 stimulates the activation of the non-canonical NF-κB pathway, which subsequently induces the transcription of IDO by directly binding the IDO promoter region[64]. Furthermore, TNF-α, which is a well-known activator of the NF-κB pathway, is implicated in MDSCs activation by regulating iNOS expression[65] . Specifically, tumour necrosis factor receptor superfamily (TNFR) 2 was observed to promote the survival of MDSCs in mice via NF-κB-mediated expression of c-FLIP[66], an anti-apoptotic regulator and a crucial player in conferring immunosuppressive activity in M-MDSCs[66].

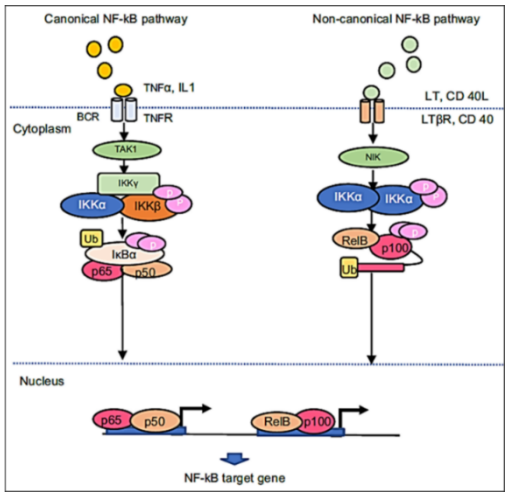

Figure 5. Schematics of canonical and non-canonical NF-κB pathways. This image is adapted from[59]

This model may explain why, at steady state, activation of STAT3 and STAT5 in response to various growth factors that are required for normal haematopoiesis, does not result in accumulation of MDSCs in the absence of strong signal from pro-inflammatory factors. It can also explain why acute inflammation, associated with the release of pro-inflammatory factors in the absence of sustained up-regulation of growth factors, also does not result in accumulation of MDSCs. It is likely that there is an overlap between these signaling pathways. In steady state, different hematopoietic factors might contribute to drive differentiation towards either one or the other subset of MDSCs. Moreover, transcription factors can modulate the activity of each other, as shown, for instance, for STAT3 and NF-κB[67,68].

Finally, this model suggests that accumulation of MDSCs is possible only if two strong signals are provided. More recently a multi-step model was suggested (**Figure 6**[69]), which does not contradict the two-stage model but adds some steps that are associated with the migratory properties of these cells. For example, the first step in the two-stage model corresponds to activation of myelopoiesis, mobilization to the blood, and migration of myeloid cells to the tumour sites. From the migratory viewpoint, the multi-step model suggests more complex setup of four steps: myelopoiesis, mobilization to the blood, recruitment, and retention. These steps comprise a crosstalk between the tumor site and myeloid cells. Cytokines,

chemokines and transcription factors released from the tumor site reach the blood and, thereafter, the BM and LNs altering different steps in myeloid cell differentiation and migration. The first step starts with the migration of myeloid cells, generated from hematopoietic stem cell and progenitor cells (HSPCs) in a process termed myelopoiesis, from BM to the blood. HSPCs also migrate from BM to secondary lymph nodes (LNs) and spleen. This first step is directed by several cytokines, among them IL-17A, G-CSF, GM-CSF and TNF-α[69]. Moreover, the mobilization of myeloid cells to the blood is selectively directed by chemokine receptors, including CCR2 for monocytic myeloid cells and CCR5 for the polymorphonuclear myeloid cells, via CCR2 key ligand CCL2 and the CCR5 key ligands: CCL3, CCL4 and CCL5[70,71]. Homing to the tumor site is likely to be directed by many chemokines and chemokine receptors largely expressed at tumor sites. Especially, CX3CL1-CCL26 pathway is involved in the M-MDSCs recruitment, whereas CXCL5/CXCL2/CXCL1 chemokines play a pivotal role to recruit PMN-MDSCs into tumor compartment. Finally, retention of these cells at the tumor sites is supposed to be directed by a limited number of chemokine receptors and/or adhesion molecules. This step is still speculative and has been mostly studied for T cells thus far[69]. CCL2 has multiple roles in cancer progression. Qian *et al*. in 2011 showed that Gr-1$^+$ inflammatory monocytes were not found at primary mammary tumor lesions, and instead were preferentially recruited by CCL2 to pulmonary metastases to assist tumor spreading. Moreover, CCL2 expression and macrophages infiltration were shown to correlate with poor prognosis and metastatic diseases in human breast cancer[72]. Recent evidence reported that the administration of anti-CCL2 monoclonal antibody (mAb) induced tumor-specific CD8$^+$ T cells activation and expansion rather than a decrease in the number of tumor-associated macrophages[73,74]. Furthermore, Ugel *et al.* demonstrated that CCL2 serum levels correlated with the expansion of immature myeloid cells in the blood of cancer patients, and CCL2 blockade re-established the immune responses in the tumor-bearing host[14].

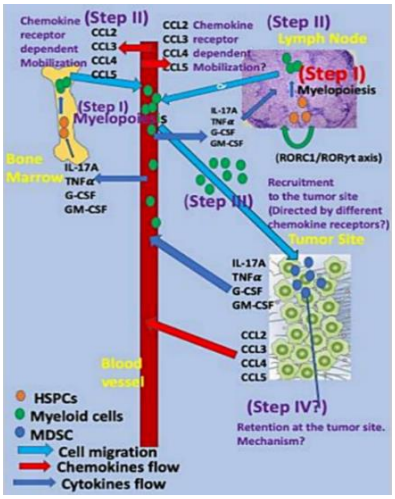

Figure 6. Multistep model for the mobilization and migration of myeloid cells to the tumor site. This image is adapted from[69]

1.5. Role of MDSCs in tumor microenvironment and cancer progression

TME is a complex network of epithelial and stromal cells as well as immune cells. Immune cell populations include myeloid cells, which are mainly composed of tumour-associated macrophages (TAMs), DCs, tumour-associated neutrophils (TANs), and MDSCs. The main inhibitory immune cells in tumor sites are MDSCs, TAMs, and Treg cells[75,76], but at present, there is growing evidence that MDSCs play a major role in tumour growth and represent a key factor for immunosuppression in cancer patients[76]. TME itself has been reported to favour the MDSCs survival and function[77,78]. TME is a hostile environment due to deficiencies in oxygen (hypoxia) and nutrients and the presence of ROS. The survival of tumour cells within the TME is governed by different mechanisms, two of which are: (a) activation of the transcription factor Nuclear Factor Erythroid-derived 2-like 2 (Nrf2) which turns on genes that attenuate oxidative stress; and (b) the presence of High Mobility Group Box Protein-1 (HMGB1), a DAMP that induces autophagy and protects against apoptosis[77]. Both Nrf2 and HMGB1 promote tumour cell survival, as well they facilitate MDSCs survival[77]. MDSCs were first observed in patients with advanced cancer, and in a variety of tumoral contexts a high number of circulating MDSCs is associated with poorer prognosis and a weaker response to treatment[73]. MDSCs fulfil their immunosuppressive role through a variety of

mechanisms blocking T cell activation, function and trafficking into lymph nodes, inducing Tregs, blocking natural killer (NK) cell-mediated cytotoxicity, promoting neo-angiogenesis and enhancement of cancer cell stemness[79] . MDSCs also favour metastatic processes by promoting the premetastatic niche "priming". Indeed, these cells convoy tumor cells into the circulation, inhibit their killing by immune cells, promote their extravasation into the tissues and enhance the engraftment of circulating tumour cells (CTCs)[80,81]. Chemokine receptors CXCR2 and CXCR4 are mostly involved in the recruitment of PMN-MDSCs to the premetastatic niches[82], where they may facilitate the escape of tumour cells by suppressing immune cells, and may promote tumour cells' engraftment by inducing matrix remodelling and angiogenesis[82]. PMN-MDSCs were shown to promote both the extravasation and engraftment of CTCs by producing high levels of matrix metalloproteinase (MMP)-8 and -9[83].

CTCs, precursors of metastasis, are often found in the circulation of cancer patients, such as patients with breast cancer[84]. Cancer patients with high percentages of CTC-neutrophil clusters in the blood had worse clinical outcomes. The neutrophils contained in the clusters showed a PMN-MDSCs like gene expression profile. Additionally, neutrophil-containing CTC clusters were able to form metastasis much faster than CTC alone[85]. These findings suggest that, at the very early stage of cancer dissemination, neutrophils can promote the formation of metastasis by enhancing the proliferative abilities of CTCs. CTCs can also be targeted by immune cells with anti-tumour activity, including NK cells and $CD8^+$ T cells[86]. In mouse models of metastasis, the depletion of NK cells prior to the injection of tumor cells increased metastasis to the lung. Moreover, PMN-MDSCs inhibited NK-mediated killing of CTCs and promoted metastasis formation into lungs[87].

Finally, recent studies have also shown that MDSCs can be used as prognostic biomarkers for the evolution of the disease as well for efficacy of cancer immunotherapy[88,89,90]. Due to the recognised prominent role that MDSCs have in cancer, they are now considered as a main therapeutic target. Although MDSCs have a short lifespan in tissues, their continuous recruitment to sites of chronic inflammation enables them to have long-lasting effects at these sites. However, because their lifespan in tissues is short, the state of pathological activation of these

cells in tissues is difficult to reverse. Therefore, effective therapies could aim at targeting MDSCs by (a) blocking immunosuppressive functions to improve antitumor immune response, (b) inhibiting their migration to the affected tissues, or (c) by manipulating the tissue microenvironment to deplete MDSC population[9]. Preclinical and clinical research is studying several novel approaches to target MDSCs with combined immunomodulatory therapies including chemotherapeutic agents and immune checkpoint-directed therapy[91].

1.6. M-MDSCs and monocyte subpopulations in cancer

Human MDSCs have been well characterized in a long list of solid tumors: breast cancer, non-small cell lung cancer, colon and colorectal cancer, sarcoma, gall bladder, melanoma[29], head and neck squamous carcinoma[92], carcinoid, renal cell carcinoma (RCC)[20], gastrointestinal cancer, oesophageal cancer[93], bladder cancer[94], urothelial cancer[21]. MDSCs were also detected in different haematological malignancies, such as non-Hodgkin's lymphoma and multiple myeloma[16]. Nevertheless, it remains very difficult to identify clearly MDSC subsets in cancer patients. Multiple human MDSCs subsets with different phenotypes have been documented in several types of tumors in the last 2 decades[16]. In many tumors, as well as in cancer patients, PMN-MDSCs are the predominant subset, representing 70 to 80% of the tumor-induced MDSCs, compared to 20 to 30% of the cells reflecting the monocytic lineage[78]. For example, patients with colon and lung cancers display increased levels of PMN-MDSCs in blood as well[18]. On the other hand, circulating M-MDSCs ($CD11b^{+}Lin^{-}CD33^{+}HLA\text{-}DR^{-}CD14^{+}$) and Tregs are increased in metastatic prostatic cancer patients compared to healthy donors (HDs) and negatively correlate with patients' survival. Circulating MDSC levels correlated with response to therapy and surgery[95] and the analysis of the clinical outcome of cancer patients revealed that MDSC frequency in blood is associated with prognosis and clinical outcome[93].

Novel insights allowed to characterize better the nature of MDSCs as cells with an intrinsic immune suppressive activity with a genomic and biochemical profile that partially permit to distinguish them from other myeloid subsets[3]. It has been

reported that M-MDSCs have stronger inhibitory effect than PMN-MDSCs and have become an important mediator of tumour-induced immunosuppression[96]. However, the emerging complexity of human monocytes subsets, together with their role in promoting tumor processes, makes a clear definition of M-MDSCs more difficult to achieve. Indeed, human monocytes are characterized by a great plasticity and heterogeneity and can exert important pro- and anti-tumoral functions[52]. Three different subsets of monocytes can be distinguished: classical monocytes ($CD14^{+}CD16^{-}$), non-classical monocytes ($CD14^{low}CD16^{+}$), and intermediate monocytes ($CD14^{+}CD16^{+}$)[97]. Classical monocytes, also known as "inflammatory monocytes" (iMo), are characterized by a high expression of chemokine receptor CCR2[98]. In steady state conditions, classical monocytes extravasate and differentiate into local tissue-resident macrophages. They can also remain undifferentiated in the tissues, acting as a local monocyte reservoir[99]. Non-classical monocytes display a distinct and characteristic motility along the vasculature; hence, they have acquired the name of "patrolling monocytes" (pMo) and are defined by a higher surface expression of C-X3-C chemokine receptor 1 (CX3CR1)[52]. These cells are mainly found in blood, but they also undergo diapedesis and were identified in parenchyma of many tissues[99]. iMo can perform a transition into pMo, by the upregulation of pMo-specific genes indicating that they are biologically linked. C/EBPβ, an important transcription factor regulating the expression of many myeloid-related genes, was identified as a key factor in epigenetic processes leading to the differentiation of iMo into pMo in steady state conditions[100]. Furthermore, C/EBPβ is also an important regulator of MDSC immunosuppressive properties[101], as already described, indicating that it could be a key factor in the development of monocytes during the emergency state. However, evidence showed that pMo development can also be independent from iMo subset, probably by direct generation from the common monocyte progenitor (cMoP)[52]. Indeed, under pathological conditions, as in case of cancer, there is a rapid recruitment of myeloid cells to sites of injury from the BM[52]. Moreover, pMo might differentiate from circulating iMo by the formation of the intermediate monocyte subset[52]. This subset is found at low frequency but has unique features and expands with cytokine treatment and in inflammation[97].

iMo recruitment into tumors seems to be negatively associated with $CD8^+$ T cells infiltration, and it was shown that inhibition of CCR2 in tumor-infiltrating macrophages prevented monocyte accumulation and increased $CD8^+$ T cells infiltration in mice with hepatocellular carcinoma. This finding suggests that iMo could be also primary precursor of MDSCs[102] . Monocytes have been also shown to be involved in the development of cancer metastasis. In particular iMo might be pre-metastatic promoters recruited to the pre-metastatic niche by CCL2/CCR2 axis[52]. Here, they can promote tumor colonization by the secretion of angiogenic factors, as VEGF-A, as demonstrated on a mouse model of spontaneous breast cancer[72]. Monocytes can also support the survival of cancer cells in the metastatic organs by direct binding of the α4-integrin, expressed on monocyte surface, with vascular cell adhesion protein 1 (VCAM-1), expressed on tumor cells. This binding allows to deliver anti-apoptotic signals favouring tumor cell survival[103]. Furthermore, extracellular vesicles (EVs) secreted by tumor cells can be involved in favouring metastatic cancer growth by myeloid cell recruitment. In the context of lung metastasis, Zhang *et al.*[104] showed the ability of lungs, alveolar and interstitial macrophages to internalize tumor-derived-EVs, after the vesicles crossed basal lamina of alveolar capillaries. The uptake of EVs by macrophages led to the release of CCL2 favouring the recruitment of iMo to the lungs, that consequently differentiated into macrophages, mostly with an M2-like phenotype[104]. M2 macrophages are, in turn, able to promote tumor growth by the release of IL-6 and deposition of fibrin[104]. Considering the increasing evidence highlighting the role of monocytes, together with MDSCs, in the immunosuppressive and pro-tumoral activities, further investigations will clarify the underlying molecular mechanisms that could represent novel and important targets for cancer immunotherapy.

1.7. Strategies to target therapeutically MDSCs

Since MDSCs fuel immunosuppressive circuits in TME, several pharmacological approaches, which involve either MDSC elimination or modulation of their functions, are currently being explored in tumor-bearing host. Moreover, these novel approaches could be potentially translated to the therapy of other diseases in which MDSCs can play a pathogenic role, such as immunosuppression/immune

deviation associated with chronic infections. For simplicity, we can divide these MDSC inhibitors in four classes according to their ability to control MDSC immune regulatory properties, MDSC development, MDSC differentiation or MDSC depletion.

Targeting MDSC immune regulatory properties. MDSCs can be functionally inactivated by targeting their suppressive machinery and, at the moment, several approaches have been already exploited. Both ARG-1, iNOS expression have been shown to be down-regulated in response to phosphodiesterase-5 (PDE-5) inhibition[105]. A clinical trial (number NCT00894413) with tadalafil, an inhibitor of PDE-5, evaluated the effect of this treatment on immune function in patients with head and neck squamous cell carcinoma (HNSCC) and reported that both ARG1 and iNOS activities were significantly reduced in tadalafil-treated patients. Moreover, this pharmaceutical treatment promoted the contraction of both circulating and tumor-infiltrating $CD33^{+}HLA\text{-}DR^{-}IL\text{-}4R\alpha^{+}$ M-MDSCs in treated patients[103]. Interestingly, [3-(aminocarbonyl)furoxan-4-yl] methylsalycylate (AT38), NO-donating compound was shown to decrease MDSC inhibitory activity by reducing the nitration of chemoattractants, such as CCL2 and CXCL12 chemokines, restoring T cell ability to migrate within tumor primary lesion. Indeed, the administration of this drug significantly reduced the expression of both iNOS and ARG1 enzymes in myeloid cells, preventing RNS generation within tumor environment[35]. Up to date, there are only two ARG inhibitors being tested in clinical trials. Both drug candidates have been developed by Calithera Biosciences and are orally available small-molecule compounds. INCB001158 (CB-1158) is being evaluated in phase 2 as a single agent and in combination with immune checkpoint inhibitors in cancer, while CB-280 in phase 1 in cystic fibrosis, exploiting the novel idea of increasing NO production to improve lung function. CB-1158 has been shown *ex vivo* to reverse human T cell immunosuppression mediated by ARG-1 produced by neutrophils as well as MDSCs[106,107]. Epacadostat, also known as INCB024360, is an orally available reversible competitive IDO1 inhibitor. It was found to enhance the antitumor effect of anti-CTLA-4 or anti-PD-L1 antibodies in the pre-clinical models. However, recent data showed that the phase III clinical trial of epacadostat in combination with pembrolizumab (anti-PD-1 immune checkpoint

inhibitor) for the treatment of patients with unresectable or metastatic melanoma did not meet the primary endpoint of improving progression-free survival in the overall population compared to pembrolizumab alone. Navoximod, also known as GDC-0919, was developed as an orally bioavailable IDO1/TDO inhibitor. In the 4T1 murine breast tumor model, this drug synergizes with doxorubicin to elicit an antitumoral immune response and to control tumor growth. PF-06840003 is a highly selective IDO1 inhibitor with favourable pharmacokinetic characteristics and a prolonged half-life in humans, which enable single-dose daily administration. Additionally, its ability to enter the central nervous system (CNS) allows for its use against brain metastases. Recently, BGB-5777, a potent CNS-penetrating IDO1 inhibitor, enabled a durable survival benefit in a fraction of patients with advanced glioblastoma when combined with nivolumab and radiation therapy[108]. Finally, inhibition of COX-2 decreased the production of immunosuppressive prostaglandin E2, limiting cancer progression. Celecoxib, the COX-2 inhibitor, supplied in combination with DCs pulsed with tumor lysates improved the survival of mesothelioma-bearing mice[109].

Inducing MDSC depletion. Accumulating evidence indicates that the antitumor activity of chemotherapy also relies on several off-target effects, especially directed at the host immune system, that cooperates for successful tumor eradication[110]. In particular, some conventional chemotherapy agents, such as gemcitabine and 5-fluoracil (5-FU), showed a highly effective cytotoxic action on MDSCs. Gemcitabine, an antimetabolite drug (nucleoside analogue), used for the treatment of pancreatic, breast, ovarian, and lung cancers, was reported to deplete MDSCs in tumor-bearing mice, resulting in enhanced antitumor immunity[111,112,113]. Another antimetabolite, 5-FU, was also shown to induce MDSC apoptosis[114]. Interestingly, MDSCs are more sensitive to these molecules than other immune cells or tumor cells. This dominant effect was explained by a lower expression of thymidylate synthase by MDSCs. This preferential targeting of MDSCs translates into increased effector lymphocyte to immunosuppressive MDSC ratio and is associated with enhanced $CD4^+$, $CD8^+$, and NK cell activation and pro-inflammatory cytokine production, that are fundamental prerequisites to establish a therapeutic effect mediated by cancer immunotherapy. For example, a chemo-immunotherapeutic

regimen based on the association of different chemotherapies with adoptive cell transfer (ACT) of antigen-specific $CD8^+$ T lymphocytes was described to restrain tumor development and improve the overall survival of tumor-bearing mice since the chemotherapeutic treatment selectively eliminated MDSCs[14,114].

Targeting MDSC depletion. Another attractive strategy is based on neutralizing the factors that are involved in MDSC expansion from the hematopoietic precursors, thus compromising their development. Although promising, this task is made complex by the plethora of TDFs involved in MDSC expansion and recruitment.

STAT3 inhibition. MDSCs are characterized by a persistent STAT3 activation induced by various alterations in tumor microenvironment, including oncogenic activation of receptor tyrosine kinase and release of IL-6, VEGF, and IL-10. The consequence of STAT3 constitutive activation is the up-regulation of the numerous STAT3-dependent genes, among which there are anti-apoptotic (Bcl-xL), pro-proliferative (survivin, cyclin D1/D2), and pro-angiogenic proteins (MMP2, MMP9, and HIF-1α). This persistent STAT3 activation also contributes to the increased production of ROS by MDSCs. A selective inhibitor of the JAK2/STAT3 pathway, JSI-124 (circubitacin I), was capable of increasing immune responses against tumors[115]. This molecule markedly reduced the number of $CD11b^+/Gr\text{-}1^+$ immature myeloid cells in the tumor microenvironment, both by increasing their apoptosis (up to 50% in a colon carcinoma model), and by promoting their differentiation into more mature cells. Another category of drugs comprises molecules already used in the clinic. Sunitinib, a tyrosine kinase inhibitor, is used for the treatment of several tumor types for its anti-angiogenic properties[116,117]. Sunitinib also acts by inhibiting the STAT3 pathway in renal carcinoma-associated MDSCs.

Finally, MDSC can be targeted by two molecules used in clinic for STAT3 inhibition are silibinin and baricitinib. Silibinin is a natural polyphenolic flavonoid and exhibits potent antioxidative, anti-inflammatory, anti-proliferative, immunomodulatory, and anti-angiogenetic activities. This drug exhibits its activity by suppressing STAT3 phosphorylation on lysine 705 (Y705) and its dimerization. In the past two decades, researchers have explored the antitumor effects of silibinin in various cancer cell lines, including skin, prostate, lung, and colon cell lines such

as HT29, LoVo, SW480, and COLO205[118]. Studies reported that the treatment with silibinin reduced the intestinal polyps in murine models[115], and ameliorated colitis and inhibited colitis-associated tumorigenesis via inhibition of IL-6/STAT3 signaling pathway[118]. Silibinin has also been used in clinic and its anti-tumor activity was reported in patients with lung cancer and brain metastases. The silibinin administration in these patients showed a STAT3 signaling decrease in the tumor microenvironment[119]. Although, treatments with baricitinib have not reported yet any evidence in cancer context, this drug is clinically approved as JAK1-2 inhibitor for the treatment of moderately-to-severely active rheumatoid arthritis (RA)[120]. Baricitinib was shown to interfere with STAT3 activation. An important clinical trial (number NCT01710358), which was performed in 2017, reported the extreme efficacy of this drug for patients with active RA who had had an inadequate response to methotrexate. This clinical trial was a randomized, phase 3, double-blind study, that was conducted for 52 weeks at 281 centres in 26 countries in which 1307 patients with active RA who were receiving background therapy with methotrexate were randomly assigned to one of three regimens: placebo, treatment with baricitinib or adalimumab (an anti-TNF-α monoclonal antibody). The clinical trial reported that treatment with baricitinib was associated with significant clinical improvements as compared with placebo and adalimumab[121]. Moreover, *in vitro* studies reported that the treatment with baricitinib was able to reduce cell death of cancer cells.

Targeting S100A8/A9. Another potential target to limit MDSC accumulation is represented by S100A8/A9 proteins together with their receptor for advanced glycan endproducts[122]. The injection of an anti-carboxylate glycan antibody (mAbGB3.1), that blocks S100A8/A9 binding and signaling, reduced MDSC accumulation in blood and peripheral lymphoid organs of tumor-bearing mice[56].

CSF-1R inhibition. The inhibition of CSF-1R signaling through small-molecules CSF-1R kinase inhibitors constitutes another strategy to affect MDSC development. GW2580 abrogated tumor recruitment of $CD11b^{+}Gr\text{-}1^{lo}Ly6C^{hi}$ MO-MDSCs in mice bearing Lewis Lung Carcinoma (LLC) and induced a decrease in expression of pro-angiogenic and immunosuppressive genes[123]. The monoclonal antibody against CSF-1R (IMC-CS4), that is used in phase I of a clinical trial

(NCT01346358), established its safety and pharmacokinetic profile in the treatment of subjects with advanced solid tumors, either refractory to standard therapy or for whom no standard therapy is available[124]. The treatment with the monoclonal antibody RG7155, that inhibits CSF-1R activation, in animal models reported a strong reduction of $F4/80^+$ TAMs accompanied by an increase of the $CD8^+/CD4^+$ T cell ratio. The administration of RG7155 to patients led to striking reduction of $CSF\text{-}1R^+CD163^+$ macrophages in tumor tissues, which translated into clinical objective responses in diffuse-type giant cell tumor (Dt-GCT) patients[125].

Targeting MDSC differentiation. In addition to targeting suppressive functions, myelopoiesis can be diverted away from generating MDSCs for therapeutic benefit. All-trans-retinoic acid (ATRA), supplemented with GM-CSF, has been shown to differentiate MDSCs into DCs and improve their immune-stimulatory capacity, inducing the up-regulation of HLA-DR, CD1a and CD40 on MDSCs[126,127]. Treatment of renal cell carcinoma patients with ATRA substantially decreased the presence pf MDSCs in peripheral blood[128]. A recent study demonstrated that lung cancer patients vaccinated against p53 showed a better immune response when immunotherapy was combined with the administration of ATRA[129] (**Table 1**[130]).

Table 1: Synopsis of clinical trials to limit MDSC pro-tumoral activity. Adapted from[130]

Drug	**Type of cancer**	**Effects on myeloid cells**
Curcubitacin B	Lung cancer	Inhibition of MDSC
PDE5 inhibitors (sildenafil, tadalafil)	Breast and colon cancer, myeloma, HNSCC	Inhibition of MDSC dependent immune suppression
Nitroaspirin	Colon carcinoma	Inhibition of MDSC dependent immune suppression
Triterpenoids (CDDO-Me)	Pancreatic adenocarcinoma	Inhibition of MDSC dependent immune suppression
Ciclooxigenase 2 inhibitors	Ovarian cancer, melanoma	Inhibition of MO-MDSC dependent immune suppression
Gemcitabine	Pancreatic adenocarcinoma	MO-MDSC apoptosis

Doxorubicin-cyclophosphamide	Breast cancer	MDSC apoptosis
Bisphosphonates	Pancreatic adenocarcinoma	TAM depletion, inhibition of MDSC expansion
CSF-1R antagonist (PLX3397)	Melanoma, AML, breast cancer	MO-MDSC expansion and recruitment
Anti-CSF1R monoclonal antibody (RG7155 and IMC-CS4)	Advanced solid tumors	Monocyte subset, tissue macrophage and TAM depletion
Tyrosine kinase inhibitor (Sunitinib)	RCC	Inhibition of MDSC expansion in patients
ATRA	RCC, lung cancer	MDSC differentiation to more mature cells
Anti-VEGF-A specific antibody (Bevacizumab)	Lung, breast, and colorectal carcinoma, RCC	Inhibition of proliferation
Vitamins (1,25(OH)2D3)	Head and neck and lung tumors	MDSC differentiation to more mature cells

2. Cellular FLICE (FADD-like IL-1β-converting enzyme)-inhibitory protein (c-FLIP)

2.1. c-FLIP structure and canonical biology

One hallmark of cancer cells is regulation of cell death signaling promoting tumour growth and metastasis formation and inducing resistance to chemo- and radiotherapies. Cellular FLICE (FADD-like IL-1β-converting enzyme)-inhibitory protein (c-FLIP) is a major apoptosis-regulatory protein frequently over-expressed in solid and haematological cancers, in which its high expression is often correlated with poor prognosis[131]. This protein was reported to be constitutively required for the development, survival, and suppressive function of murine M-MDSCs ($CD11b^{+}Ly6G^{low}Ly6C^{+}$ cells)[3,87]. c-FLIP is encoded by the *CFLAR* gene (located on chromosome 2q33.1) and is expressed in humans as 13 distinct spliced variants, three of which are expressed as proteins, namely c-FLIP long ($c\text{-}FLIP_L$), c-FLIP short ($c\text{-}FLIP_S$), and c-FLIP Raji ($c\text{-}FLIP_R$). Each of these three spliced variants

possesses 2 tandem N-terminal protein–protein interaction domains termed death effector domains (DEDs). These DEDs facilitate homotypic interactions with other proteins bearing DEDs, most importantly procaspase-8, procaspase-10 and Fas-associated protein with death domain (FADD). While each c-FLIP splice form has equal N-terminal DEDs, they differ at their C terminus (**Figure 7**)[131]:

- c-FLIP$_S$ is a 26 kDa protein comprising a C-terminal 20 aminoacidic unstructured sequence, which plays an important role in its ubiquitination and subsequent proteasomal degradation;
- c-FLIP$_R$ is a 24 kDa protein notable for its restricted expression pattern, being found mainly in T cells. Its C-terminal region lacks the additional carboxy-terminal amino acids that are present in c-FLIP$_S$, due to alternative splicing;
- c-FLIP$_L$ is a 55 kDa protein and its C terminus is longer than c-FLIP$_S$ one containing a caspase-like protease domain that is catalytically inactive. c-FLIP$_L$ contains a caspase-8 cleavage site at position Asp-376, which produces a N-terminal fragment p43-c-FLIP$_L$ when the longer isoform is cleaved at this site.

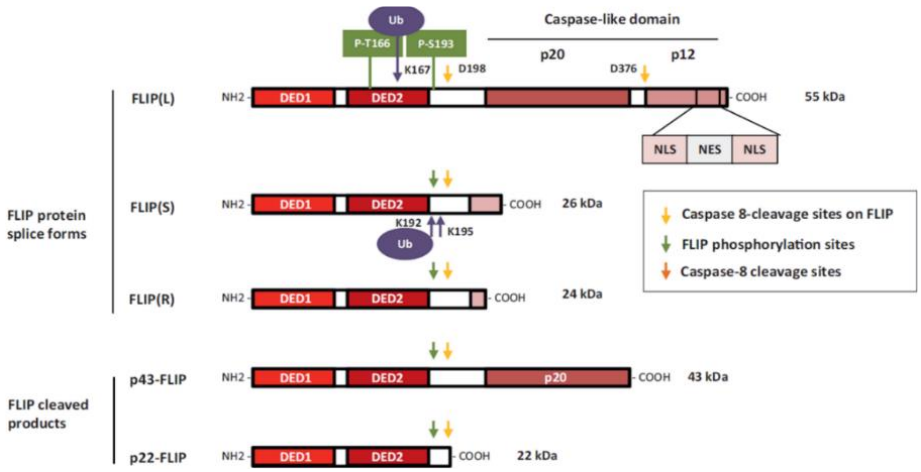

Figure 7. Schematic representation of c-FLIP splice variants. This image is adapted from[130]

In humans, the production of c-FLIP$_S$ and c-FLIP$_R$ is determined by a single nucleotide polymorphism in a 3' splice site of *CFLAR*; however, because of different protein translation rates, c-FLIP$_S$ is produced in higher amount compared to c-FLIP$_R$.

c-FLIP is an anti-apoptotic regulator and resistance factor that suppresses Fas-L- and TNF-related apoptosis-inducing ligand (TRAIL)-induced apoptosis. These factors are all involved in the extrinsic apoptosis (or death-receptor mediated) pathway, which is triggered when TNF receptor superfamily members (as TRAIL-R1/DR4, TRAIL-R2/DR5 and Fas/CD95) are activated by their cognate ligands (TRAIL and FasL)[131]. TNF receptor activation leads to the recruitment of the adapter FADD and formation of the death-inducing signaling complex (DISC), in which procaspases-8 and -10 are recruited and cleaved into active caspases. In this context c-FLIP, containing a DED, is recruited to the DISC complex and regulates the activation of caspases-8 and -10 by competing with them for the recruitment to the DISC complex[132]. This cascade is in turn able to activate other caspases of apoptosis, such as caspase-3[131]. c-FLIP, by caspase-8 and -10 inhibition, down-regulates also the mitochondrial apoptotic pathways, whose cascade starts with the cleavage of Bid, a pro-apoptotic Bcl-2 family member, by caspases-8 and -10. When cleaved, truncated Bid (tBid) induces mitochondrial cytochrome c release, promoting procaspase-9 activation.

Different splice forms can be recruited to the DISC, where the heterodimerization with procaspase-8 occurs. However, each splice form could act in different ways[130]. c-FLIP$_S$ and c-FLIP$_R$ inhibit the formation of procaspase-8 homodimers. The regulatory role of c-FLIP$_L$ is more complex and not only inhibitory. Indeed, its heterodimerization with procaspase-8 leads to the formation of an active enzymatic complex, which can promote the cleavage of both adjacent procaspase-8 homodimers and c-FLIP$_L$/procaspase-8 heterodimers. In the first case, c-FLIP$_L$ drives an activator function of caspase-8; in the second case, the protein does not have any apoptosis-inducing activity[133]. The activating or inhibitory function of c-FLIP$_L$ is strictly affected by the level of the protein recruited to the DISC. When the recruitment of c-FLIP is high and consistent, an apoptosis inhibitory mechanism takes place, since there is a prevalent formation of c-FLIP$_L$/procaspase-8 heterodimers rather than procaspase-8 homodimers, and their subsequent cleavage is not able to activate downstream caspases[131]. In case of low c-FLIP expression, there will be a prevalent formation of procaspase-8 homodimers at the DISC, which can trigger the downstream apoptotic pathway after their cleavage[131]. It was

recently defined the stoichiometry of c-FLIP$_L$:procaspase-8 at the DISC at which these two opposing functions operate. Generally, total cellular levels of procaspase-8 exceed those of c-FLIP$_L$ even in cancer cells which reports elevated c-FLIP expression, however c-FLIP recruitment at DISC complex is more efficient. At low levels of receptor activation, the number of DISCs formed will be low and there will therefore be a predominance of heterodimers (c-FLIP$_L$:procaspase-8 ratio ≈ 1:1) and apoptosis will be inhibited. At high levels of receptor activation, c-FLIP$_L$ levels will become depleted relative to the more highly expressed procaspase-8 (c-FLIP$_L$:procaspase-8 ≈ ratio 1:1) and there will therefore be a predominance of homodimers.

c-FLIP is also involved in the regulation of extrinsic apoptosis mediated by tumor necrosis factor receptor-1 (TNFR1) signaling. In this case, TNFR1 recruits the TNFR1-associated death domain (TRADD) protein, which, in turn, recruits an initial complex, called complex I, that leads to the activation of NF-κB and MAP kinase signaling pathways[134]. When TRADD and receptor-interacting kinase (RIPK1) associate with FADD and procaspase-8, leads to complex II formation which, in turn, promotes the apoptosis. c-FLIP inhibits FADD-induced caspase-8 homo-dimerization in complex II, blocking apoptosis[134]. In necrosome, RIPK1, interacting with RIPK3, can activate the so-called mixed lineage kinase-like (MLKL), under conditions of distruption of the inhibitory complex formed by FADD, caspase-8 and FLIP. Necrosome leads to necrosome translocation to the plasma membrane, where oligomerization takes place and pores are formed, exerting a pro-inflammatory necroptosis[135].

2.2. Non-canonical c-FLIP biology

c-FLIP has been recently reported[132] to be involved in other different signaling pathways which are related to cell survival and proliferation (**Figure 9**[136]). c-FLIP provides also non-canonical pseudoenzyme functions that are independent of caspase-8[136]. These nonclassical pseudoenzyme functions enable c-FLIP to play key roles in the regulation of a wide range of biological processes some of which are herein described:

- *Inflammasome activation*. Inflammasome is an intracellular multimeric protein complex which assembles in response to a range of DAMPs and PAMPs. The inflammasome platform comprises the zymogen procaspase-1 that, one activated, leads to a particular form of cell death called pyroptosis[137]. Inflammasomes are classified based on the protein upon which their scaffold structure is formed[138]. One of the most important and best understood is the NACHT, LRR, and pyrin domain (PYD)-containing protein 3 (NLRP3) inflammasome, which is triggered in response to the most diverse range of inflammatory stimuli. c-FLIP$_L$ has been shown to influence directly the NLRP3 inflammasome assembly and activation. Through its pseudo-caspase domain, c-FLIP$_L$ can interact directly with both NLRP3 and procaspase-1, thereby enhancing caspase-1 processing and IL-1β production[139].
- *Wingless-related integration site (Wnt) signaling*. c-FLIP$_L$ has also been implicated in playing a role in the Wnt signaling pathway. The binding of Wnt proteins to the N-terminal region of Frizzled receptors and to low-density lipoprotein receptor-related protein (LRP) 5 and 6, essential Wnt coreceptors[140], results in increased intracellular levels of β-catenin and in inhibition of GSK (serine-threonine kinase)-3/Axin/APC β-catenin degradation machinery. The process leads to stabilization of β-catenin, which then translocate to the nuclear compartment where it cooperates with the T-cell factor/lymphoid enhancer-binding factor (Tcf/Lef) to drive expression of various genes that regulate stemness and proliferation[141]. c-FLIP$_L$ has been reported to inhibit β-catenin ubiquitination, leading to increase in cytosolic β-catenin and its translocation to the nucleus[142]. Notably, c-FLIP$_L$ has both a nuclear localization signal (NLC) and a nuclear export signal (NES) within its C terminus (not present in the other FLIP splice forms). These features allow the accumulation of c-FLIP$_L$ in both cytoplasmic and nuclear compartments. More recently, it has been reported that c-FLIP$_L$ could interact via its DED with the nuclear protein TBP-interacting protein 49 (TIP49) and that this interaction was crucial for the ability of c-FLIP$_L$ to modulate Wnt signaling[143].
- *Autophagy* is a cytoprotective degradation process which consists in elimination of potentially harmful cytosolic material, such as damaged mitochondria or protein aggregates. Autophagy is also used by cells to secrete cytoplasmatic constituents. This process occurs in response to different forms of stress and its deregulation

modulates many pathologies[144]. Beclin-1 protein is involved in autophagosome formation by inducing the localization of autophagic proteins to the pre-autophagosomal membrane. It has reported that in multiple myeloma cells[145] c-FLIP$_L$ could play the role of negative regulator of Beclin-1-mediated autophagy. In addition to this direct modulation of autophagy, c-FLIP$_L$ has been shown to affect autophagy also through its interaction with procaspase-10[146].

- *NF-κB and MAPK signaling*. This signaling pathways can be modulated by c-FLIP$_L$ through interaction with both TNFR-associated factors 1 (TRAF-1) and 2 (TRAF-2) (**Figure 8**[136]), as well as with RIPK1 and proto-oncogene serine/threonine-protein kinase (Raf-1)[147]. Our research group has recently reported in c-FLIP enforced human monocytes the direct NF-κB activation[66]. Moreover, an alternative c-FLIP mechanism of NF-κB signaling regulation was reported. p22-FLIP, a cytoplasmic NH_2-terminal procaspase-8 cleavage product of c-FLIP, strongly induces activation of NF-κB signaling pathway by interacting with the IKK complex via IKKγ subunit. Finally, c-FLIP$_L$ was shown to be essential for TNF-α-induced MAPK activation by interacting with Raf-1 in a Ras-independent manner or with hcc 7 (MKK7)[148].

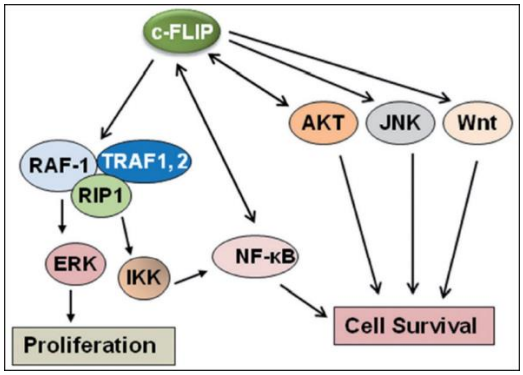

Figure 8. Multifunctional roles of c-FLIP on various signaling pathways. This image is adapted from[136]

- *Endoplasmic reticulum (ER)*. c-FLIP$_L$ localizes at ER and mitochondria-associated membranes (MAMs) playing a role as a modulator of ER morphology and ER-mitochondria crosstalk. Moreover, it has reported that c-FLIP ablation resulted in a disruption of ER morphology and in a decrease of ER-mitochondria

tethering[149]. Conti *et al.* demonstrated that absence of c-FLIP$_L$ resulted in a protein kinase B (AKT) activation which in turn inhibited PERK signaling and promoted cell survival in response to ER stress[150].

- *Aerobic glycolysis*. it was recently reported in hepatocellular carcinoma (HCC) that c-FLIP$_L$ over-expression induces a significant increase in cell aerobic glycolysis indexes including glucose uptake and consumption and lactate production. The co-localization and interaction of c-FLIP$_L$ with sodium/glucose cotransporter 1 (SGLT1), a major active glucose transporter in HCC cells, induces an increase of SGLT1 protein stability by inhibiting its ubiquitination and degradation[151].

- *Cell motility*. c-FLIP$_L$ can enhance cell motility and adhesion to extracellular matrix proteins through the Rho-associated signaling pathway, leading to focal adhesion kinase (FAK) activation, which in turn activates extracellular signal-regulated kinase (ERK). In addition, c-FLIP$_L$ can increase the MMP9 expression promoting further increased cell motility[152].

- *Interferon signaling*. Interferon (IFN) regulatory transcription factor 3 (IRF3) is a transcription factor that promotes expression of IFN-α, IFN-β, which in turn moderate cellular responses to, for instance, viral infection[153]. c-FLIP$_L$ was found to function as an inhibitor of IRF3-induced gene expression[154]. This activity associated with c-FLIP$_L$ preventing of IRF3's interaction with CREB-binding protein.

2.3. c-FLIP regulation

c-FLIP splice forms are regulated at transcriptional, translational, and post-translational levels by various stimuli in a cell-specific manner. The multiple levels at which splice form-specific expression of c-FLIP is controlled underline its fundamental importance in regulating cell fate.

- *Transcriptional regulation*. Induction or repression of *CFLAR* gene are regulated by different transcription factors. NF-κB[155] represents an important effector of TNFR1 signaling promoting c-FLIP upregulation and, consequently, a pro-survival response. In addition, c-FLIP transcription has been reported to be upregulated[131] by CREB, NFATc2, EGR1, androgen receptor, SP1 and p63 factors. *CFLAR* gene

expression can be repressed by several transcription factors[131], including c-Fos, c-Myc, FoxO3a, IRF5, E2F1 and SP3. The transcription factor c-Myc is involved in multiple pathways including Wnt, MAPK signaling, TGF-β and T cell receptor pathways and highly activated in many cancer types[156]. It has been observed that c-Myc directly binds to *CFLAR* promoter to repress its transcription, contributing to apoptotic processes activation in different types of human cancer cell lines[156]. For this reason, c-Myc-mediated regulation of c-FLIP transcription has been proposed as a potential therapeutic strategy for cancer treatment[131].

- *Post-transcriptional regulation*. In general, c-FLIP proteins have a short half-life (30 minutes for c-FLIP$_S$, 3 hours for c-FLIP$_L$) and their degradation involves the ubiquitin-proteasome system (UPS)[131]. Both c-FLIP$_S$ and c-FLIP$_L$ share some C-terminal amino acid residues which can be ubiquitinated, regulating their turnover via UPS[131]. Although these residues are shared, the effect on c-FLIP stability is not the same in the different splice forms, showing a major degradation susceptibility of c-FLIP$_S$ compared to c-FLIP$_L$[131]. Another molecule involved in regulating c-FLIP degradation is TRAF2, that has an E3-ubiquitin ligase function. A multi-protein cytosolic complex termed the FADDosome regulates a p53/ATR/Caspase 10-and TRAF2-dependent cell death mechanism relying on the ubiquitination of FLIP leading to its degradation, caspase-8 activation and cell autonomous apoptosis[131]. ITCH is another E3-ubiquitin ligase which is activated by c-Jun N-terminal kinase (JNK)-mediated phosphorylation and, in the context of hepatitis, has been observed to interact directly and ubiquitinate c-FLIP$_L$, allowing its degradation and sensitization of cells to TNF-α-induced cell death and DNA damage in hepatocytes[157]. These findings suggested that the pro-apoptotic function of JNK could antagonize NF-κB pro-survival signaling, since both are downstream of TNF-α signal.

2.4. c-FLIP in cancer and as therapeutic target for oncology treatment

FLIP has been shown to be over-expressed in several cancer types, including non-small-cell lung cancer (NSCLC)[158], colorectal cancer (CRC)[159], pancreatic cancer[160], stomach cancer[161], urothelial cancer [162], prostate cancer[163], acute myeloid leukaemia[164], cervical carcinomas[165], and breast cancer[160]. c-FLIP over-expression

is associated with an increased resistance to apoptosis mediated by Fas and TRAIL, and studies have demonstrated that in some tissue types high levels of c-FLIP expression correlate with a more aggressive tumour[166]. In most cases, c-FLIP$_L$ represents the most over-expressed isoform in malignancy, however some studies[167] show that also c-FLIP$_S$ upregulation is involved in the tumorigenesis[168]. Over-expression of c-FLIP$_S$, but not c-FLIP$_L$, was reported in human tissues of lung adenocarcinoma[169]. In a cohort of 184 NSCLC patients, it was also recently found that high cytoplasmic but not nuclear c-FLIP levels significantly correlated with a ≥2-fold decrease in overall survival[158]. Simultaneous down-regulation of c-FLIP$_L$ and c-FLIP$_S$, as well as knockdown of either isoform by RNA interference, significantly enhances TRAIL and CD95-induced caspase activation and caspase-dependent apoptosis in pancreatic intraepithelial neoplasm lesions and in pancreatic ductal adenocarcinomas[160]. Several studies have observed the ability of c-FLIP in conferring resistance to many chemotherapeutic agents[131]. It has been demonstrated that c-FLIP over-expression confers resistance to apoptosis induced by 5-Fluorouracil and oxaliplatin in H630 and RKO colon cancer cells[170]. In addition, it has also been shown that c-FLIP can induce adaptive resistance mechanism to molecules that do not directly engage the apoptosis machinery, such as MEK inhibitors (MEKi) used for CRC treatment[171]. Therefore, c-FLIP could represent an important adverse prognostic indicator and clinical marker of drug resistance. The ability of c-FLIP to induce a resistance to multiple anticancer drugs[170,172,173], highlights c-FLIP as a critical target for therapeutic intervention. It has been suggested that targeting c-FLIP, both c-FLIP$_L$ and c-FLIP$_S$ isoforms, could sensitize cancer cells to chemotherapy in order to maximize clinical benefit of conventional therapy for the treatment of several cancers[170,174]. Small molecules that selectively down-regulate c-FLIP$_S$ or c-FLIP$_L$ and gene therapy strategies that knock down a specific c-FLIP variant have been used to down-regulate these isoforms. c-FLIP isoforms can be inhibited by compounds that inhibit their transcription or translation, trigger their degradation, which sensitize a wide range of cancer cell types to apoptosis. Pre-treatment with DNA damaging drugs such as cisplatin, 5-FU, oxaliplatin, doxorubicin and camptothecin is effective in inducing the down-regulation of c-FLIP isoforms in various tumor cells by inhibiting its transcription

and rendering cells sensitive to death receptor-triggered apoptosis[170,175,176]. In addition, histone deacetylase inhibitor (HDACi) compounds have been shown to down-regulate c-FLIP expression in various cancer cells both at the transcriptional and translational levels[177] and a number of agents that modulate Akt, PI3K, NF-κB, and Ras pathways, as well as an inhibitor of STAT3, have also been shown to transcriptionally silence c-FLIP expression[178].

Longley's group identified selective inhibitors of the FLIP-FADD protein-protein interaction (PPI). They found a druggable cleft on the surface of the DED2 domain of FLIP. This cleft is considered a key element of the FLIP-FADD protein-protein interaction (PPI) since it favors the binding of FLIP with an α-helix of FADD. The inhibitors identified by Longley's group, by inhibiting the PPI, are able to void the binding of FLIP to procaspase-8. Treatment with FLIP inhibitors in A549 NSCLC (lung carcinoma, epithelial-like, human cell line) murine xenograft has revealed an increase of apoptosis sensitivity of tumor cell and it has reported the decrease of tumor volume in the cancer murine model[131].

2.5. c-FLIP in monocytic subset of MDSCs

c-FLIP has reported to regulate tumor progression not only by inhibiting cancer cells apoptosis, but also by influencing the functional activity of immune system cells. In keeping with an important role for c-FLIP in favouring local immunosuppressive tumor microenvironment[131], c-FLIP has recently been shown to be critically important in maintaining FoxP3$^+$ Tregs[179] . Importantly, in DCs, loss of c-FLIP was shown to induce higher MHC II expression on the cell surface, increased IL-2, GMCSF and TNF-α expression and enhanced T-cell activation[180]. Even in the peripheral sites (i.e. outside the lymph nodes), c-FLIP seems to play an important role in the maintenance of an immunosuppressive milieu[131]. More interestingly, our research group has recently shown the critical role of c-FLIP in monocytic MDSCs subset. We reported that the percentage of circulating CD14$^+$ c-FLIP$^+$ cells significantly increased in cancer condition and especially in pancreatic ductal adenocarcinoma (PDAC) patients[66]. Moreover, our laboratory unveiled that not only c-FLIP favours the survival of this subset by inhibiting of extrinsic

apoptosis pathway, but also mediates its immunosuppression mechanisms. Fiore *et al.*[66] have demonstrated a direct role mediated by c-FLIP in triggering immunosuppressive properties in human monocytes isolated from HDs, which in physiological condition do not display any immunosuppressive activity. Indeed, the enforced over-expression of c-FLIP was able to activate in HDs monocytes the ability to inhibit T cell activation and induced the upregulation of many genes typical of M-MDSCs signatures and responsible for their immunosuppressive activity, such as STAT3, IL-6, IDO1 and PD-L1 (**Figure 9**)[66].

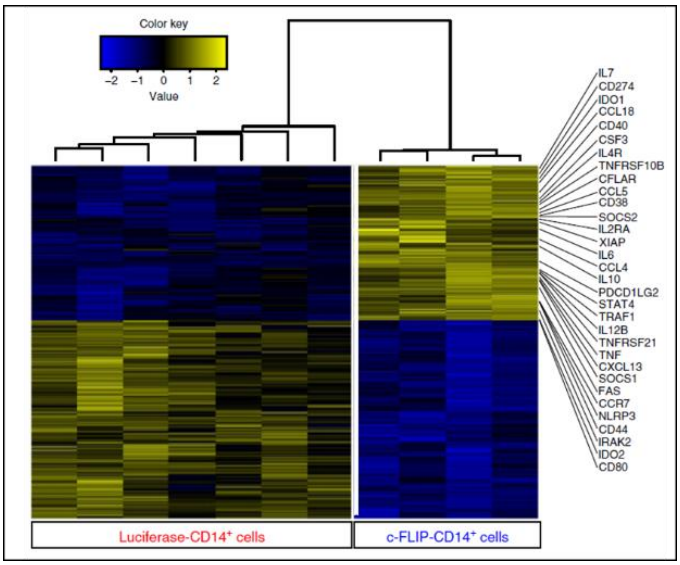

Figure 9. Transcriptome analysis of c-FLIP-infected $CD14^+$ cells isolated from HDs compared to luciferase-infected ones used as control. This image is adapted from[66]

Gene set enrichment analysis (GSEA), performed on c-FLIP-over-expressed $CD14^+$ cells isolated form HDs, revealed several signaling pathways modulated by c-FLIP over-expression (**Figure 10**[66]). Among them, genes upregulated by IL-6 via STAT3 and several genes belonging to NF-κB pathway in response to TNF-α resulted enriched, confirming the crucial role of such pathways, c-FLIP-induced, in controlling an immunosuppressive program in monocytes[66].

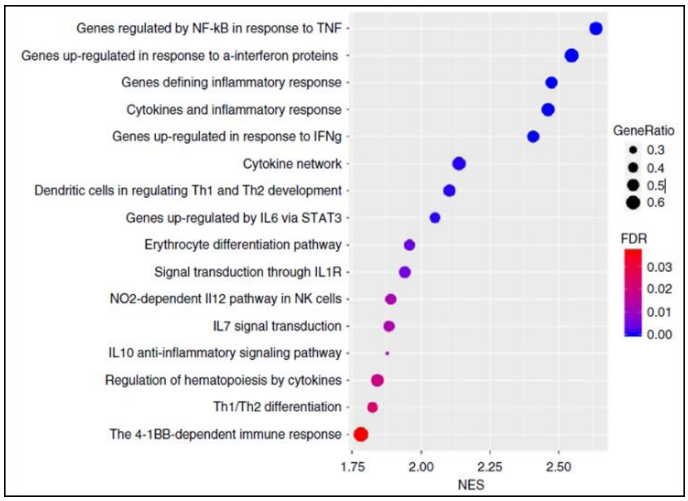

Figure 10. Signaling pathways up-regulated by c-FLIP over-expression in c-FLIP-infected $CD14^+$ cells evaluated by GSEA. This image is adapted from[66]

Give the key role of c-FLIP in different pathological settings, we will deeply investigate the involvement of c-FLIP in two types of immune dysregulation, tumor setting (lung cancer), and infectious disease (SARS-CoV-2 infection).

3. Lung Cancer (LC), MDSCs and therapeutical treatments

3.1. Lung Cancer (LC) and staging

Lung cancer (LC) represents the second most diagnosed cancer (11.6% of all cancer cases) and the leading cause of cancer death in the world (18.4% of all cancer deaths). According to the 2015 World Health Organization (WHO) Classification of Lung Tumors[181], the main types of epithelial lung cancer include adenocarcinomas, squamous cell carcinomas and neuroendocrine tumors. Next to epithelial tumors, mesenchymal, lymphohistiocytic and tumors of ectopic origins can also affect the lung, but they are generally less common. Malignant neoplasms of the lung can be divided into Small Cell Lung Cancer (SCLC) and NSCLC. The former is a specific subtype belonging to neuroendocrine tumors, while the latter includes both adenocarcinomas and squamous cell carcinomas, along with the rarer large cell carcinoma[182]. NSCLC constitutes 85% of the overall LC and comprises a

variety of neoplasms such as adenocarcinoma (ADC), squamous cell carcinoma (SCC), large cell carcinoma (LCC), and other less-differentiated variants. ADC is the most prevalent type of NSCLC[183] followed by SCC and LCC. NSCLC is often only diagnosed in patients with locally advanced or metastatic disease and is poorly responsive to chemotherapy. Despite tremendous advances in LC treatment, the overall survival (OS) of LC patients remains poor, with a 5-year survival rate of 18%, the lowest of all malignancies[184].

The eight editions of TNM classification, published in 2017, is currently used for the LC staging. The three key components used to describe the anatomic extent of a tumor and subsequently determine the cancer stage are T for the extent of the primary tumor, N for lymph node involvement, and M for distant metastasis (**Table 2**)[185].

Table 2: TNM classification of LC. TX, NX: T or N status not able to be assessed[185]

T (Primary Tumor)	
T0	No primary tumor
Tis	Carcinoma in situ
T1	Tumor ≤3 cm
T1a(mi)	Minimally Invasive Adenocarcinoma
T1a	Tumor ≤1cm
T1b	Tumor >1 but ≤2cm
T1c	Tumor >2 but ≤3 cm
T2	Tumor >3 but ≤5cm or tumor involving visceral pleura, main bronchus, atelectasis to hilum
T2a	Tumor >3 but ≤4cm
T2b	Tumor >4 but ≤5cm
T3	Tumor <5 but ≤7cm or tumor invading chest wall, pericardium, phrenic nerve, or separate tumor nodule(s) in the same lobe
T4	Tumor >7cm or tumor invading mediastinum, diaphragm, heart, great vessels, recurrent laryngeal nerve, carina, trachea, esophagus, spine, or tumor nodule(s) in a different ipsilateral lobe
N (Regional Lymph Nodes)	
N0	No regional node metastasis
N1	Metastasis in ipsilateral pulmonary or hilar nodes
N2	Metastasis in ipsilateral mediastinal/subcarinal nodes
N3	Metastasis in contralateral, mediastinal/hilar, or supraclavicular nodes
M (Distant Metastasis)	
M0	No distant metastasis

M1a	Malignant pleural/pericardial effusion or pleural/pericardial nodules or separate tumor nodules in a contralateral lobe
M1b	Single extrathoracic metastasis
M1c	Multiple extrathoracic metastases (1 or >1 organ)

By combining each parameter's value, lung cancer is classified into four stage groups (**Table 3**)[186]. In this classification, stage IV consists of all metastatic tumors (M1). According to the current Italian guidelines for lung cancer treatment, IIIC stage patients are considered locally advanced and non-resectable, whereas IIIA and IIIB stages include both patients with a respectable or non-resectable disease based on lymph nodes status[187].

T/M	Subcategory	N0	N1	N2	N3
T1	T1a	IA1	IIB	IIIA	IIIB
	T1b	IA2	IIB	IIIA	IIIB
	T1c	IA3	IIB	IIIA	IIIB
T2	T2a	IB	IIB	IIIA	IIIB
	T2b	IIA	IIB	IIIA	IIIB
T3	T3	IIB	IIIA	IIIB	IIIC
T4	T4	IIIA	IIIA	IIIB	IIIC
M1	M1a	IVA	IVA	IVA	IVA
	M1b	IVA	IVA	IVA	IVA
	M1c	IVB	IVB	IVB	IVB

Table 3: Stage grouping of lung cancer[186]

3.2. MDSCs and Lung Cancer (LC)

In patients with NSCLC it has been reported that MDSCs can inhibit T cell activity, enhance immunosuppression, and accelerate tumor progression through arginase, ROS, and the IL-13/IL-4R axis[184]. Li *et al.*[188] showed that patients suffered from brain metastasis had an expansion of peripheral MDSCs and Tregs population and an increase of PD-L1 expression compared to pre-metastatic LC. Lee *et al.*[189] found that, using a transgenic LC mouse model, PD-L1 was highly expressed in both tumoral cells and MDSCs, thus confirming that MDSCs played an important role in promoting LC development. Li *et al.*[42] also showed that tumor-induced HIF-1α activation upon hypoxia or TGF-β induction is able to stimulate CD39/CD73 ectonucleotides' expression in MDSCs in NSCLC patients. CD39 and CD73 can

produce adenosine inhibiting the antitumor activity of NK cells and effector T cells, so promoting further the escape of tumor cells from cytotoxic T cell responses. Furthermore, MDSCs in lung cancer can also promote tumor angiogenesis and metastasis by producing VEGF, MMPs and exosomes. A growing number of studies have demonstrated that MDSC-released exosomes have a role in immunosuppression and, interestingly, exosomes from tumor cells also contribute to the function of MDSCs[98]. Moreover, the expression of PD-L1 in MDSCs could be increased after tumor-derived exosomes were transferred from tumor cells to MDSCs in glioma and LC tumor models. This expression was related to the increased expression of ARG1 in MDSCs, the production of TGF-β, and the strengthened immunosuppressive activity of these cells[190].

In detail, some studies clearly showed the PMN-MDSCs and M-MDSCs subsets involvement in the LC progression. A significant increase in the frequency of circulating M-MDSCs was observed in the NSCLC patients compared with HDs. It has also been reported that the frequencies of PMN-MDSCs and M-MDSCs were higher in the tumor tissue than in the peripheral blood of the same patients[191]. This accumulation was associated with elevated concentrations of inflammatory mediators (i.e.CCL2, CCL3, CCL4, CCL5, IL-8, and CXCL10) involved in MDSC migration to and activation in the TME. The frequency of CCR5 expression on circulating M-MDSCs was significantly higher in the patients than in the HDs. Moreover, an analysis performed on MDSC immunosuppressive pattern showed that tumor PMN-MDSCs displayed higher PD-L1 expression levels than the same cell type in the peripheral blood in NSCLC patients[191].

As described in other cancer settings, several clinical studies have been reported that high levels of MDSCs in LC patients were associated with chemotherapy and immunotherapy resistance and thereby with a poor prognosis (**Table 4**[192]).

Table 4. Clinical significance of different MDSCs phenotypes in NSCLC - (PB=peripheral blood; TT=tumor tissue; PR=partial response; SD=stable disease; PD=progressive disease; PFS=progress free survival; RFS=recurrence free survival; OS=overall survival)[192]

Phenotype (*MDSC*)	**PB/ TT**	**No. of patients**	**Implications**
$CD11b^{+}$ $CD14^{-}$ $CD15^{+}$ $CD33^{+}$	PB	41	Decreased in the advanced-stage patients who had clinical benefit (PR or SD) and in the early-stage patients after removal of tumor.
$CD11b^{+}$ $CD14^{+}$ $S100A9^{+}$	PB	24	Poor chemotherapy response and short PFS
$CD16^{low}$ $CD11b^{+}$ $CD14^{-}$ HLA-DR^{-} $CD15^{+}$ $CD33^{+}$	PB	185	Significantly increased compared to healthy controls
$CD14^{+}$ HLA-$DR^{-/low}$	PB	60	Negatively correlated with PFS
$B7^{-}$ $H3^{+}$ $CD14^{+}$ HLA-$DR^{-/low}$	PB	111	Decreased RFS
$CD11b^{+}$ $CD14^{-}$ HLA-DR^{-} $CD33^{+}$ $CD15^{+}$ $ILT3^{high}$	PB	105	Decreased OS
PMN-MDSCs; lin^{-} $CD14^{-}$ $CD11b^{+}$ $CD39^{+}$/$CD73^{+}$ *M-MDSCs*: lin^{-} $CD14^{+}$ $CD11b^{+}$ $CD39^{+}$/$CD73^{+}$	PB	24	Decreased with chemotherapy cycles in SD and PR groups, increased in PD group.
Lin^{-} $CD14^{+}$ $CD15^{+}$ $CD11b^{+}$ $CD33^{+}$ HLA-DR^{-}	PB	110	Independent prognostic marker for decreased PFS and OS.
Lin^{-} $CD14^{-}$ HLA-DR^{-}	PB	46	After three cycles, bevacizumab-based chemotherapy significantly reduced the level of $Lin^{-}CD14^{-}HLA\text{-}DR^{-}$ cells.
Lox-1^{+} *PMN-MDSCs*	PB	34	Patients with a higher ratio of Tregs to Lox-1^{+}PMN-MDSCs in the blood after the 1^{st} nivolumab had better PFS.

Lin^- $CD33^+$ $CD14^+$ $CD15^-$ $HLA\text{-}DR^-$	PB	61	Decreased OS in anti-PD-1 treatment.
SSC^{low} Lin^- $HLA\text{-}DR^{-/low}$ $CD33^+$ $CD13^+$ $CD11b^+$ $CD15^+$ $CD14^-$	PB	53	PMN-MDSCs (≥6 cell/µl) showed a significan-tly improved survival in anti-PD-1 treatment.
PMN-MDSCs: $CD33^+$ $CD11b^+$ $CD14^-$ *M-MDSCs*: $CD33^+$ $CD11b^+$ $CD14^+$ $HLA\text{-}DR^{-/low}$	PB	7	Both subtypes decreased after SBRT treatment.
PMN-MDSCs: $CD11b^+$ $HLA\text{-}DR^{-/low}$ $CD14^-$ $CD15^+$ *M-MDSCs*: $CCR5^+$ $HLA\text{-}DR^{-/low}$ $CD11b^+$ $CD14^+$ $CD15^-$	PB and TT	42	TT PMN-MDSCs displayed higher PD-L1 expression levels than the same cells in the PB. Significant correlations between lower total PMN-MDSCs and $CCR5^+$ M-MDSCs frequencies in the peripheral blood and improved RFS.

Studies revealed that increased levels of PMN-MDSCs in NSCLC treatment naïve patients, compared to HDs, reported a decrease after treatment in patients responsive. Nevertheless, high levels of $CD11b^+$ $CD14^+$ $S100A9^+$ M-MDSCs were associated with a poor response to cisplatin-based chemotherapy and predicted shortened progress free-survival (PFS). Further analysis revealed that the percentage of $CD39^+CD73^+$ MDSCs was decreased with increasing numbers of chemotherapy cycles in the stable disease (SD) and partial response (PR) groups, whereas there was a trend toward an increase in the percentage of $CD39^+CD73^+$ MDSCs in the progressive disease (PD) group. These data suggested that the ectoenzymatic activities of CD39 and CD73 are required for MDSC-mediated suppressive and tumor chemoprotective effects[39] and that the changes in $CD39^+CD73^+$ MDSC frequency in NSCLC patients could be used for predicting chemotherapeutic response.

It is also relevant to underline the role of MDSCs in LC resistance to immune checkpoint inhibitors (ICIs; T cell targeted immunomodulators blocking the

immune checkpoints PD-1/PDL-1 axis and CTLA-4) which are the most relevant novel immunotherapy extensively studied and used in LC treatment. Many studies have reported that in patients suffering from LC, levels of MDSCs, which are characterized by elevated PD-L1 expression, are associated with response of patients to anti-PD-1 therapy[193,194]. Thus, targeting MDSCs has the potential to increase anti-PD-1 efficacy. Studies by Li *et al.*[195] provided preclinical evidence that anti-PD1 resistance in LC was associated with over-expression of IDO1 in $F4/80^{+}Gr1^{int}CD11b^{+}$ MDSCs. Thus, IDO1 inhibition represents another immunotherapeutic strategy to overcome immunosuppression in anti-PD-1 therapy-resistant tumors. Moreover, Feng *et al.* showed that although both $CD11b^{+}CD14^{+}$ and $CD11b^{+}CD14^{-}$ cell populations are expanded in NSCLC patients, only $CD11b^{+}CD14^{+}$ MDSC numbers were associated with treatment response, thereby concluding that monocytic MDSCs are the most relevant subgroup when it comes to NSCLC[184].

Therefore, there is increasing evidence that MDSCs are involved in the development of LC and may be used to predict the efficacy of immune checkpoint blockade treatment, but there are still a wide range of unknown mechanisms and interactions that require further research within this topic. Several findings suggest that targeting MDSCs and their molecular immunosuppressive mechanisms may be a promising strategy to use in combination with existing immunotherapeutic strategies, such as boosting the immune system by vaccination or immune checkpoint inhibition. Using these strategies to treat LC may produce more breakthroughs that overcome current treatment limitations. However, these findings still require more solid research before clinical translation. Firstly, unlike other immunosuppressive cells (i.e., Treg cells and TAMs), MDSCs do not have a uniform molecular phenotype. Secondly, the results for the relationships between different MDSC subtypes and the prognosis of LC are not consistent. For example, some studies suggest that elevated PMN-MDSC numbers are an indicator of a poor prognosis[192,196], while other studies show that M-MDSCs have a better prognostic value than PMN-MDSCs[134,194]. Thirdly, it is difficult to use the level of MDSCs in the peripheral blood to represent the distribution in tumor tissues, and the monitoring of their suppressive function is not predictable. Therefore, more in-

depth explorations of the MDSCs mechanisms in tumor tissues are still needed for LC patients.

3.3. Immune Checkpoint Inhibitors (ICIs) in NSCLC

For NSCLC-affected patients who are not eligible for local treatment, a molecular characterization of the tumor, for all stage IV and stage IIIC, has become essential to identify specific features of the disease and potential targets, which influence therapeutic options. Some markers are critical in the diagnostic workup of these advanced cancers. Current recommendations include the analysis of Epidermal Growth Factor Receptor (EGFR) mutations, Anaplastic Lymphoma Kinase (ALK) and c-Ros Oncogene 1 (ROS-1) rearrangements, BRAF-V600 mutations and PD-L1 expression levels. In patients harboring oncogene-addicted tumors, guidelines recommend the treatment with molecular targeted therapy (i.e., tyrosine-kinase inhibitors TKIs) as first-line treatment. In the case of disease progression, further lines of treatment consist of other TKIs or platinum-based chemotherapy[197]. For patients who do not present any of these mutations or rearrangements, the analysis of PD-L1 expression becomes central. Its levels are used to evaluate the possibility and modality of using immunotherapeutic drugs, specifically PD-1 inhibitor pembrolizumab, in treating NSCLCs that test negative for the other four markers mentioned above[197]. PD-L1 is expressed by a percentage of NSCLC tumor cells that ranges between 24 and 60%[198]. PD-L1 expression levels are assessed on samples containing a minimum of 100 cells through immunohistochemistry (IHC) and validated antibodies; the results are expressed as a percentage according to the Tumor Proportion Score (TPS). This score is calculated by considering the proportion of neoplastic cells which express, even if only partially, PD-L1 on their membrane[198].

Targeting negative regulators of the immune response, known as immune checkpoints, has transformed the treatment for many cancers[199]. Several immune checkpoint molecules including PD-1, CTLA-4, LAG-3, and TIM-3 are expressed upon T-cell activation. The activity of CTLA-4 and the PD-1 immune checkpoints is well known in NSCLC patients and their action mechanisms (**Figure 11**)[199] are

the most studied in this lung tumor context. CTLA-4 is typically expressed on $CD4^+$ and $CD8^+$ T lymphocytes and provides an early inhibitory signal that regulates the immunological synapse between T cells and dendritic cells in lymph nodes, thereby suppressing T-cell activation[199]. Indeed, T-cell activation requires antigen presentation by MHC class II molecules on APCs and a second activation signal that can be blocked by CTLA-4 binding with CD80 or CD86[200]. Mechanisms engaged in PD-1/PD-L1 axis, between T cells and tumour cells in the tumour microenvironment, hamper immune rejection or the effector phase promoting T-cell apoptosis. PD-1 and PD-L1 are currently the most relevant targets for LC immunotherapy[198]. It was reported that the expression of PD-L1 is up-regulated in NSCLC cells and causes T cells suppression[199] .

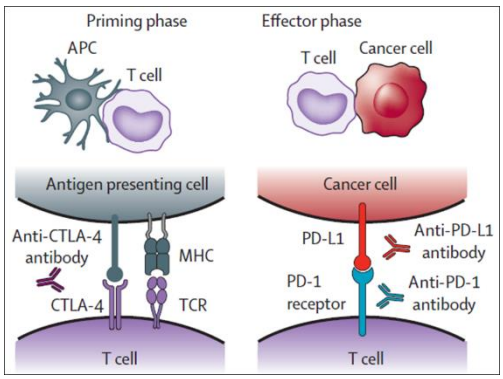

Figure 11. Mechanisms of Immune Checkpoint Inhibitors CTLA-4 and PD-1. This image is adapted from[199]

ICIs are monoclonal antibodies that target CTLA-4, PD-1 and PD-L1. Anti-CTLA-4 antibodies inhibit the CTLA-4 binding with CD80 or CD86 costimulatory molecules, avoiding a negative regulatory signal. Whereas anti-PD-1 and anti-PD-L1 antibodies inhibit T-cell apoptosis interfering with PD-1-PD-L1 axis. NSCLC was thought to be poorly immunogenic, but treatment with anti-PD-1 and anti-PD-L1 antibodies consistently showed superior patient survival compared with second line chemotherapy and has emerged as important immunotherapy in patients with treatment-naïve NSCLC (**Figure 12**)[199].

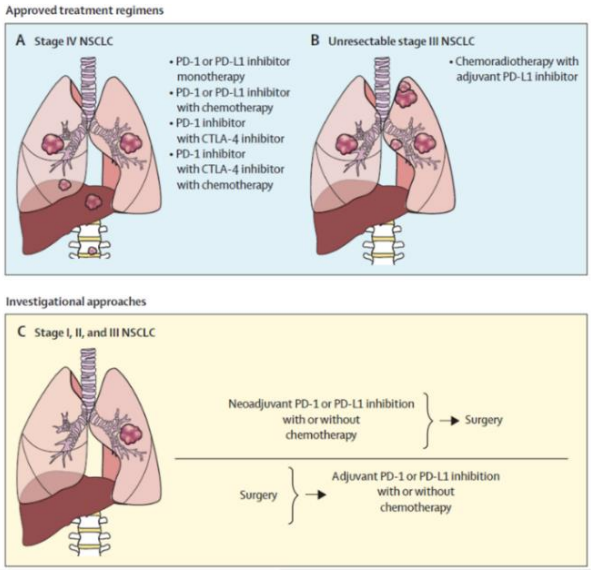

Figure 12. Different approaches of immunotherapy treatment in NSCLC according to different severity stage. This image is adapted from[199]

Several pre-clinical studies and clinical trials have evaluated the role of immune checkpoints. Among them, tremelimumab and ipilimumab (CTLA-4 blockers), pembrolizumab, nivolumab and cemiplimab (PD-1 blockers), and durvalumab, avelumab, and atezolizumab (PD-L1 blockers) have been developed and approved for lung and other cancers treatment[201]. Numerous trials have revealed a correlation between the NSCLC tissue expression of PD-L1 and the efficacy of the treatment. Moreover, since PD-L1 expression in NSCLC was associated with poor prognosis[202,203] many clinical trials, which provide anti-PD-1 and anti-PD-L1 monotherapy, were defined with tumour PD-L1 expression as a predictive biomarker (**Figure 13**)[199].

Two clinical trials compared the efficacy of atezolizumab (IMpower110)[204] or pembrolizumab (KEYNOTE-042)[205] treatment to chemotherapy effects in NSCLC patients with tumor expression of PD-L1≥1%. Survival benefit was mainly observed in the ICIs groups in patients with tumor expression of PD-L1≥50%, and higher frequency of side effects was reported in chemotherapy-treated patients (41–53% vs. 13–27% in ICIs-treated patients)[205]. On the other hand, studies investigating nivolumab and durvalumab treatment as first-line in NSCLC patients did not show a survival benefit compared with chemotherapy treatment[206].

Checkmate-227 clinical trial[207] has studied the efficacy of dual immunotherapy compared to monotherapy in patients with advanced NSCLC. First-line combinatory treatment with nivolumab plus ipilimumab reported a longer duration of OS than did monotherapy, independent of the PD-L1 expression levels. Up to the 2019 guidelines, PD-L1 expression level was used to establish which patients, among those with non-oncogene-addicted tumors, were eligible for immunotherapy with pembrolizumab in the first or second line of treatment. In the KEYNOTE 024 study[208,209], 305 patients affected by NSCLC were randomized to receive either pembrolizumab or platinum-based chemotherapy. Only tumors expressing at least 50% of PD-L1 could receive pembrolizumab as first-line treatment. For patients who did not meet this criterion, the alternative first-line treatment was represented by platinum-based chemotherapy, with or without bevacizumab, an anti-VEGF therapy. When it comes to second-line treatment, an expression level of at least 1% was needed to use pembrolizumab. Usage of other ICIs, namely Nivolumab and atezolizumab, was limited to second-line treatment in patients who had progressed after platinum-based chemotherapy. In this study, only the group who received pembrolizumab as first-line treatment, compared to the group undergone to chemotherapy, showed a better OS.

Likewise, the combination between ICIs and chemotherapy succeeded. In the phase 3 KEYNOTE-189[210] clinical trial performed in non-squamous NSCLC[210], the combination of pembrolizumab and platinum chemotherapy showed a longer median OS (22.0 months) compared to patients treated with chemotherapy alone (10.7 months). Improvements in OS of patients receiving combination treatment were reported for all subgroups classified according to PD-L1 tumor expression, including the subgroup with PD-L1<1%. Similar side effects were observed in both monotherapy and combinatory treatments. Starting from the guidelines published in the year 2020, indeed, the role of immunotherapy has changed significantly. ICIs are recommended earlier and in combination with platinum-based chemotherapy to treat some metastatic forms, even in patients with PD-L1 expression levels lower than 50%. In lung cancer patients with an expression level of 50% or greater, guidelines recommend a first-line treatment with pembrolizumab, and, in the case of disease progression, these patients receive chemotherapy as second-line

treatment. Moreover, patients affected by non-squamous carcinoma with a PD-L1 expression <50% and in good general conditions can receive pembrolizumab plus platinum-based chemotherapy (chemoimmunotherapy) as first-line treatment[211]. Patients with squamous cell cancer with PD-L1 expression level of 1-49%, receive platinum-based chemotherapy only as first-line treatment, and immunotherapy with pembrolizumab (PD-L1≥1%), nivolumab or atezolizumab as second-line treatment after a documented progression[212]. In 2021, Checkmate-9LA clinical trial has shown improved OS in patients with advanced NSCLC after dual immunotherapy combined with two cycles of platinum-doublet chemotherapy[213]. As expected, side effects were mainly observed in patients treated with combination therapy compared with the chemotherapy alone. The regimen proposed by Checkmate-9LA is now approved and indicated in several countries for first-line treatment of patients with metastatic or current NSCLC[199].

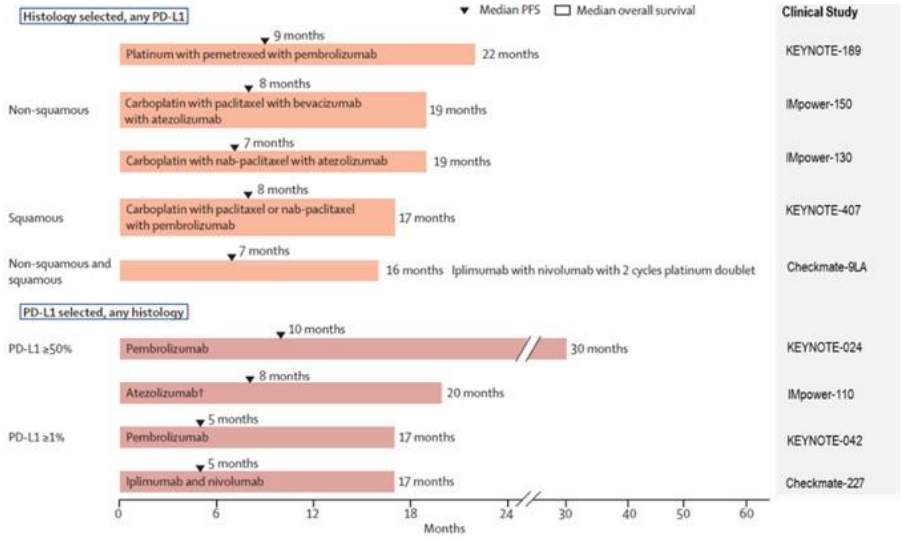

Figure 33. Approved therapies for upfront treatment for NSCLC. Chemo-immunotherapy regimens have been approved for squamous and non-squamous NSCLC, irrespective of PD-L1 expression. Single-agent immune checkpoint inhibitors and dual blockade with ipilimumab and nivolumab are approved based on tumor PD-L1 expression. This image is adapted from[199]

In conclusion all these data show that ICIs are important in the initial management of metastatic NSCLC. According to current guidelines (for patients enrolled within

2019)[148], pembrolizumab or atezolizumab monotherapy, can be used as first-line therapy in patients with tumour PD-L1 expression ≥50%,. For patients with tumour PD-L1 expression ≥1% (<50%), combinatory treatment with chemotherapy plus anti-PD-1 or anti-PD-L1 inhibitors is the standard approach.

Despite the clinical outcome improvement obtained with ICIs in NSCLC, many patients do not register benefit from immunotherapy. Moreover, although PD-L1 expression remains the only predictive biomarker used in daily clinical practice for patients affected by NSCLC, its expression in tumor cells is highly heterogeneous and it is far from an ideal marker. On the one hand, some patients with PD-L1 negative tumors respond to ICIs, and, on the other hand, a significant percentage of selected patients does not respond. There are many possible explanations, and they can be attributed to both technical and biological factors. Spatial and temporal PD-L1 expression heterogeneity is likely to be the most relevant factor. Its evaluation on a single biopsy specimen can lead to inaccurate results[214]. Moreover, there is a variation of PD-L1 expression over time. PD-L1 expression is regulated by different signaling pathways and can be modulated by several factors[215]. Among these factors, some chemotherapeutic agents may change PD-L1 expression levels[216]. Cavazzoni and colleagues demonstrated that pemetrexed increased PD-L1 levels in non-squamous NSCLC cell lines, thus giving a probable explanation to the positive results of the combination of pemetrexed-based chemotherapy and pembrolizumab even in PD-L1 negative NSCLC[217].
Therefore, the identification of further predictive biomarkers may help to anticipate treatment sensitivity or resistance of patients, reducing exposure to potential toxicity and obtaining a patient-specific therapy.

4. SARS-CoV-2 infection

Viruses have evolved a myriad of ways to escape host apoptotic process and thereby preserve infected cells from early death[218]. Several viruses including hepatitis C virus[219], hepatitis B virus[220], human T cell leukemia virus-1[221], human immunodeficiency virus 1[222], Epstein Barr Virus[223] and influenza A virus[224] induce the expression of the anti-apoptotic protein c-FLIP, which blocks caspase-mediated

cell death[132]. Kaposi's herpesvirus K13/vFLIP and the herpesvirus saimiri orf71 can encode proteins with high homology to c-FLIP, which harbor DED domains responsible for blocking procaspase cleavage, preventing apoptosis and favoring viral latency[225]. Thus, FLIP expression is not only linked to oncology or inflammatory conditions but also to viral replication by favoring the suppression of host cell death. In order to deepen the c-FLIP involvement in the viral infection, we put our attention on severe acute respiratory syndrome coronavirus-2 (SARS-CoV-2). This virus is responsible for the current world pandemic and its capacity to escape the host immune responses seem to be associated to c-FLIP expression induced in myeloid cells by virus in order to favor an immunosuppressive landscape.

4.1. SARS-CoV-2 infection: epidemiology, symptoms

Near the end of 2019 an unknown upper respiratory tract infection has spread worldwide. This infection was caused by a novel coronavirus SARS-CoV-2, with the disease being named COVID-19 (coronavirus disease 2019)[226]. By the beginning of March 2020, the World Health Organization (WHO) officially labeled the disease as a pandemic[227]. This infection originated from China, and within April 2020, it has affected 214 countries and territories, spreading extremely quickly[228]. There are over 264.300.000 cases worldwide of COVID-19 and over 5.248 million of deaths[229]. Although the origin of this pandemic is uncertain, it is widely believed that the disease spread from bats, which act as intermediate hosts between the virus and humans[230]. Additionally, there is a possibility that pangolins were the intermediate between bats and humans for SARS-CoV-2 transmission[231]. There is no evidence that this virus was made in a lab and the overwhelming evidence suggests a zoonotic shift from animals to humans[232].

SARS-CoV-2 is the seventh coronavirus to date that is known to infect humans[233]. Two of these previously identified coronaviruses were responsible for major epidemics in the past two decades; SARS-CoV, also originating from China in 2002–2003, and the Middle East Respiratory Syndrome Coronavirus (MERS-CoV), originating from the Middle East in 2012[234, 235]. All three of these coronaviruses are considered zoonotic in origin and have the ability to cause severe

and fatal illness in humans[235]. Unfortunately, given their large genetic diversity and the frequent recombination of their genomes coupled with the increase in human-animal interface activities due to modern agricultural practices, novel coronaviruses are likely to continue to develop and cause periodic seasonal spreads[235].

Symptoms caused by SARS-CoV-2 are similar to MERS and SARS, and include in over 80% of cases mild fever, dry cough, and shortness of breath. Severe cases displayed dyspnea in 44% of patients, hypoxia (oxygen depletion in body tissues) in about 50% of patients, and a high fever in around 14% of total patients[236, 237]. 5% of the severe cases are reported as critical disease with respiratory failure, shock, and/or multi-organ failure[238]. There are two main clinical symptoms that appear for critically ill patients with COVID-19: low levels of oxygen due to poor breathing (Acute Respiratory Distress Syndrome, ARDS) and fever[239]. Asymptomatic infection was mainly found in young patients between 18 and 29 years of age[240]. A study involving 634 patients infected with COVID-19 on a cruise ship in Japan found that 17.9% were asymptomatic[241]. The majority of patients with SARS-CoV-2 infection have been found to start with mild symptoms and, during the course of a week, progress to moderate or severe disease. A study done in Wuhan showed that, in the majority of patients, the median time to the development of dyspnea was 5 days, to hospital admission was 7 days, and to the development of ARDS was 8 days from the start of illness[242].

4.2. Structure and viral transmission of SARS-CoV-2 virus

Coronaviruses are enveloped, positive single-stranded RNAs viruses with the largest known RNA genome ranging from 26 to 32 kilobases in length[243]. They are spherical virions with a core shell and a surface that resembles a solar corona based on its surface protein projections[243]. There are four main subfamilies: α-, β-, γ- and Δ- coronaviruses. α- and β-coronaviruses originate from mammals, mainly bats, and are thought to cause more severe and fatal diseases in humans, while γ- and Δ-viruses mainly originate from birds and pigs and are thought to cause asymptomatic or mild disease in humans[244]. SARS-CoV-2 belongs to the β-coronavirus group, which also includes MERS-CoV and SARS-CoV. The latter shares 75–80% of its viral genome with SARS-CoV-2[243]. β-coronaviruses have three important envelope

proteins: Spike (S) protein, Membrane (M) protein, and Envelope (E) protein. S protein mediates viral attachment to the cell membrane receptor, membrane fusion, and ultimately viral entry into the host cell. M protein, the most abundant membrane protein, together with E protein are responsible for the coronavirus membrane structure. Another component of the β-coronavirus is the N protein, which is the protein component of the helical nucleocapsid that includes the genome RNA (**Figure 14**)[245].

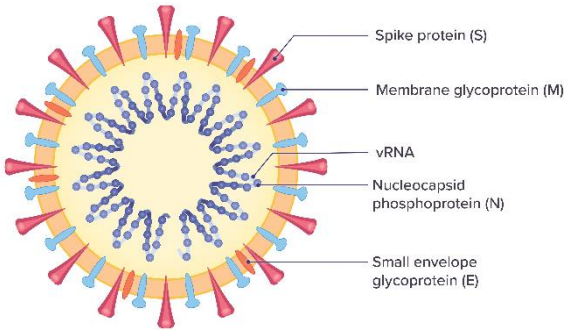

Figure 44. Viral structure of SARS-CoV-2 with its protein components and viral RNA (vRNA). This image is adapted from[245]

According to current evidence, the WHO reports that SARSCoV-2 transmission occurs via respiratory droplets and contact routes. Droplet transmission occurs through direct contact within 1m from someone with respiratory symptoms including coughing and sneezing. Airborne transmission may be possible when aerosol-generating procedures are performed including endotracheal intubation, cardiopulmonary resuscitation, administration of nebulized treatments, and others. Transmission can also occur through indirect contact by way of fomites on surfaces in the immediate environment around the infected person[246]. Transmission of the virus can occur in the pre-symptomatic incubation period. A study showed that people who resulted positive for SARS-CoV-2 infection and most likely contributed to transmission were pre-symptomatic (pre-symptomatic patients were defined those who were asymptomatic at the time of symptoms assessment but developed symptoms within 7 days after evaluation)[247]. COVID-19 is significantly more infectious than SARS and MERS in terms of human-to-human transmission, causing the number of cases to skyrocket and outweigh both MERS and SARS[248].

4.3. Viral replication cycle of SARS-CoV-2 and host immune responses

SARS-CoV-2 binds to epithelial cells in the oral and nasal cavities and can also migrate further down the respiratory tract into the conducting airways. SARS-CoV has been shown to infect primary ciliated cells in the conducting airway and therefore, it has been hypothesized that the same occurs with SARS-CoV-2. The virus can progress even further and can infect the alveolar type II pneumocyte cells, similar to SARS-CoV, causing cell apoptosis. Type II pneumocyte cells normally comprise 10–15% of total lung cells. They produce surfactant, which is responsible for the maintenance of surface tension in alveolar walls. These cells are also responsible for maintaining the lung epithelium after injury through epithelial regeneration[244]. Therefore, as replicated viral particles are released from the cell and move on to infect more type II pneumocytes, the resulting apoptosis eventually causes diffuse alveolar damage and impaired gas exchange, which is hypothesized to lead to ARDS[249] (**Figure 15[250]**). SARS-CoV-2 has been shown to use the angiotensin-converting enzyme 2 (ACE2) receptor for cell entry. ACE2 receptors have been found in various organs and cells including the nasopharynx, nasal and oral mucosa, small intestine, colon, kidney, liver, vascular endothelium, and epithelial cells of lung alveoli[251]. The receptor binding domain (RBD) in the S protein of SARS-CoV-2 specifically recognizes its host ACE2 receptor. It is thought that a genetic recombination event in the RBD region of SARS-CoV-2 may be the cause of its higher transmission rate as compared to SARS-CoV[252]. After cell entry, the viral RNA positive sense genome is released into the cell cytoplasm and undergoes translation and replication forming progeny genomes and sub-genomic mRNAs. The latter translates into membrane proteins, N protein, and a variety of accessory proteins[245]. The formed membrane proteins (S, M, and E) are then inserted into the rough endoplasmic reticulum (RER) and are transported to the endoplasmic reticulum-Golgi intermediate compartment (ERGIC). N proteins along with genomic RNA then form nucleocapsids, which fuse into the ERGIC. Finally, the pathogen gets transported to the plasma membrane and is exported out of the cell via exocytosis[245] (**Figure 15[250]**). When the virus enters the cell, its antigen is presented by the antigen-presenting cells (APCs) such as dendritic cells

and macrophages. SARS-CoV mainly depends on MHC I molecules[253]. The antigen presentation leads to the activation of the body's humoral and cellular immunities, which are mediated by virus specific B and T cells[254]. The innate immune response increases within a couple of hours of infection limiting viral replication, recruiting effector cells that eventually will limit viral load and prime the adaptive response of T- and B-cells[255]. Within a week, $CD4^+$ and $CD8^+$ virus-specific T-cells with effector functions arise[256]; $CD4^+$ T cells are crucial to control primary SARS-CoV-2 infection, activate B lymphocytes and allow the generation of plasma cells, which will produce antibodies after 10-15 days[256, 257]. It is essential that B and T cells work together to clear rapidly and specifically the viral-infected cells and circulating virions. Once $CD4^+$T cells are activated, they cause the release of cytokines and chemokines. If exaggerated, this leads to the development of cytokine storm syndrome[253].

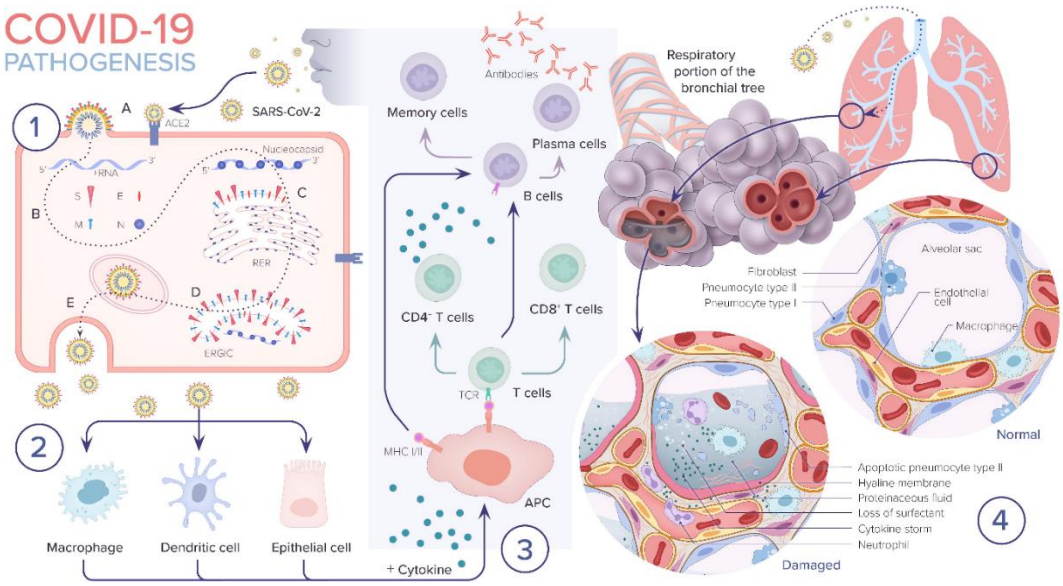

Figure 15. COVID-19 pathogenesis. 1. A. SARS-CoV-2 enters the epithelial cell either via endocytosis or by membrane fusion through binding to ACE2 receptor and releasing its RNA into the cytoplasm. B. Viral RNA uses the cell's machinery to translate its viral non-structural and structural proteins and replicate its RNA. C. Viral structural proteins S, E, and M assemble in the rough endoplasmic reticulum (RER). D. Viral structures and nucleocapsid subsequently assemble in the endoplasmic reticulum Golgi intermediate (ERGIC). E. New virion packed in Golgi vesicles fuse with the plasma membrane and get released via exocytosis. 2. SARS-CoV-2 infection induces inflammatory factors that lead

to activation of macrophages and dendritic cells. 3. Antigen presentation of SARS-CoV-2 via major histocompatibility complexes I and II (MHC I and II) stimulates humoral and cellular immunity resulting in cytokine and antibody production. 4. In severe COVID-19 cases, the virus reaches the lower respiratory tract and infects type II pneumocytes leading to apoptosis and loss of surfactant. The influx of macrophages and neutrophils induces a cytokine storm. Leaky capillaries lead to alveolar edema. Hyaline membrane is formed. All of these pathological changes result in alveolar damage and collapse, impairing gas exchange. This image is adapted from[250]

4.4. The immunopathological background

The high viral burden in COVID-19 patients is likely to be associated with low ability to mount a "harmonized" immune response and with alterations in immune cell composition involving both innate and adaptive immunity, and within the adaptive response, both T- and B-cell compartments[258, 259] (**Figure 16**[250]).

Monocyte-macrophages. Airway macrophages and monocytes exhibit hyper-inflammatory signatures, producing chemokines such as CCL2 and CCL3, while the blood counterpart contain aberrant $CD14^{+}$ $CD16^{+}CD163^{hi}$ $HLA\text{-}DR^{lo}$ monocytes expressing the chemokine receptor CCR2 and secreting IL-6[260, 261]. Thus, through a feed forward-loop mediated by CCL2/CCR2 axis, aberrant monocytes from the blood infiltrate the alveolar spaces, perpetuating tissue inflammation and damage. Monocyte-derived alveolar macrophages expressing CD163 (with a gene signature recalling M1-like macrophages) and CD206, productively infected by SARS-CoV-2, contribute to propagate the inflammatory status in severe COVID-19[262]. Single-cell transcriptome analysis performed on this cell subset segregated mild and severe forms of the disease according to the myeloid cell composition. In depth analysis revealed a trend to accumulate inflammatory $HLA\text{-}DR^{high}$ $CD11c^{high}$ blood monocytes in mild patients, suggesting a scenario in which these monocytes prolong the activation and expansion of antigen-specific T cells, via the contribution of IFN-stimulated genes[263]. While, in severe patients, increased number of monocytes expressing $HLA\text{-}DR^{low}$ $CD11c^{low}$ $CD163^{high}$ $CD69^{high}$ $CD226^{high}$ is reported paralleled by the progressive loss of non-classical $CD14^{-}$ $CD16^{high}$ cells. The expression of CD69 and CD226 in classical monocytes

promoted diapedesis and tissue infiltration and retention[264]. Moreover, these monocytes were reported to express CD34, a marker commonly associated to immature phenotype, and they present the potential to suppress T-cell activation and effector functions[259,260]. Moreover, the expression of surface ACE2 receptors in alveolar macrophages provides sufficient evidence for the central role of monocytes in cytokine storm and lung pathology (**Figure 16**[250]). It should be noted that a failure to shift macrophages form pro-inflammatory classically activated phenotype (M1) to a wound-healing alternatively activated phenotype (M2) could contribute to the excessive inflammatory injuries and fibrosis lesions commonly found in ARDS patients[265]. Monocytes are capable of differentiating into macrophages and DCs when activated by innate immune response. Morphological changes and the expression of inflammatory related phenotypes in monocytes may be involved in disease aggravation. Indeed, the hyper-activation of pathogenic Th-1 cells may generate extensive IFN-γ and GM-CSF signals. Monocytes, which function as the responsive cells of pathogenic GM-CSF, are activated and converted into high levels of $CD14^{+}CD16^{+}$ inflammatory monocyte subsets in infected patients. These atypical monocytes can enter the pulmonary circulation and are capable of secreting high levels of GM-CSF and IL-6 to induce further monocyte migration and mediate the infiltration of inflammatory macrophages and DCs, ultimately leading to aggravating lung injuries[266] (**Figure 16**[250]).

Polymorphonuclear cells. Increase in neutrophils occurs in the lungs of COVID-19 patients[267] . Transcriptional analysis of broncho-alveolar lavage fluid (BALF) from COVID-19 patients reported high levels of CXCL2 and CXCL8, chemokines that facilitate the PMN recruitment to the site of infection[267]. An extensive and prolonged activation of these cells can lead to detrimental effects in the lungs and result in pneumonia and/or ARDS[268]. Activated neutrophils release neutrophil extracellular traps (NETs), a web of chromatin, microbicidal proteins, and oxidant enzymes with the function to contain infectious agents. However, when not properly regulated, NETs have the potential to propagate inflammation and microvascular thrombosis, as observed in the lungs of patients with ARDS and severe COVID-19 patients. Therefore, activated neutrophils forming NETs have been repeatedly linked to the immunopathogenesis of severe COVID-19[260, 263].

Moreover, the presence of $CD16^{int}CD44^{low}CD11b^{int}$ low-density neutrophils (LDNs), expressing IL-6 and TNF-α, is typical of severe COVID-19 patients and correlates with poor clinical outcomes[260, 263] . Among the LDN subsets, severe patients present MDSC-like phenotype (PMN-MDSCs defined as HLA-DR^- $CD11b^+CD33^+CD15^+CD14^-$ cells), whose expansion is sustained by the inflammatory milieu. These cells were shown to suppress T-cell activation via mechanisms dependent on TGF-β and iNOS[269].

T-cells. Lymphopenia characterizes COVID-19 and can predict disease severity. A reduction in $CD4^+$ and $CD8^+$ T-cell responses was reported in patients progressing to a fatal outcome[270] . The absolute numbers of central memory ($CD45RA^-$ $CCR7^+$) and terminally differentiated effector memory (TEMRA, $CD45RA^+$ $CCR7^-$) $CD8^+$ T-cells were reduced in patients with severe disease[271]. Perturbation in Tregs also translated into COVID-19 disease severity showing a higher expression of FoxP3 and an over-expression of a range of suppressive effectors, but also pro-inflammatory molecules like IL-32, thus mirroring the behavior already evidence in cancer [272]. Moreover, Th-1 and Th-2 related cytokines were both activated and detectable during COVID-19 courses, suggesting that an extensive upregulation of adaptive immunity occurred during COVID-19 infection[239] (**Figure 16**[250]).

B cells. In regard to the long-term effect of antibodies in COVID-19 recovered patients, one study observed elevated antibody titres as early as 1 week after the onset of symptoms, and the majority of patients experienced seroconversion within 3 weeks[273]. Although virus-specific antibody to SARS-CoV-2 favor the neutralization of virus, higher titers have been associated with more severe clinical cases[274] suggesting that a robust antibody response alone is insufficient to avoid severe disease. In severely ill COVID-19 patients, studies reported a profound reduction of absolute umber of total $CD19^+$ B-cells, naive (IgD^+CD27^-), early transitional T1 and T2 ($IgD^+CD27^-CD10^+CD45RB^-$), and $CXCR5^+$ follicular ($IgD^+CD27^-CD10^-CD73^+$) cells[275] . Another study suggested that high antibody titres act as a risk factor of critical illness, likely due to an antibody-dependent enhancement (ADE) effect[276] (**Figure 16**[250]). ADEs were proposed to exert

distinctive effects in SARS infection[227].

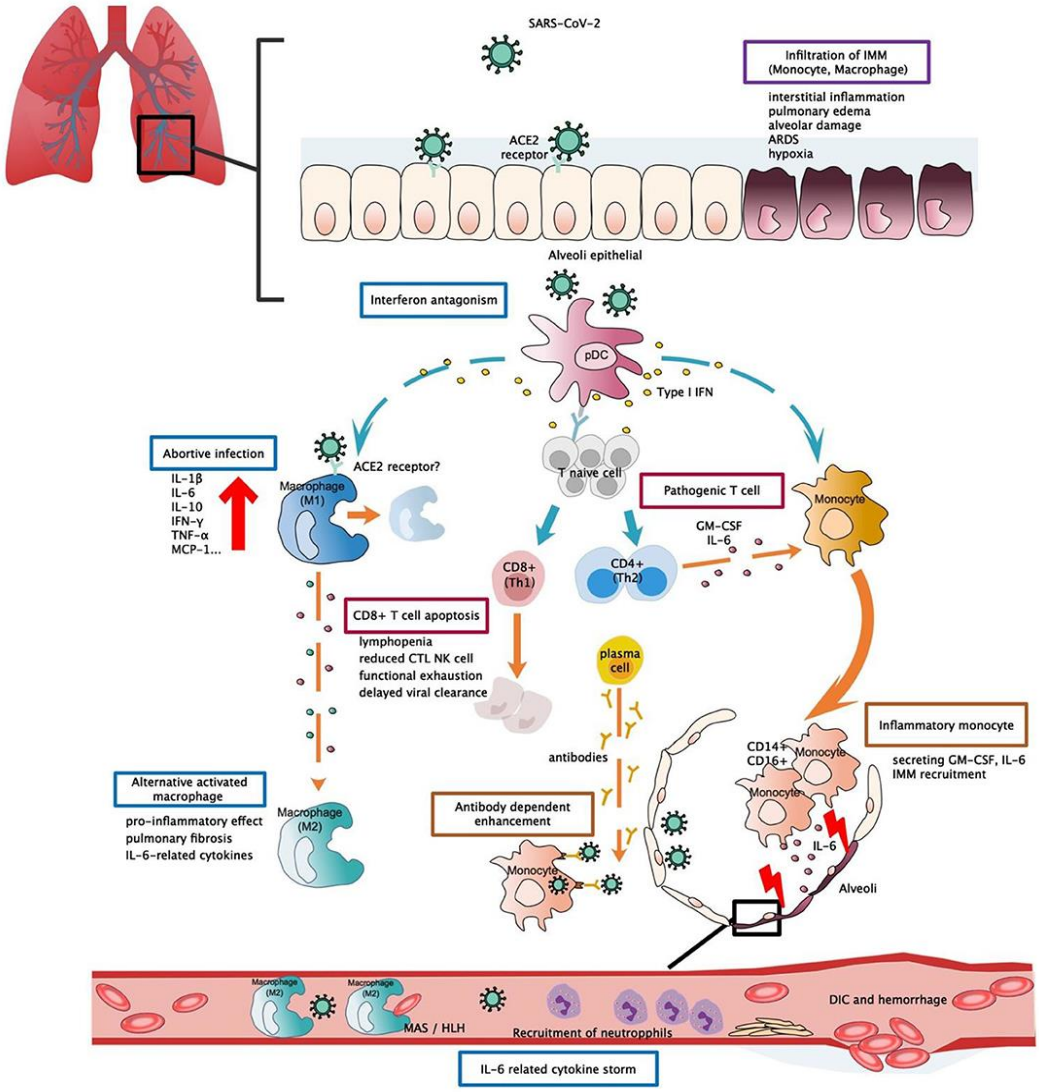

Figure 16. Potential immunopathogenesis in SARS-CoV-2 infection. This figure shows the potential immunopathogenesis during SARS-CoV-2 infection, inferred from previous SARS-CoV and MERS-CoV studies. Coloured boxes labelled the potential strategies or deleterious events involved in SARS-CoV-2 pathogenesis. Words below each box indicate the pathological consequences. Dashed arrows indicate causal relations between target cell and cell mediators. (A) Initially host-viral entry was found at alveoli epithelial. The virus invades host defences via binding with ACE2 by S-protein RBD. Abortive infection was observed in PBMC and haematopoietic cells—a process that induces expression of pro-inflammatory mediators rather than effective viral production. Another potential viral entry strategy relies on the presence of specific antibodies that form bridges between viral-host and facilitate viral entry rather than expressing ADCC effect. SARS-CoV-2 might have

evolved to encode specific proteins to counteract the host anti-viral response and optimise viral entry. Strategies such as interferon antagonism (not shown on the figure) allow viral evasion and prolonged viral shedding. (B) Regarding the host immune response, increased viral loads, and chemokines from abortive infection further enhance infiltration of IMM, an intense release of inflammatory cytokines that results in lung tissue injuries. Delayed viral clearance, aberrant cytokine production, and altered interferon levels hinder the proper functioning of the immune system, such as shifting of functional phenotype in macrophages and lymphocytes which would result in the impaired wound-healing function T cell apoptosis, pathogenic T cell response, functional exhaustion, dysregulated cytokine storm (i.e., MAS/HLH) and impaired viral clearance. Cascades activation of cytokine and chemokine ultimately led to systemic cytokine storm, manifested as sepsis, DIC, haemorrhage, and shock. RBD, receptor binding-domain; ADCC, antibody-dependent cell-mediated cytotoxicity; ACE2, Angiotensin-converting enzyme 2; pDC, Plasmacytoid dendritic cell; IMM, Inflammatory monocyte/macrophage; MAS, macrophage activation syndrome; HLH, Hemophagocytic lymphohistiocytosis; DIC, Disseminated intravascular coagulation. This image is adapted from[250]

4.5. Cytokine storm disease (CSD) and COVID-19-associated cytokine storm

Cytokine storm disease (CSD) is an umbrella term encompassing several disorders of immune dysregulation. Three criteria are used for identifying cytokine storm: elevated circulating cytokine levels, acute systemic inflammatory symptoms, and either secondary organ dysfunction (often renal, hepatic, or pulmonary) due to inflammation beyond that could be attributed to a normal response to a pathogen (if a pathogen is present), or any cytokine-driven organ dysfunction (if no pathogen is present)[277]. Nearly all patients with cytokine storm are febrile, and the fever may be high grade in severe cases. These symptoms may be due directly to cytokine induced tissue damage or acute-phase physiological changes or may result from immune cell–mediated responses. Cases can progress rapidly to disseminated intravascular coagulation either vascular occlusion or catastrophic hemorrhages, dyspnea, hypoxemia, hypotension, hemostatic imbalance, vasodilatory shock, ARDS and death)[277]. Cytokine storm can occur as a result of inappropriate recognition of pathogen antigen (i.e., in hypersensitivity) or ineffective recognition

with immune evasion (i.e., in Epstein–Barr virus [EBV]–associated hemophagocytic lymphohistiocytosis [HLH]), an inappropriate triggering with a response initiated in the absence of a pathogen (i.e., idiopathic multicentric Castleman's disease) or failure to terminate homeostasis or return to homeostasis (i.e., in HLH))[277].

Innate cells that are most often implicated in the pathogenesis of cytokine storm include neutrophils, macrophages, and NK cells. A complex, interconnected network of cell types, signaling pathways, and cytokines is involved in cytokine storm disorders. IFN-γ, IL-1, IL-6, TNF, and IL-18 are key cytokines that often have elevated levels in cytokine storm and are thought to have central immunopathologic roles)[277]. Levels of IL-6 are highly elevated across various underlying immunopathologic disorders and in mouse models of cytokine storm [278]. Drugs which neutralize interleukin-6 directly (tocilizumab, siltuximab), have been shown to be effective in a number of cytokine storm disorders, including HLH or idiopathic multicentric Castleman's disease[279]. The excessive secretion of soluble IL-6 is able to activate the JAK/STAT3 signaling in cells that do not express the membrane-bound IL-6 receptor (IL-6R), such as endothelial cells resulting in systemic hyperinflammation involving secretion of monocyte chemoattractant protein 1 (MCP-1), IL-8, and additional IL-6, as well as increased VEGF and reduced E-cadherin expression on endothelial cells, which contribute to vascular hyperpermeability, leakiness, hypotension, and pulmonary dysfunction[280]. TNF can induce cellular apoptosis and regulate immunity. It is a potent inducer of NF-κB, leading to the expression of multiple pro-inflammatory genes, and in mouse models of toxic shock, TNF is the cytokine driver of superantigen-driven cytokine storm[281]. IL-18 has recently associated with CSD. Patients with cytokine storm have high levels of IL-18 in serum, and it is considered as a biomarker of severity of the syndrome[282]. Macrophages and DCs are the primary sources of bioactive IL-18, which has many proinflammatory effects. Most important, it synergizes with IL-12 or IL-15 to stimulate secretion of IFN-γ from T cells and NK cells, and thus promotes Th1-type inflammatory responses. IL-1β and IL-18 are also potent inducers of IL-6 secretion from macrophages favoring further multi-organ damage[283] . Moreover, regulatory cytokines such as IL-10 are associated to CSD.

IL-10 inhibits the production of TNF, IL-1, IL-6, and IL-12 and down-regulates antigen presentation. Furthermore, in mice lacking IL-10, infection leads to cytokine storm[284].

Cytokine storm can also occur in a number of infections. CSD has been described in prior viruses including SARS-CoV, MERS-CoV. Acute lung injury, including its severe form ARDS and inflammatory conditions, is a common consequence of cytokine storm syndrome[253]. Although most of the COVID-19 patients recover with mild and moderate disease in one week, some develop to severe pneumonia in the second week followed by cytokine storm, ARDS, multi-organ failure, and disseminated intravascular coagulation (DIC) within the 3rd week of the disease. A study done in Wuhan noted that patients infected with SARS-CoV-2 had high amounts of pro-inflammatory cytokines and chemokines in their plasma. Critically ill patients who required intensive care unit (ICU) admission were found to have higher concentrations of cytokines in their plasma as compared to those with milder illness, suggesting that cytokine storm was connected to disease severity[239]. The cytokines, whose serum level was reported to be elevated in COVID-19 patients, include IL-1β, IL-6, IL-10, TNF, IFN-γ, macrophage inflammatory protein (MIP) 1α and 1β, and VEGF[239,277], colony-stimulating factor 3 and 2 (CSF3, CFS2), chemokines (CLL2, CXCL1), suggesting hyperactivation of Th1 cell responses[285]. The reduction in circulating T-cells has been firmly linked to the increment in serum levels of IL-6, TNF-α and IL-10[286]. In a recent study, the RNA sequencing transcriptional analysis revealed that in peripheral blood mononuclear cells (PBMCs) specimens from COVID-19 patients, several immune pathway, pro-inflammatory cytokines and CC chemokine ligands (CCL) and C-X-C motif chemokine ligand (CXCL), were induced by SARS-CoV-2 infection. The induction of CCL-2, CXCL2, CCL8, CXCL1, CCL3L1, IL-33, interferon-γ-inducible protein-10 (IP-10), tumor necrosis factor superfamily (TNFSF)10, tissue inhibitors of metalloproteinases (TIMP)1, IL-8, and IL-10, in COVID-19-derived PBMC indicate sustained inflammatory condition in the patients[287]. CCL-2 and CCL-4 were observed to be elevated selectively in patients with fatal outcome but not in those with mild disease. Of interest, IL-18 blood levels emerged along with IL-6 as a biomarker of severity, suggesting that the inflammasome pathway could be

important in determining the major outcomes[288]. IFNs play also a key role in the viral replication. Type I and III IFNs, once activated by binding their specific receptors (IFNAR and IFNLR), induce a powerful network of defense elements encoded by hundreds of IFN stimulated genes (ISGs) which cooperate to inhibit different steps of viral replication[289]. Early observations demonstrated that SARS-CoV-2 is sensitive to IFN-I/III pretreatment in vitro[290,291,292], highlighting that type I/III IFNs can effectively limit coronavirus-dependent infection[293,294]. Moreover, SARS-CoV-2 has evolved several mechanisms to interfere with antiviral immunity such as limiting host pattern recognition receptors (PRR) activation[295] and blocking the type I/III IFNs production[290]. Autoimmune blockade of IFN-dependent antiviral response was postulated in at least 10% of life-threating COVID-19 patients, due to the presence of neutralizing auto-antibodies towards type I IFN at the onset of critical disease and undetectable levels of serum type I IFN levels during acute disease[296]. On the contrary, recent evidence has reported that host IFN response defect can also contribute to the COVID-19 disease evolution, suggesting that IFN-I might orchestrate a dysregulated immune response that leads to COVID-19 aggravation (**Figure 16**)[250]. Growing evidence also pinpoints type III IFN signaling in the regulation of immunity and in the antiviral response[297]. Homozygosity for IFNλ3-IFNλ4 variants was associated with a reduction in viral clearance among children affected by acute respiratory infections[298].

IL-6. An excessive generation of IL-6 during infections and tissue injury is believed to be responsible for CSD[299]. IL-6 dysregulation leads to the activation of complement and coagulation, inducing vascular leakage[300]. The activation of IL-6 is thought to be the key feature of the progression of COVID-19 pneumonia to ARDS and hyperinflammation[301]. The respiratory epithelium, in presence of SARS-CoV-2 virus, releases IL-6 inducing the activation of DCs and alveolar macrophages. A cascade of the cytokines IL-1β, IL-12, and TNF-α results, and their secretion induces white blood cells (WBCs) to release cytokines, thus effectively perpetuating an inflammatory cycle. These cytokines also enter the circulation and cause systemic multi-system pathology[302]. The persistent secretion of IL-6 and GM-CSF that has been observed in COVID-19 patients supports the pathogenic role of atypical innate immune cells, thus suggesting their participation in COVID-19

pathogenesis (**Figure 16**[250]). Patients with severe SARS-CoV infection showed higher levels of IL-6, and chemokines in their serum compared to those with mild disease[253].

Although with limited efficacy, many agents or methods have been proposed for the treatment of CSD, such as IFN-γ neutralization, IL-6 receptor blockade, IL-6 neutralization, corticosteroids, B-cell ablation with rituximab, T cell–directed immunomodulation, blockade of IL-1 family member cytokines, IL-18 binding protein, and JAK inhibition[284].

4.6. Immunosuppressive landscape in COVID-19 patients

Research that was carried out in initial stage of COVID-19 infection, reported a lung interstitial pneumonia and an alteration of the pulmonary structure characterized by distortion of the alveolar architecture and diffuse vascular modifications[303]. The lymphoid and myeloid infiltration, that characterizes this initial stage of infection, is scattered, and epithelial cells show an intense expression of phosphorylated STAT3 (pSTAT3), suggesting their initial involvement on the activation of STAT3-dependent inflammatory process. Moreover, the endothelial cells of the new blood vessels that distinguish this infection phase, show a diffuse expression of both immunoregulatory PD-L1 molecule and tolerogenic enzyme IDO1[303]. A proteomic profiling of COVID-19 autopsies of different tissues (lung, spleen liver, heart, kidney, thyroid and testis) reported the significant dysregulation of 5,000 proteins including fibrosis markers, inflammation factors, as well as coagulation system- and angiogenesis-associated proteins[304], confirming the multisystem abnormal activation of inflammation pathways. In particular c/EPBβ, STAT3, STAT1, NF-κB2, RelA subunit of NF-κB, and transcription factor jun-B (JUNB) emerged as pervasive drivers of COVID-19 inflammation in multiple tissues. Most of the molecules mentioned, were observed to be involved in the immunosuppressive landscape of MDSCs. Moreover, aberrant levels of soluble mediators, inflammatory cytokines, chemokines that characterize the initial stage of COVID-19 infection and are responsible of the ARDS severity, can promote emergency myelopoiesis[305] leading to the mobilization of myeloid cell subsets with

immunosuppressive functions[3]. Circulating MDSC frequency increases during COVID-19 aggressiveness [306, 307], likely supporting the progression to lymphopenia in COVID-19 patients by actively inhibiting immune effector expansion and functionality (i.e., NK cells and T cells)[78]. Immunosuppressive functions of circulating MDSCs, in particular in the monocytic cell fraction ($CD14^+$ cells), isolated from COVID-19 patients depend on the expression of ARG1 enzyme and can predict patients' outcome[259] . The accumulation of immunosuppressive cells in SARS-CoV-2-infected patients and inflammatory cytokines (i.e., IL-6) highlights the existence of similar traits between cancer and COVID-19. For instance, high frequencies of $STAT3^+ARG1^+CD14^+$ immunosuppressive cells have been identified in PDAC patients[66,55] . More interestingly, in autopsy samples from lung in COVID-19 patients, c-FLIP was reported to be over-expressed in in myeloid cells[308]. c-FLIP favors the maintenance of an immunosuppressive milieu[131] and in monocytic subset of MDSCs promotes the upregulation of genes responsible for their immunosuppressive activity such as STAT3, IL-6, IDO1 and PDL-1[66] and enhances an aberrant STAT3-signallig[66, 308]. These data suggest that c-FLIP might play a key role in the progression and severity of COVID-19-induced ARDS disease. Indeed, c-FLIP could participate in favoring the unrestrained and persistent immunosuppressive and inflammatory milieu that establishes the terminal contexture of the COVID-19 disease characterized by a fatal immune silence[309].

4.7. Therapeutic intervention according to immune phases

Avoiding the need for mechanical ventilation is a key therapeutic strategy in COVID-19 management. Current evidence suggests that approximately 79-86% of patients who require ventilator support experience mortality[310]. Therefore, the period of time before respiratory decline to the point at which ventilator support is needed may be especially important during the COVID-19 disease course. Specific therapeutic approaches in this time period may be crucial for recovery and for preventing progression to ARDS, which can cause irreversible lung damage. Different kind of approaches have been tested in COVID-19 patients and several trials have been published in the last year aimed at dampening the inflammatory spread from the lung to other organs.

Monoclonal antibodies directed against epitopes of S protein can help to stop the invasion of the virus and several drugs have been tested in controlled trials (Umifenovir, Lopinavir/Ritonavir, Favipiravir, Sofosbuvir and Daclatasvir, Hydroxychloroquine) with no evidence of clinical efficacy[311]. *Bamlanivimab* has an activity against the RBD of SARS-CoV-2. It blocks the attachment of the virus to the host cell and prevents its entry into human cells. In the phase 2 clinical trial for bamlanivimab in outpatients, a reduction in viral load was observed at day 11 when compared to the placebo group. The symptom severity and COVID-19 hospitalization rate were also reduced in patients who received bamlanivimab[312]. It currently has received emergency use authorization by the food and drug administration (FDA) for the treatment of COVID-19 in recently diagnosed patients[313]. *Remdesivir*, an inhibitor of the viral RNA-dependent, RNA polymerase with *in vitro* inhibitory activity against SARS-CoV-1 and MERS-CoV (Middle East respiratory syndrome) originally created to be used against the Ebola virus, was shown to be clinically useful in hospitalized patients, in the very early phases of the disease. The structure of remdesivir prevents the propagation of viruses by blocking a crucial piece RNA duplication machinery, the RNA-dependent RNA polymerase (RdRp)[314]. *Interferons* were used against MERS and SARS to stimulate active immunity. It was identified that the IFN-1β was most effective against coronaviruses as it upregulates anti-inflammatory cells in the lungs. Early testing of interferons in human epithelial cell lines showed a reduction of viral concentration by injection[315]. *EIDD-2801,* known also as molnupiravir, is a novel antiviral agent with potent activity against severe acute SARS-CoV-2. It is a ribonucleoside analog and it is able to induce lethal mutagenesis by accumulating deleterious transition mutations in the viral RNA while having many off-target effects. The results of EIDD-2801 treatment have shown the greatest promise out of all these drugs, having been shown to reduce the concentration of SARS-CoV-2 as well as other coronaviruses (MERS and SARS) when taken prophylactically[316]. As of April 7th, 2020, the FDA has given the company responsible for EIDD-2801 approval to perform human trials[317]. A recent randomized, controlled trial, based on *dexamethasone* treatment on COVID-19 patients, showed that dexamethasone reduced mortality among the most severe cases[318]. Dexamethasone enters the

immune cells, binds to the glucocorticoid receptor (GR) in the cell cytoplasm. The ligand bound GR complex is rapidly translocated into the nucleus, interacts with NF-κB to block its transcriptional activity hence negatively regulating target gene expression, including IL-1, IL-2, IL-6, IL-8, TNF-α, and IFNγ[318].

Il-6/STAT3 pathway inhibitors. An important role is played by this class of inhibitors for the COVID-19 patients' treatment. Indeed, many viruses might have developed strategies to trigger STAT3 signaling to dampen the antiviral innate immune response during the acute phase, either by preventing IFN responses or triggering the negative immune-regulatory effects of IL-6[319, 320]. STAT3 pathway is relevant to produce some cytokines during the cytokine release syndrome (CRS). From the immune standpoint, a reduction of STAT3 in NK cells promotes a consistent increase in perforin and granzyme B, improving NK-mediated surveillance against pathogens[321]. On the other hand, preventing STAT3 phosphorylation in monocytes and neutrophils affects the ability to produce and release pro-inflammatory cytokines as well as their immunosuppressive properties on T lymphocytes[55]. Moreover, STAT3 in cytotoxic $CD8^+$ T cells controls lymphocyte differentiation from an effector to a long-term central memory phenotype[301]. The initial phase of COVID-19 infection comprises the activation of JAK1-2 and STAT-1 and the consequent phosphorylation of STAT3. JAK1 and JAK2 inhibitors, which are approved for the treatment of a number of autoimmune and neoplastic conditions, have the potential to inhibit signaling downstream of type I IFN, IL-6 (and other gp130 family receptors), IFN-γ, and IL-2, among other cytokines[322]. COVID-19 patients treated with baricitinib, showed a marked reduction in serum levels of IL-6, IL-1β, and TNF-α, a rapid recovery of circulating T and B cell frequencies, and increased antibody production against the SARS-CoV-2 spike protein. Moreover, a reduction of pSTAT3 expression in blood cells was reported in these patients (**Figure 17** [323]). These data suggested that baricitinib prevented the progression to a severe, extreme form of the viral disease by modulating the patients' immune landscape[250]. Furthermore, a randomized controlled trial with baricitinib showed a reduced progression to mechanical ventilation or mortality in COVID-19 patients[324]. The study COV-BARRIER RCT, in which baricitinib was administrated with Dexamethasone in COVID-19 patients,

demonstrated that the combinatory treatment offered the greatest chance of reducing mortality[325]. These results likely derive from the efficacy of baricitinib in modulating the inflammatory pathways via JAK1-2 inhibition, and in determining a dose-dependent inhibition of IL-6-induced STAT3 phosphorylation[308, 323] with decrease in immune factors.

Tocilizumab and *Sarilumab,* two IL-6R inhibitors used to treat rheumatoid arthritis[326], administrated in combination with Dexamethasone in COVID-19 patients, showed to protect from death with a hazard ratio of 1.61[327]. The estimates of this combinatory treatment were greater than the estimates for any intervention on its own, and the estimated interaction between IL-6R antagonists and glucocorticoids was additive and slightly in the direction of synergistic. These results were confirmed further in the RECOVERY randomized controlled trial, in which the death rate was reduced from 4.2% to 35%[328].

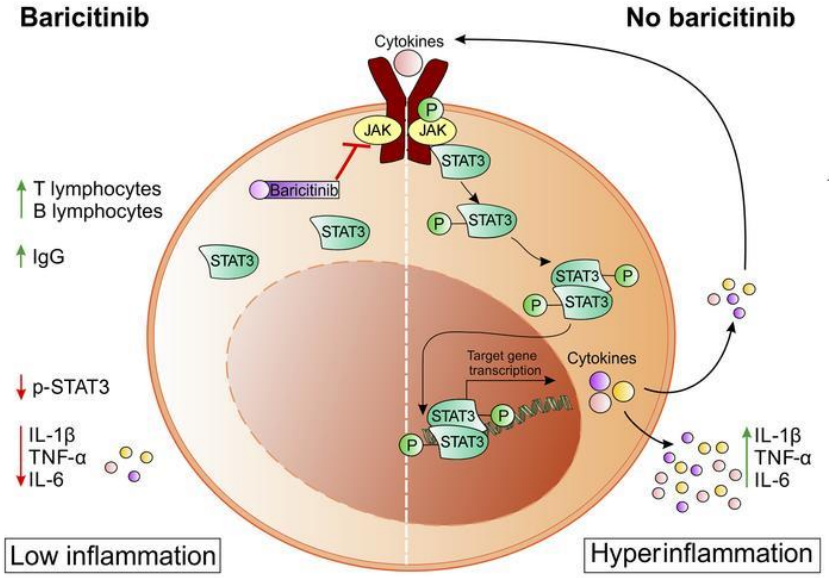

Figure 17. Baricitinib restrains the immune dysregulation in patients with severe COVID-19 recovering the peripheral T and B cell frequencies, reducing the serum levels of IL-6, IL-1β, TNF-α and the expression of p-STAT3 in blood cells, increasing IgG production against SARS-CoV-2 spike protein. This image is adapted from[316].

AIM OF THE STUDY

Several evidence report the clinical significance of MDSCs in different pathological settings such as cancer, inflammation disorders and infectious diseases[4, 7, 8,329]. The lack of conclusive markers do not allow to identify and target MDSCs without affecting other leukocytes. Recently, we characterized c-FLIP as a pivotal player on MDSC-associated functions and fitness since it regulates several M-MDSCs genes involved in monocytes suppressive activity[66, 158, 330]. STAT3-associated pathway represents one of the most upregulated networks in c-FLIP-over-expressing monocytes and, overall, it is responsible for the acquisition of immunosuppressive functions by MDSCs[55, 66].

Starting from these premises, we demonstrated that strategies based on STAT3-targeting might be promising to restrain the FLIP-mediated immune dysregulation in diseases in which MDSCs can play a pathogenic role. Indeed, STAT3 pathway is relevant to produce some cytokines during the CRS[55] in which FLIP was reported to play an essential role[66] . Therefore, treatments against STAT3 pathway might represent a key goal to mitigate FLIP-dependent cytokine storm via STAT3-activation. Availing of ROSA26.vFLIP Tg mouse model that over-expresses v-FLIP in the myeloid lineage and shows a systemic immune dysregulation, and inflammatory scenario[66], we generated a new mouse model, vFLIP chimera mouse, by engrafting immunocompetent mouse recipients with BM cells isolated from either ROSA26.vFLIP; LyzM-CRE (CD45.2) and wild type mice (CD45.1). This model recreated the v-FLIP-induced immunological landscape that characterized the ROSA26.vFLIP Tg mice[66] and offered a novel tool for defining molecular mechanisms, which fuel inflammation and CRS-associated immune dysfunctions. *In vivo* STAT3-targeting treatments, by using two drugs silibinin[331] and baricitinib[120, 121, 332], allowed us to verify the therapeutic impact on controlling systemic inflammation and MDSC-dependent immunosuppression.

The second aim of this work was the demonstration of the FLIP involvement in the progression of COVID-19 infection caused by SARS-CoV-2 virus. Indeed, FLIP expression was observed to be also linked to viral replication by favoring the

suppression of host cell death[132, 218, 224]. This part of the study was carried out on 2 cohorts of COVID-19 patients, Moreover, by availing of mouse transgenic for hACE2 (HFH4-hACE2 mice)[333] , we demonstrated that the solid link between FLIP and STAT3 dysregulation following SARS-CoV-2 infection. All data obtained in COVID-19 patients and in mouse model mirrored the immunological scenario observed in vFLIP chimera mice. Finally, the *in vitro* STAT3 targeting was able to inhibit immunosuppressive functions of FLIP-expressing monocytes isolated from COVID-19 patients.

In the third part of this work, we decided to investigate the role of c-FLIP as potential biomarker in oncology to predict the outcome of cancer subjects to immunotherapy. Currently, NSCLC remains poorly responsive to chemotherapy, and immunotherapy with ICIs stands for the main current approach to treat this malignancy[200]. c-FLIP was reported to be over-expressed in several cancer settings[158, 330] and our research group has recently reported that percentage of $CD14^+$ $c\text{-}FLIP^+$ cells significantly increased in PDAC patients[66]. A NSCLC cohort undergoing to ICIs immunotherapy was used for this project. Through the c-FLIP evaluation in peripheral monocytes, our study confirmed the hypothesis that c-FLIP assessment was able to predict the clinical evaluation of patients to immunotherapies suggesting c-FLIP as promising predictive biomarker to optimize the current oncology treatments for this or other cancer setting.

Finally, our research group has recently revealed that canonical NF-κB pathway was mainly involved in c-FLIP-induced suppressive phenotype[66] and it has hypothesized c-FLIP function as transcriptional regulator through nuclear translocation in a complex with p50 subunit. Furthermore, to confirm our hypothesis we investigated c-FLIP/p50 physical interaction and we analyzed, through Chromatin Immunoprecipitation sequencing (ChIP-seq) analysis, the DNA sequences linked to c-FLIP. For this part of the study, we enforced the expression of target gene by transient transfection of THP1 human monocytic cell line with c-FLIP-encoding mRNA. This study confirmed our hypothesis and revealed several DNA sequences involved in different immune system processes that were identified as c-FLIP linked.

Data obtained from this work could give the possibility to exploit this "moonlighting" protein and transcriptionally c-FLIP-regulated genes to develop prospective novel therapeutic strategies aimed at regulating the immunosuppressive program of myeloid cells in different pathological setting such as cancer context, inflammatory disorders, and infectious diseases.

MATERIALS AND METHODS

1. Mice

All genetically Tg mice and their respective controls were gender and age-matched (typically 3–10 weeks) and both males and females were used in this study. Mice were assigned randomly to experimental groups. C57BL/6 (H-2^b) mice were originally purchased from Charles River Laboratories Inc., OT-1 TCR-Tg mice (C57BL/6-Tg (TcraTcrb)1100Mjb/J), CD45.1^+ congenic mice (H-2^b, *B6.SJL-Ptrc^{a}Pepc^b/BoyJ*) and LySM-CRE mice (H-2^b, *B6.129P2-Lyz2$^{tm1(cre)Ifo}$/J*) were purchased from Jackson Laboratories; Rosa26.vFLIP mice were a gift from Dr. Ethel Cesarman (Weill Cornell Medicine, NY, USA). All mice were maintained under specific pathogen-free conditions in the animal facility of the University of Verona. Food and water were provided *ad libitum*. Animal experiments were performed according to national (protocol number C46F4.26 approved by the Ministerial Decree Number 993/2020-PR of July 24, 2020 [PI: Stefano Ugel] and protocol number C46F4.8 approved by the Ministerial Decree Number 207/2018-PR of February 21, 2018 [PI: Vincenzo Bronte]) and European laws and regulations. All animal experiments were approved by Verona University Ethical Committee and conducted according to the guidelines of Federation of European Laboratory Animal Science Association (FELASA). All animal experiments were in accordance with the Amsterdam Protocol on animal protection and welfare: mice were monitored daily and euthanized when displaying excessive discomfort.

2. Generation of vFLIP chimera mice

To generate the vFLIP-chimera mouse model, C57BL/6 female of 8 weeks of age received 9 Gy total body irradiation (TBI) using ^{137}Cs-source irradiator. Six hours after pre-conditioning, irradiated recipient mice were intravenously injected with 5x10^6 BM cells obtained from CD45.1 WT and ROSAvFLIP Tg (CD45.2) donor mice at different ratio (100% WT-0% vFLIP; 75% WT-25% vFLIP; 50% WT-50% vFLIP; 0% WT-100% vFLIP). BM cells over-expressing FLIP protein from Kaposi's sarcoma virus (v-FLIP) in myeloid compartment were collected from

ROSA26.vFLIP Tg knock-in mice. These mice were obtained by crossing ROSA26.vFLIP knock-in mice with mice expressing Cre recombinase under control of the endogenous *Lyz2* promoter. For the therapeutic studies, 50% WT-50% vFLIP ratio was used to generate the vFLIP-chimera mice. Four weeks post bone-marrow transplantation, peripheral blood of recipient mice was analyzed for the presence of donor-derived cells.

3. Ethics and acquirement of human samples

All 48 patients with COVID-19 and 4 HDs in this study were admitted, within the period from March 12th to April 20th 2020 to the University Hospital of Verona or Hospital of Pescara. At sampling, the stage of disease was categorized as mild (patients not requiring non- invasive/mechanical ventilation and/or admission to intensive care unit (ICU)) or severe (patients requiring admission to ICU and/or non-invasive/mechanical ventilation). For immunohistochemistry (IHC) analysis of lung autopsy, this study includes a group of 4 non-respiratory disease (NRD) patients, 4 bacterial pneumonia (BP) patients and 23 COVID-19 patients. The clinical features are recapitulated in **Table 5A-B**. For molecular data (i.e. single cell transcriptomic analysis), phenotypic analysis (myeloid characterization in terms of expression of immune suppression hallmarks) and functional data (myeloid immune suppressive assay), this study includes a group of 14 severe COVID-19 patients admitted to ICU, 11 mild SARS-CoV-2 patients and 4 HDs (**Table 5C**).
All the patients (and/or initially their families) provided written informed consent before sampling and for the use of their clinical and biological data. This study was approved by the local ethical committee (protocol 17963; PI: Vincenzo Bronte; ClinicalTrials.gov identifier NCT04438629). All clinical investigations were conducted according to Declaration of Helsinki principles, and informed consent was obtained from all study participants.

32 patients with stage IIIC/IV NSCLC adequate for immune-based treatment with ICIs were enrolled in the study at the Department of Medical Oncology of AOUI from January 2019 to June 2020. Enrolled patients met all the following inclusion criteria: age of at least 18 years, Eastern Cooperative Oncology Group performance

status (ECOG PS) ≤ 2; unresectable, locally advanced or metastatic NSCLC (histologically or cytologically confirmed); no prior immunotherapy (**Table 6A-B**). According to the current guidelines (AIOM. Linee guida NEOPLASIE DEL POLMONE Edizione 2019. Published online 2019) for patients enrolled before January 2020, Pembrolizumab was used as first line treatment in patients with PD-L1≥50% (13 patients), whereas Nivolumab, Atezolizumab or Durvalumab (for PD-L1≥1%) were chosen as second or further line treatment after chemotherapy. For second-line immunotherapy, 14 patients received Nivolumab, 3 received Atezolizumab, and only one received Durvalumab. Atezolizumab was administered for all patients receiving ICIs as third line of treatment (1 patient). All patients enrolled after January 2020 fulfilled the criteria for Pembrolizumab monotherapy as first line of treatment (PDL1≥50%). For the study reported in this thesis, we selected the patients undergone only immunotherapies. After enrollment, patients were periodically re-evaluated, and all data pertaining to therapy response was recorded. Tumor staging was performed according to the TNM staging system. According to routine local clinical practice, periodic tumor assessments were performed through computed tomography (CT), scan or magnetic resonance imaging (MRI) every three months. Response evaluation criteria in solid tumors (RECIST) 1.1 criteria were used to evaluate tumor response. According to RECIST 1.1 criteria and clinical evaluation, patients were classified as responders (13 subjects) or non-responders (19 subjects) 6 months after the first ICIs administration (the clinical parameters and the tumor evaluation for both responders and non-responders are reported in Table 6A and 6B respectively). This study was approved by the local institutional review board and conducted according to Good Clinical Practice guidelines and the Declaration of Helsinki. Written informed consent for biomarkers analysis and clinical data collection was obtained from all patients before enrollment in the study. Data were anonymized to ensure patients' privacy.

Table 5: Main clinical data of: (A) patients for IHC analysis of lung autopsy; (B) COVID-19 patients for IHC analysis of lung autopsy, and (C) patients for molecular, phenotypic, and functional data.

	NRD	**BP**	**COVID-19**
(A) Main clinical data of patients for IHC analysis of lung autopsy			
Parameters	$N = 4$	$N = 4$	$N = 23$
Age (year), median (range)	64.5 (48–80)	63 (44–82)	82 (54–95)
Gender, *n* (%)			
Males	2 (50%)	4 (100%)	11 (48%)
Females	2 (50%)		12 (52%)
Co-morbidity, *n* (%)			
Absent	0	1 (25%)	3 (13%)
1	1 (25%)	2 (50%)	8 (34.8%)
2	0	1 (25%)	8 (34.8%)
3	3 (75%)	0	4 (17.4%)
(B) Main clinical data of COVID-19 patients for IHC analysis of lung autopsy			
		c-FLIP^{-}CD68^{-}pSTAT3^{-}	c-FLIP^{+}CD68^{+}pSTAT3^{+}
Days of hospitalization, median (range)		25 (11–52); $N = 10$	18 (0–32); $N = 13$
CRP (mg/L), median (range)		75.79 (9–271.2); $N = 10$	80.83 (5.92–242.5); $N = 12$
Pro-calcitonin (ng/mL), median (range)		2.12 (0.14–9.45); $N = 9$	0.81 (0.2–9.45); $N = 10$
(C) Main clinical data of patients for molecular, phenotypic, and functional data			
	Healthy controls	Mild patients	Severe patients
Characteristics	$N = 4$	$N = 11$	$N = 14$
Anagraphic			
Age, Yr: Median (IQR)	66 (64–73)	71 (63–86)	70 (60–71)
Male, no. (%)	3 (75)	10 (90.9)	6 (85.7)
Clinical features at sampling			
APACHE score, median (IQR)	–	–	25 (13.5–28)
SOFA score, median (IQR)	–	–	7 (4–8)
Score on ordinal scale (1–8), median (IQR)	–	4 (3–4)	5 (3–7)

Table 6: Main clinical data of NSCLC cohort: (A) clinical parameters; (B) tumor parameters. PS=presence of metastatic disease; SCC=squamous cell carcinoma.

A		**RESPONDERS**	**NON-RESPONDERS**	**P value**
Sex	Males	9 (0,69)	12 (0,63)	0.722
	Females	4 (0,31)	7 (0,37)	
Familiarity	No	5 (0.50)	8 (0.50)	1
	Yes	5 (0.50)	8 (0.50)	
Previous cancer	No	8 (0.61)	17 (0.89)	0.091
	Yes	5 (0.39)	2 (0.11)	
Comorbidity	No	3 (0.23)	3 (0.16)	0.666
	Yes	10 (0.77)	16 (0.84)	
PS	0	7 (0.37)	6 (0.46)	0.598
	≥ 1	8 (0.63)	11 (0.54)	
Symptomatic at diagnosis	No	5 (0.38)	6 (0.32)	0.721
	Yes	8 (0.62)	13 (0.68)	
Death occurrence	No	11 (0.85)	1 (0.05)	**<0.001**
	Yes	2 (0.15)	18 (0.95)	

B		**RESPONDERS**	**NON-RESPONDERS**	**P value**
Histology	Adenocarcinoma	7 (0.64)	13 (0.76)	0.671
	SCC	4 (0.36)	4 (0.23)	
N parameter	0	4 (0.31)	2 (0.11)	0.150
	≥1	9 (0.69)	17 (0.89)	
M parameter	0	4 (0.31)	4 (0.21)	0.684
	1	9 (0.69)	15 (0.79)	

4. Cell lines

THP1-Blue™ NF-kB cell line (InvivoGen) is a human monocytic cell line derived from a patient with acute monocytic leukemia (AML-M5). It was grown at 37 °C and 5% CO_2 in arginine and glutamine-free RPMI 1640 supplemented with 2 mM L-glutamine, 10 mM Hepes, 4.5 g/L glucose, 1 mM sodium pyruvate, 10% heat-

inactivated fetal bovine serum (FBS), 50 U/ml penicillin-streptomycin, 100 μg/ml normocin and 10 μg/ml blasticidin.

5. Cytokines and synthetic peptides

Mouse recombinant GM-CSF and mouse recombinant IL-6 were purchased from Miltenyi Biotec. Kb-restricted $OVA_{257-264}$ peptide (SIINFEKL), was synthesized by JPT (Berlin, Germany).

6. STAT3 targeting

The *in vitro* effect of drugs treatment was investigated in differentiated MDSCs obtained from $CD45.1^+$ congenic mice, and in peripheral $CD14^+$ cells isolated from COVID-19 patients. The cells were treated for 30 minutes with either baricitinib or silibinin at different concentrations to determine the appropriate doses which kept unaltered the cell viability and differentiation. The data reported were obtained by using 200μM of baricitinib for both type of cells, 500μM of silibinin for MDSCs treatment and 200μM of silibinin for COVID-19-derived $CD14^+$ cells. The *in vivo* effect of drugs treatment was investigated in the vFLIP-chimera mouse model, four weeks after the BM cells transplantation. Chimera mice that displayed at least 20% of donor-derived cells were randomized before beginning treatment. Chimera mice were treated using 8 intraperitoneal administrations of baricitinib (10 mg/kg; Cayman chemicals) or silibinin (100mg/kg; Sigma-Aldrich) every two days, for a total of 9 treatments. IHC and flow cytometry analysis were performed at the end of the experiment (2 weeks after the first treatment). Chimera mice were euthanized when the weight loss reached the 20% of body weight as an animal protocol-defined endpoint.

7. Detection of cytokines and serology

Cytokines released by patients' monocytes and the peripheral cytokines in vFLIP chimera mice were quantified by 25-Plex Human ProcartaPlex™ according to manufacturer's instructions. In the results we reported the data more significant relative to following cytokines: IL-1β, IL-6, IL-18, TNF α, IL-10 (eBioscience,

Thermo Fisher Scientific, Waltham, MA, USA). Samples with a purity greater than 95% were assessed for their cytokine production. Briefly, $5x10^5$ COVID-19-derived $CD14^+$cells were plated in 24-well plates for 12 hours. At the end of the incubation, viability was evaluated by flow cytometry.

8. Preparation of cell suspensions from organs

Mice were euthanized by CO_2 inhalation. For lung flow cytometry analysis, mice were immediately perfused with 20 mL ice-cold PBS. Organs were harvested and processed as follows. Spleens were mechanically disaggregated and filtered (Corning Inc). Lungs were cut in small pieces with scissors, enzymatically digested at 37°C for 45 minutes with a solution containing collagenase IV (1mg/ml), hyaluronidase (0.1mg/ml) and DNase (4.5mg/ml) (Sigma-Aldrich). For BM, tibias and femurs were flushed in RPMI 1640 (Euroclone) supplemented with 10% heat-inactivated FBS (Superior, Merck), 2mM L-glutamine, 10mM HEPES, 1mM sodium pyruvate, 150U/mL streptomycin, 200U/mL penicillin/streptomycin (all from Euroclone). Cells were then collected, filtered and red blood cells were lysed at RT for 5 minutes with ACK Lysing Buffer (Lonza). Peripheral blood was washed with PBS and red blood cells were lysed twice at RT for 10 minutes. Single-cell suspensions were then analysed by flow cytometry.

9. PBMCs and $CD14^+$ cells isolation from human samples

Cells were isolated from EDTA-teated tubes (BD Biosciences, NJ, USA) and peripheral blood mononuclear cells (PBMCs) were freshly isolated by Ficoll-Hypaque (GE Healthcare) gradient centrifugation. In the NSCLC cohort, the cells were isolated from whole blood of patients before treatment initiation, six weeks after the first administration and at each tumor re-evaluation, every three months approximately. $CD14^+$ monocytes were freshly isolated from PBMCs by immunomagnetic sorting using CD14 MicroBeads (Miltenyi Biotec) according to manufacturer's instructions. Isolated cell purity was evaluated by flow cytometry using anti-human CD14 antibody. Samples with a purity greater than 95% were assessed for their suppressive capacity. NSCLC-derived PBMCs and $CD14^+$ cells

were frozen at −80 °C and stored in liquid nitrogen until use, whereas the COVID-19-derived PBMCs and $CD14^+$ cells were freshly used.

10. Immunosuppression assay

Mouse: The immunosuppressive activity was evaluated plating *in vitro* differentiated MDSCs in 96 wells plate at a final concentration of 24% of total cells in culture in presence of splenocytes from OT-1 Tg mice, labelled with 1μM CellTrace (Thermo Fisher Scientific) and diluted 1:10 with $CD45.1^+$ splenocytes , in the presence of SIINFEKL peptide (1μg/ml final concentration). After 3 days of co-culture, cells were stained with APC-Cy7 conjugated anti-CD45.2 (clone 104, eBioscience, Thermo Fisher Scientific) and PerCP-Cy5.5 conjugated anti-CD8 (clone SK1, eBioscience, Thermo Fisher Scientific). CellTrace signal of gated lymphocytes was used to analyze cell proliferation. Samples were acquired with FACS-Canto II (BD Biosciences) using TruCount™ tubes (BD Biosciences) to determine the absolute number of $CD8^+$ cells in the samples. Data were analyzed by FlowJo software (Tree Star Inc).

Human: Isolated monocytes were co-cultured *in vitro* with allogeneic PBMCs. PBMCs were isolated from leukocyte-enriched buffy coats from HDs by Ficoll-Hypaque (GE Healthcare) gradient centrifugation, frozen at -80 °C and stored in liquid nitrogen. PBMCs were recovered and incubated with 1μM CellTrace Violet stock solution (Thermo Fisher Scientific) for 5 minutes at 37 °C, protected from light. Cells were then washed and resuspended in culture medium. Labelled PBMCs were stimulated with coated 0.6 μg/ml anti-CD3 (clone OKT-3, eBioscience) and 5 μg/ml soluble anti-CD28 (clone CD28.2, eBioscience) for 4 days and co-cultured with isolated $CD14^+$ cells from patients at 3:1 ratio ($CD14^+$ cells: PBMCs) in 384 flat bottom well plates. Cell cultures were left at 37 °C and 5% CO_2 in arginine and glutamine-free RPMI 1640, supplemented with 2 mM L-glutamine, 150 μM arginine, 10% heat-inactivated FBS, 10 U/ml penicillin and streptomycin, and 0.1 mM Hepes. Following incubation, cells were stained with human anti-CD3-PE-Cy7 (UCHT1, eBioscience) antibody and samples were acquired with FACS-Canto II (BD Biosciences). TruCount™ tubes (BD Biosciences) were used to determine the

absolute number of $CD3^+$ cells. Data were analyzed by FlowJo software (Tree Star Inc.) and CellTrace signal of $CD3^+$ cells was used to analyse cell proliferation.

11. Flow cytometry

0.5-2x10^6 cells were washed in PBS and incubated with FcReceptor Blocking reagent CD16/32 (Biolegend) or FcReceptor Blocking reagent (Miltenyi Biotec) in staining buffer (2% FBS in PBS) for 10 min at 4 °C to saturate FcR. The following mAbs were then used for cell labelling: anti-mouse CD3 (17A2), CD45.1 (A20), CD45.2 (104), CD11b (M1/70), Ly6C (HK1.4), Ly6G(1A8), FOXP3 (NRRF-30), CD25 (PC61.5), CD3ξ (145-2C11), CD62L (MEL-14), CD8a (53-6.7), CD4 (RM4-5), LAG-3 (C9B7W), TIM-3 (B8.2C12), NK1.1 (PK136), IL-6 (MP5-20F3), TNFα (MP6-XT22), or anti-mouse/human CD44 (IM7), p-STAT3 (Tyr705) using clone LUVNKLA, or anti-human CD16 (3G8), CD3 (UCHT1), HLA-DR (L243), CD14 (MφP9), PD-L1 (MIH1). LIVE/DEAD™ dye (Fixable Aqua Dead Cell Stain Kit, Thermo Fisher Scientific), and 7-AAD and Annexin-V (Apoptosis Detection Kit) were used to determine cell viability. All antibodies were purchased from the following companies: BD Biosciences (San Jose, CA, USA), eBiosciences (Thermo Fisher Scientific, Waltham, MA, USA), Biolegend (San Diego, CA, USA) and Cell Signaling Technologies (Danvers, MA, USA). Extracellular antigens were stained for 30 minutes at 4°C in staining buffer. For cytokines and transcriptional factor analysis, cells were fixed and permeabilized with FoxP3/Transcription Factor Staining Buffer Set (eBioscience) following manufacturer instructions. Intracellular antigens were stained for 1 hour in the appropriate 1x Perm/Wash buffer. Samples were acquired with a FACSCanto II (BD, Franklin Lakes, NJ, USA) and analyzed with FlowJo software (Treestar Inc.).

To determine the intracellular levels of p-STAT3 (Tyr705) using clone LUVNKLA, after surface markers staining, cells were fixed with 2% paraformaldehyde (Sigma-Aldrich) and permeabilized with 90% cold methanol. All steps were performed in ice.

To assess $CD14^+$ or THP1 cells transfection efficiency, percentage of GFP^+ cells were estimated at FACS by fluorescence signal in FITC-fluorochrome canal.

FLIP protein expression was evaluated by flow cytometry by indirect amplification on intracellular signal. In details, after surface markers staining, 1×10^6 PBMCs were fixed and permeabilized with FoxP3/Transcription Factor Staining Buffer Set (eBioscience). Before the intracellular staining, cells were incubated with FcReceptor Blocking reagent (Miltenyi Biotec) for 10 min at RT in the appropriate 1x Perm/Wash buffer. Rabbit anti-FLIP antibody (D5J1E; 1:100; Cell Signaling Technologies) was added for 2 h at 4 °C. Signal was amplified with a secondary anti-rabbit IgG (H+L) (#8885, Cell Signaling Technology) for 30 minutes at 4 °C. To normalize the c-FLIP expression level between the analyzed samples of COVID-19 cohort, we applied the following formula: Normalized MFI = (MFI sample – MFI FMO)/ MFI FMO.

12. Immunofluorescence (IF) and immunohistochemistry (IHC)

To determinate the presence of pSTAT3 Tyr705 or c-FLIP in human $CD14^+$ cells and in c-FLIP transfected THP1 cell line, the cells were plated on coverslips (ibidi GmbH; Cat#80826), fixed in 4% formaldehyde for 10 minutes at RT, and blocked with 0.1% Triton X-100 in PBS 1x for 10 minutes at RT. To detect the intracellular signal, permeabilization was performed in 0.1% Triton X-100 in PBS 1x and 20% of normal goat serum (Vector Laboratories) for 2 hours at RT. Primary mAbs rabbit anti-FLIP antibody (D5J1E; 1:100; Cell Signaling Technologies) and mouse anti-pSTAT3 (Try705) (LUVNKLA; 1:50; Invitrogen) were diluted in PBS1x supplemented with 0,05% Tween 20 (Biorad, Cat#1706531) solution overnight at 4°C. Signal was amplified with secondary antibodies goat anti-rabbit IgG Alexa Fluor 488 (1:1000; CAT#A11034; Invitrogen) and donkey anti-mouse IgG Alexa Fluor 647 (1:1000; Cat#A-31571 Invitrogen) in 0.1% Triton X-100 in PBS 1x and 20% of normal goat serum for 1 hour at RT followed by nuclei staining with Hoechst 33342 (H1399; 1:500; Invitrogen) in PBS 1x for 10 minutes at RT.
Images regarding c-FLIP signal in THP1 cell line was acquired by Leica TCS SP5 AOBS inverted confocal microscopy, and the colocalization analysis of Pearson's correlation about nuclear c-FLIP was performed by Imaris software. As autofluorescence control, unstained GFP positive cells were used.

Tissues were fixed in 10% neutral buffered formalin and embedded in paraffin; after embedding, 5μm thick sections were cut and stained with Hematoxylin and Eosin (Bio-Optica, Italy) for histological examination. For immunohistochemical and immunofluorescence analysis of samples, slides were deparaffinized, serially rehydrated and, after the appropriate antigen retrieval procedure, incubated with the following primary antibodies: rabbit anti-mouse pSTAT3 antibody (#9145, Cell Signaling), rat anti-mouse B220 antibody (550286, BD Pharmigen), mouse anti-human CD68 antibody (M0814, Dako), mouse anti-Human/Mouse/Rat FLIP antibody (MAB8430, R&D), rabbit anti-mouse CD3 antibody (ab16669, Abcam), rabbit anti-mouse F4/80 antibody (#70076, Cell Signaling), rabbit anti-mouse CD62P antibody (ab255822, Abcam), rabbit anti-mouse Neutrophil Elastase antibody (ab68672, Abcam), rabbit anti-mouse CD4 antibody (#25229, Cell Signaling) and rat anti-mouse FoxP3 antibody (14-5773-82, eBioscience), followed by the appropriate secondary antibodies. Immunostainings were developed with streptavidin peroxidase methods and the DAB Chromogen system (Dako). After chromogen incubation, slides were counterstained in Hematoxylin (Bio-Optica) and images were acquired by Leica DMRD optical microscope (Leica). For immunofluorescence, immunostainings were developed using TSA Plus Cyanine 3, TSA Plus Cyanine 5 or TSA Plus Fluorescein Systems (NEL744001KT, NEL745001KT or NEL741001KT respectively, Akoya Biosciences), goat anti-rabbit Alexa Fluor 488 (A11008, ThermoFisher), goat anti-rat Alexa Fluor 546 (A11081, ThermoFisher), goat anti-mouse Alexa Fluor Plus 647 (A32728, ThermoFisher) and nuclei were stained with Dapi (Sigma). Images were acquired by Zeiss LSM800 confocal microscope.

For histological assessment of collagen deposition, trichrome staining was performed using the Masson Trichrome with Aniline Blue Staining Kit (04-010802, Bio-Optica). Pathological score was independently evaluated by two pathologists in double-blind using the standard guideline previously published[334].

The percentage of CD3, B220 or F4-80 positive cells was evaluated on digital images of total reconstructed spleen section (5-10 X 50 microscopic fields per sample); clear brown positive cells were selected with the Magic Wand Tool of Adobe Photoshop. For each spleen, the number of positive cell pixels indicated in

the histogram window was reported as % on the number of total spleen area (expressed in pixel). The number of $FoxP3^+$ cells was evaluated on digital images of immunofluorescence section as percentage on CD4 positive cells.

13. RNA synthesis

The sequences encoding for GFP, c-$FLIP_S$, c-$FLIP_L$ were subcloned in the pST-T7-hAg-MCS-FI-A30LA70 vectors and IVT mRNA were produced as previously described[335, 336] . The 3′ UTR (F-I) of this construct have been shown to enhance stability and translation efficiency, as it has the 100-nucleotide poly(A) tail interrupted by a short linker. Plasmids were linearized with EarI and served as the template for IVT mRNA synthesis using T7 RNA polymerase and a transcription kit (MegaScript, Ambion, Austin, TX, USA). The UTP in the reaction was replaced with 1-methylpseudouridine triphosphate (N1-methylpseudouridine-5′-triphosphate, m1ΨTP) (TriLink). β-S-ARCA(capD1) IVT mRNAs were generated as described elsewhere[329]. Upon IVT mRNA production, single-stranded RNA was enriched by cellulose purification and the absence of double-stranded RNA (dsRNA) was confirmed using the dsRNA-specific mAb J2 (10010200, English and Scientific Consulting)[328]. The quality of the purified dsRNA-free IVT mRNA was assessed by spectrophotometry on a 2100 Bioanalyzer (Agilent), and the mRNA was stored at −80 °C.

14. RNA transfection

THP1-Blue™ NF-kB cells were transiently transfected with non-immunogenic GFP mRNA (Biontech) or a combination of c-$FLIP_L$ and c-$FLIP_s$ (50 + 50%) mRNAs (Biontech) using VIROMER RED technology (Lypocalyx) following the instructions provided by the supplier. In a 6 well plate, 3 x 10^6 cells were seeded per well at a concentration of 2.5 x 10^6 cells/ml and treated with 300 µl of a transfection mix composed by 270 µl of mRNA (1.1 µg/10^6 cells) in Viromer Red Buffer and 30 µl of Viromer Red solution (diluted 1/25 in Viromer Red Buffer). Human $CD14^+$ mRNA-transfection was performed using the same mRNAs and technology, with the following protocol: in a 6 well plate, 3 x 10^6 $CD14^+$ cells were

seeded per well at a concentration of 2 x 10^6 cells/ml in RPM1 1640 supplemented with 10% FBS, 1% L-glutamine, 1% penicillin-streptomycin, 1% sodium pyruvate, 1% Hepes. $CD14^+$ cells were transfected with 360 µl of a transfection mix composed by 324 µl of mRNA (3.3 µg/10^6 cells) in Viromer Red buffer and 36 µl of Viromer Red solution (diluted 1/25 in Viromer Red Buffer). All cells were left at 37 °C, 5% CO_2 for 6 hours. Then, cells were collected, washed with PBS and pellets were prepared and stored at -80 °C. Transfection efficiency was evaluated by FACS detecting GFP^+ cells.

15. Real-time qPCR

Total RNA from both c-FLIP- or GFP-transfected THP1 cells was extracted with TRIzol reagent (Thermo Fisher Scientific). RNA quantification and purity evaluation were assessed by ND-100 Spectro-photometer (NanoDrop Technologies). 1 µg of cDNA was prepared mixing 1 µg of RNA with the reverse transcription reaction mix, composed of: 4 µl of 5x Run buffer, 1 µl of random primers, 2 µl of dNTP mix and 1 µl of 200 U/ µl Euroscript reverse transcriptase (Euroclone). Real-time qPCR was performed using 2x SYBR Green master mix (ABI). Alternatively, for the analysis of c-FLIP-linked genes expression selected by ChIP-seq, total RNA was extracted by spin column utilizing "RNeasy Mini Kit" (Qiagen). 1 µg of cDNA was prepared using "Superscript VILO cDNA Synthesis Kit" (Invitrogen) and following manufacturer's instructions. Real Time qPCR was performed by using "TaqMan Fast Advanced Master Mix" (ThermoFisher) and Custom plates designed for the specific amplification of the ChIP-seq selected genes. All samples were normalized by using GAPDH endogenous control primers and GFP-encoding mRNA transfected THP1 cells. Gene expression was analyzed by the comparative Ct method ($2^{-\Delta\Delta Ct}$).

16. Lysate preparation and quantification

Total protein lysates, collected from c-FLIP and GFP transfected THP1 cell line, were prepared diluting cell pellets in RIPA buffer, composed of 0.5% TritonX-100, 50 mM Hepes, 150 mM sodium chloride, 5 mM EDTA, with the addition of 1 mM

sodium orthovanadate, 2 mM PMSF, and 1:100 (v/v) protease cocktail inhibitor. Cytoplasmic and nuclear extracts were prepared from cell pellets (from both transfected THP1 cell line and HDs-isolated $CD14^+$ cells) by using "NE-PER Nuclear and Cytoplasmic Extraction Reagents" (Thermo Fisher Scientific) following manufacturer's instructions. Protein quantification was performed by bicinchoninic acid assay (BCA), using Quantum Protein Bicinchoninic Protein Assay Kit (EuroClone). Bovine serum albumin (BSA) was used for the standard curve.

17. Immunoprecipitation

p105/p50 immunoprecipitation (IP) was performed on c-FLIP-transfected THP1 total lysates or cytoplasmic/nuclear extracts using Dynabeads™ Protein G Immunoprecipitation Kit (Invitrogen), following manufacturer's instructions. p105/p50-IP was executed by using the following antibodies: 1 μg of α-p105/p50 antibody (0.5 μg clone D7H5M + 0.5 μg clone D4P4D, Cell Signaling Technologies) and 1 μg of Rabbit IgG isotype (used as a control). For p105/p50-IP, 200 μg of whole cell lysate was used, while 300 μg and 50 μg of cytoplasmic and nuclear extracts were used for each condition, respectively. Elution of immunoprecipitated complexes was performed in denaturing condition upon the addition of 2mM DTT to NuPAGE LDS Sample buffer (Invitrogen). Western blot analysis was performed to ensure to IP efficiency.

18. Western Blot analysis

Lysates of transfected THP1 cell line and $CD14^+$ cells were diluted in NuPAGE LDS Sample Buffer (4x, Invitrogen) and all samples were supplemented of 5% 2β-mercaptoethanol. The samples were loaded on 10% denaturing Bis-Tris NuPage gel (Invitrogen) to perform a polyacrylamide gel electrophoresis. Proteins were transferred on nitrocellulose membrane. Membranes were blocked in 5% non-fat milk dissolved in Tris-buffered saline (TBS) + 0.1% Tween-20 for 1 hour at room temperature (RT) and incubated with the appropriate primary antibody overnight at 4 °C. Membranes were washed three times with TBS-Tween-20 0.1% and

incubated with the appropriate secondary antibody, horseradish peroxidase (HRP)-conjugated, for 1 hour at RT. Proteins were detected by using Pierce ECL Western Blotting Substrate (Thermo Fisher Scientific). The following primary antibodies were used: anti-human p105/p50 (D7H5M clone, Cell Signaling Technologies) + anti-human p105/p50 (D4P4D clone, Cell Signaling Technologies), anti-human FLIP (D5J1E clone, Cell Signaling Technologies, and 7F10 clone, Enzo Life Sciences), anti-human GAPDH, anti-human Lamin B1 and anti-human α-tubulin (Cell Signaling Technology). The following secondary antibodies were used: donkey anti-rabbit IgG, HRP-conjugated (NA934V, Amersham), sheep anti-mouse IgG, HRP-conjugated (NXA931, Amersham), mouse anti-rabbit IgG, light chain specific, HRP-conjugated (Jackson ImmunoResearch), goat anti-mouse IgG, light chain specific, HRP-conjugated (Jackson ImmunoResearch).

19. Chromatin Immunoprecipitation sequencing (ChIP-seq)

c-FLIP- and GFP- (as control) transfected THP1 cells, after 6 hours from transfection, were treated with formaldehyde (1% final concentration) to cross-link proteins to DNA. Later, crosslinking reaction was stopped upon glycine addition and cells were washed twice with ice cold PBS. Cell lysis was performed in a membrane extraction buffer. Nuclei were recovered by centrifugation and resuspended by sonication to shear the chromatin. The lysate was clarified by centrifugation and an aliquot (INPUT DNA) was withdrawn and stored. Then, the chromatin preparation was diluted in immunoprecipitation buffer and supplemented with the primary antibody (mouse anti-human c-FLIP, clone 7F10, Enzo Life Sciences). Each sample was left incubating at 4 °C for 16 h on a rotating agitator. After that, samples were supplemented with protein A/G beads mixes and left incubating at 4 °C for 1-2 h with rotation, to immunoprecipitate. After centrifugation, sample supernatant was removed, and beads were washed. ChIP DNA elution was performed by diluting the beads in elution buffer. Samples were left incubating at 65°C for 4h/overnight to reverse cross-link ChIP DNA and INPUT DNA. Tris-HCl 1M ph 6.5 and proteinase K were added, and incubation was prolonged for 1h at 45°C. Finally, DNA was purified by column chromatography using Qiagen PCR purification Kit. DNA sequences were

identified by PCR, sequenced, and analyzed. ChIP-seq analysis was performed selecting the DNA sequences significantly enriched in c-FLIP transfected THP1 cells compared to GFP transfected ones. Downstream sequencing analysis focused on the selection of protein coding genes and "upstream 10 Kb sequences". Genes obtained from the selection were further filtered by gene ontology (GO) annotation in order to screen only the genes involved in the immune system processes.

20. Single-cell RNA sequencing (scRNA-seq)

Lung from WT and vFLIP chimera mice, were digested as described in "Preparation of cell suspensions from organs" section. For human samples, bronchoalveolar lavage fluids (BALs) from fatal COVID-19 patients were used. Single cell suspension (10^4 cells) was loaded on a GemCode Single Cell Instrument (10x Chromium System) to generate single cell GEMs. Raw bcl files were demultiplexed using bcl2fastq v2.20 from Illumina and processed using 10x Cell Ranger v3.1.0. In particular, 'cellranger count' command with parameter '--expect-cells=4000' was used to quantify reads mapped to mouse (mm10) and human (GRCh38) genomes and to obtain the unique molecular identifier (UMI) count tables. Human scRNA-seq data from BALs was obtained from the Gene Expression Omnibus (GEO) under accession GSE157344. The quality control steps before data integration were performed individually for each sample using the R package 'Seurat'[337, 338, 339] and Scrublet[340] for removing putative doublets. In particular, to retain high quality transcriptomes, the cells were filtered according to the following parameters: percentage of mitochondrial counts, minimum number of expressed genes, min./max. number of UMIs and doublet score. For both mouse and human only cells with less than 20% of total counts explained by mitochondrial genes were maintained. Scrublet thresholds were chosen seeing at the histograms of observed transcriptomes and simulated doublets as recommended by the author guidelines (https://github.com/AllonKleinLab/scrublet/blob/master/examples/scrublet_basics.ipynb). The other filtering thresholds were chosen looking at the distribution of the data in order to remove cells with a potential outlier behaviour. The complete list of filtering thresholds is summarized in **Table 7**.

Both for mouse and human cells all the samples were integrated using the standard Seurat v3 integration procedure[331]. Before data integration, the original count matrices were normalized using log-normalization from the Seurat package with default parameters. Next, both for mouse and human the scRNA-seq data was integrated using the first 30 dimensions of canonical correlation analysis (CCA). After integration, count matrices were scaled regressing for the total number of genes, UMIs and percentage of mitochondrial gene expression. Next, principal component analysis (PCA) was performed on the top 2,000 most variable features obtained using the 'vst' procedure of Seurat. The top 20 principal components were used to execute t-distributed stochastic neighbor embedding (tSNE) algorithm and to project the cells into a 2-dimensional space.

Table 7: Complete list of filtering thresholds used for scRNA-seq analysis.

Sample	**Min. number of expressed genes**	**Min. number of UMIs**	**Max. number of UMIs**	**Doublets threshold Scrublet**
WT 1	250	1,000	60,000	0.38
WT 2	250	1,000	60,000	0.399
vFLIP 1	250	1,000	75,000	0.38
vFLIP 2	250	1,000	75,000	0.52
Chimera UT	250	1,000	75,000	0.46
Chimera Silibinin	250	1,000	75,000	0.5
Chimera Baricitinib	250	1,000	75,000	0.38
BAL3	200	500	40,000	-
BAL7	200	500	40,000	0.689
BAL10	200	500	100,000	0.4
BAL29	200	500	60,000	0.627
BAL18	200	500	40,000	0.661
BAL24	200	500	100,000	-
BAL25	200	500	60,000	-

21. Cell type identification

After data integration, cell type identification both for mouse and human was performed using multiple reference-based cell annotation and manual inspection.

For mouse, SingleR[341] with gene expression profiles from Immunological Genome Project[342] and Mouse RNA-seq[343] was used in combination with scMCA[344] . For human data, SingleR was executed using reference gene signatures from Blueprint/ENCODE[345, 346] , Human primary cell atlas and Monaco immune data[347]. Prior to final cell classification, cell labels were simplified in order to discard ultra-rare (< 20 cells) cell annotations and harmonized to match corresponding main population labels across the different reference datasets. Final cell identity was obtained taking the classification determined by 2 out of 3 reference datasets and annotating as "Unclassified" the cells labeled differently with all the 3 datasets. Overall, about 2% of mouse and human cells were labeled as Unclassified.

22. Mapping between human and mouse genes

To map mouse to human gene symbols the ortholog table from the Mouse Genome Informatics (MGI, http://www.informatics.jax.org/downloads/reports/HMD HumanPhenotype.rpt) was used keeping only the genes with a one-to-one mapping between the two species.

23. Gene set analysis

Gene set analysis for scRNA-seq and bulk RNA-seq data was performed using 'fgsea'[348] that performs pre-ranked gene set enrichment analysis (GSEA[349]). Gene level statistics for scRNA-seq data used as input for GSEA were calculated using the Seurat function 'FindMarkers' with the Wilcoxon Rank Sum test with average log-fold change threshold of 0 for bulk-like analyses and 0.1 for cluster-level analyses. For the analysis of bulk RNA-seq of previous published Sars-CoV-2 ACE2-transgenic mice dataset (GSE154104), gene-level statistics were obtained through DESeq2 package[350]. In particular, after removing duplicated gene symbols, differential expression analysis was performed to compare Sars-CoV-2 ACE2-transgenic mice 7 days post infection (dpi) and mock-infected mice (0 dpi) with log2-fold change different from 0. The 50 hallmark gene sets from MSigDB[351] were used as input both for GSEA and GSVA. For GSEA, only up- or down-regulated gene sets with adjusted p-value < 0.05 were considered statistically significant.

In general, the bioinformatics figures were obtained using functions of the R packages Seurat and ggplot2[352] . The scRNA-seq data generated in this study have been deposited in the Gene Expression Omnibus (GEO) under accession number GSE168098.

24. Statistical analysis

All data are reported as mean ± standard error (SE) of the mean. Statistical analyses were performed using Graph Pad Prism (version 8.0.2). Student *t* test and Wilcoxon–Mann–Whitney test were used to determine statistical significance of differences between two treatment groups. Values were considered significant at $P \leq 0.05$.

RESULTS

1. The inhibition of STAT3 pathway modulates MDSCs immunosuppressive activity

The role of MDSCs in altering the immune response was described in several pathological contexts such as cancer, inflammation disorders and infectious diseases[4, 7, 8,329]. MDSCs ability in inhibiting T-cells and promoting tumor growth has been reported for several tumor settings[184]. MDSCs were initially observed in patients with advanced cancer, and in a variety of tumoral contexts a high number of circulating MDSCs is associated with poorer prognosis and a weaker response to treatment[83]. It has been reported that the main mediator of tumor-induced immunosuppression is represented by M-MDSCs subset[96]. Moreover, c-FLIP has been identified as an important regulator of tumor progression not only by inhibiting cancer cells apoptosis, but also by influencing the functional activity of immune system cells. c-FLIP has been shown to be over-expressed in several cancer settings[158, 330] and our research group has recently reported that percentage of $CD14^+$ $c\text{-}FLIP^+$ cells significantly increased in PDAC patients[66]. Our laboratory demonstrated a direct role mediated by c-FLIP in triggering immunosuppressive properties in human c-FLIP over-expressing monocytes, which in physiological condition do not display any suppressive activity. Indeed, the enforced over-expression of c-FLIP in monocytes was able to induce the upregulation of many genes typical of MDSCs signatures and responsible for their immunosuppressive activity, such as STAT3, IL-6, IDO1 and PD-L1[66]. GSEA, performed on c-FLIP-over-expressed human $CD14^+$ cells isolated form HDs, revealed the upregulation of several signaling pathways, including genes belonging to NF-κB pathway in response to TNF-α and to STAT3 pathway correlated to pro-inflammatory IL-6 cytokine. These data highlighted the crucial role of such pathways, c-FLIP-induced, in controlling an immunosuppressive program in monocytes[66]. Moreover, the MDSCs-like phenotype induced by c-FLIP in monocytes suggests not only a common signaling network among these myeloid cells, but also the same expression of *CFLAR*[4]. FLIP is reported to be required for the survival and suppressive function of murine M-MDSCs ($CD11b^+Ly6G^{low}Ly6C^+$ cells)[7, 15]. Our

research group silenced the kinase IKKα and IKKβ, both indispensable for canonical NF-κB activation, in $CD11b^{+}Ly6G^{low}Ly6C^{+}$ cells isolated from BM of ROSA26.vFLIP Tg mice. This murine model, generated by our laboratory[66], is able to express in myeloid compartment a FLIP protein homolog from Kaposi's sarcoma virus (vFLIP), which harbor DED domains responsible for blocking procaspase cleavage, preventing apoptosis and favoring viral latency[225]. This model was obtained by crossing ROSA26.vFLIP knock-in mice with mice expressing Cre recombinase under the control of the endogenous Lyz2 promoter, this resulting in v-FLIP expression in the myeloid lineage. The suppressive activity of monocytic MDSCs subset was strongly compromised by treatments with NF-κB pathway inhibitors[66]. Even though the strategies directly targeting the essential components of the NF-κB pathway may negate its cancer-promoting activities, they also seem to fail to sustain the important NF-κB pathway physiological functions. For this reason, strategies targeting NF-κB pathway have not yet been approved in the clinic[341]. Moreover, since the enforced expression of FLIP in monocytes promotes the over-expression of pro-inflammatory cytokines by a "steered" NF-κB activation, which also results in enhanced STAT3-signaling activation, as reported by our group[66], we argue that a pervasive inflammatory loop is established by FLIP through the joint activation of NF-κB and STAT3. Indeed, a synergy between NF-κB and STAT3 molecules based on pro-inflammatory cytokines (i.e., IL-6), which acts as inflammation amplifier, has been reported in several multiple inflammatory and autoimmune diseases[353].

Therefore, given all the above data, we decided to focus on targeting STAT3 pathway in order to restrain the FLIP-mediated immune dysregulation. For our experiment we availed of two STAT3 pathway inhibitors: silibinin, STAT3 inhibitor that blocks the Y705 phosphorylation related and STAT3 dimerization[331], and baricitinib, a clinically approved inhibitor of JAK1 and JAK2 able to interfere with STAT3 signaling activation[120, 121, 332]. In our starting *in vitro* experiments, we assessed the suppressive function of MDSCs after treatment with STAT3 inhibitors through a standardized proliferation assay. The MDSCs include M- and PMN-MDSCs and are reported to play suppressive functions[7]. Researchers supposed that the suppressive activity reported in MDSCs was associated, among other factors, to

CFLAR expression, as suggested by over-expressing c-FLIP monocytes showing a MDSCs-like phenotype[4]. MDSCs were differentiated *in vitro*[101] from BM cells isolated from $CD45.1^+$ congenic mice (B6.SJL-PtrcaPepcb/BoyJ). After differentiation, the cells were treated for 30 minutes with either baricitinib or silibinin at different concentrations to determine the appropriate doses which kept unaltered the cell viability and differentiation (**Figures 18A-C**). We carried out a proliferation assay using 200µM of baricitinib and 500µM of silibinin. The MDSCs were plated at 24%, 12%, and 6% of total cell co-cultured for testing their suppressive activity by measuring the T cells ($CD8^+$ cells) proliferation. Both treatments were able to restore the $CD8^+$ T cells proliferation. Baricitinib was able to impact the suppressive activity of target cells even in presence of high amount of MDSCs (**Figure 18D**). Collectively, these data suggested that blocking STAT3 could decrease FLIP-mediated immunosuppressive activity in suppressive myeloid cells.

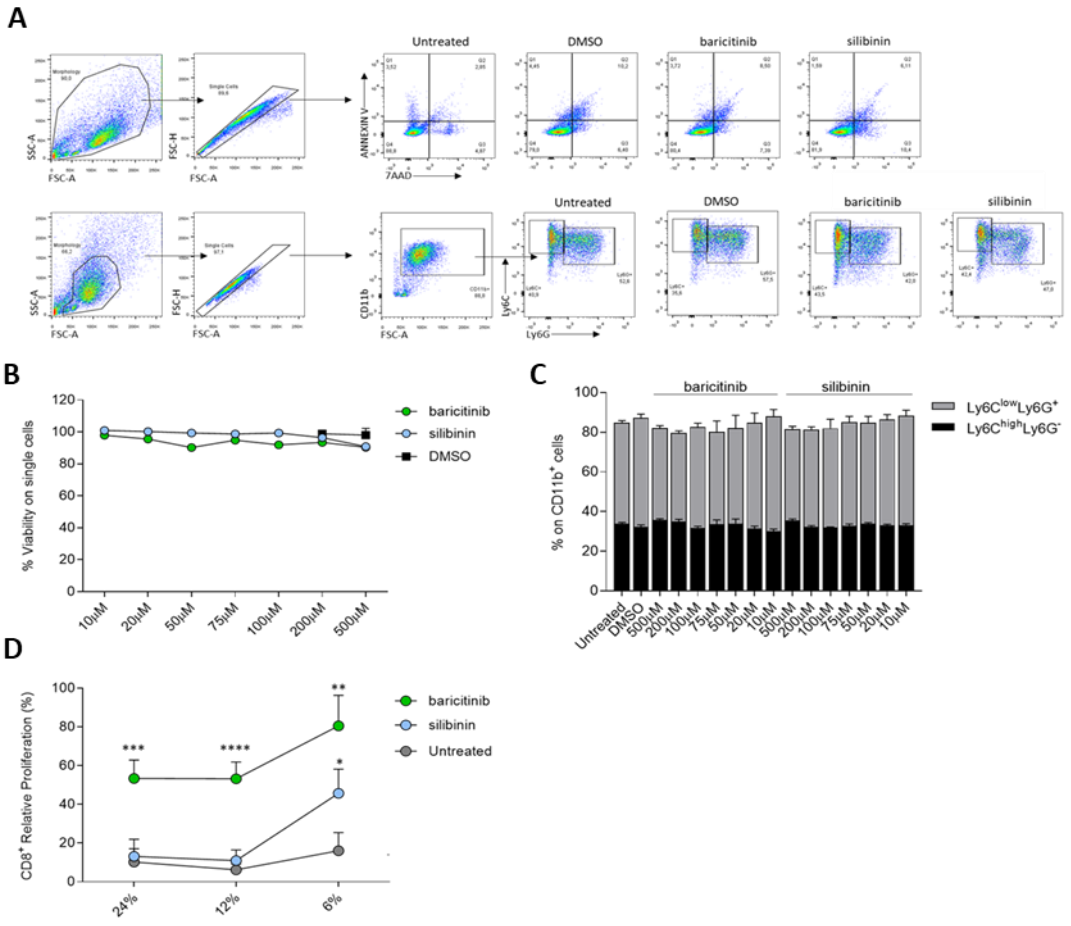

Figure 18. Treatment with STAT3 inhibitors impairs the functional activity of MDSCs without impacting their viability and differentiation. (A) FACS gating strategy for viability and differentiation analysis performed on *in vitro* differentiated MDSCs obtained from wild-type mice. The following conditions were examined: Untreated (UT), MDSCs cultured for 30 minutes in presence of DMSO (the solvent of STAT3 inhibitors), MDSCs treated with baricitinib or silibinin. The viability analysis was performed by using ANNEXIN V and 7AAD markers, whereas the differentiation analysis was performed by using CD11b, Ly6C and Ly6G markers. The higher doses for DMSO, baricitinib and silibinin, selected for the experiments, are showed. **(B)** The percentage of viability after treatment with baricitinib and silibinin at different doses, was reported on single cells and normalized for UT condition. The cells were cultured in presence of DMSO as control. **(C)** The percentage of $Ly6C^{low}Ly6G^{+}$ and $Ly6C^{high}Ly6G^{-}$ cells after baricitinib and silibinin treatment, at different doses, was reported on $CD11b^{+}$ cells. The cells were cultured in presence of DMSO as control. **(D)** Immunosuppressive assay on *in vitro* differentiated MDSCs after STAT3 inhibitors treatment (baricitinib 200 µM, silibinin 500µM). MDSCs were co-cultured with CellTrace labelled splenocytes from OT-1 Tg mice at 24%, 12% and

6% of total cell coculture. Data are reported as percentage of $CD8^+$ relative proliferation. Data are reported as mean ± SEM. Statistical analyses were performed by Mann-Whitney test **(B, C, D)**. *p<0.05, **p<0.01, ***p<0.001, ****p<0.0001 **(D)**.

2. FLIP-mediated immune dysregulation distinguished vFLIP chimera model

To investigate further the impact of targeting STAT3 pathway in FLIP-over-expressing contexts, we moved to *in vivo* experiments by exploring a mouse model recently generated in our laboratory, vFLIP chimera mouse[308]. Since Tg mice expressing vFLIP in myeloid lineage, ROSA26.vFLIP Tg mice, die prematurely within 4 weeks of life due to systemic immune disorders[66], we engrafted sub-lethally ablated (9 Gy total body irradiation (TBI) using ^{137}Cs-source irradiator) immunocompetent mouse recipients with BM cells isolated from either ROSA26.vFLIP; LyzM-CRE (CD45.2) or wild type mice (CD45.1) (**Figure 19A**) mixed at different ratios (vFLIP/WT ratio 0/1; 1/1; 3/1; 1/0). For the engraftment 5 x 10^6 BM cells were intravenously injected six hours after pre-conditioning in recipient mice. Firstly, we evaluated the impact of vFLIP over-expression on immune system in order to recreate the hematopoietic dysregulation, systemic cytokine storm and massive infiltration of myeloid cells in several organs that characterized the ROSA26.vFLIP Tg mice[66]. Through IHC analysis of spleen in vFLIP chimera mice, we observed a systemic lymphopenia, that is reported by reduction of $B220^+$ cells and $CD3^+$ cells, and an extensive accumulation of myeloid cells, that is reported by an increase of $F4/80^+$ cells. Besides, the analysis showed a highly compromised alteration of splenic architecture (**Figure 19B**). Moreover, H&E-stained microscopy images and Masson's Trichrome analysis, which were carried out on several organs such as intestine, lung and liver, showed a complete morphological alteration of tissue architecture with a massive lung infiltration, a destroyed lamina propria of the gut lumen and a cell accumulation mostly condensed around the portal triad and the bile duct in the liver (**Figure 19C**). These data suggest the development of multi-organ injuries and areas of fibrosis induced by over-expression of vFLIP. For subsequent analyses in this study, we employed chimeras generated by transplantation of a 1:1 ratio of $vFLIP^+$ and WT BM cells.

This chimera model provided an appropriate time window for our experiments. In detail, histopathologic analysis of 1:1 vFLIP chimera lungs showed a highly inflamed framework defined by interstitial enlargement, enrichment of giant cell clusters, diffuse perivascular myeloid infiltrate and alveolar damage, vascular congestion and intravascular thrombi. Severe cases also showed infarctions and extensive fibrosis (**Figure 20A**).

IF staining of lung tissue revealed a clear increase of both mononuclear phagocytes (hereafter identified as $CD68^+$ cells) and neutrophils (hereafter identified as neutrophils elastase [NE^+] positive cells) compared to normal mice (**Figure 20B**). Finally, to evaluate the tissue disfunction induced by vFLIP over-expression in this mouse model, we analyzed, through H&E-staining, the presence of the endothelial dysfunction marker p-selectin (CD62P) in the pulmonary environment of vFLIP chimera mice. P-selectin is normally stored in Weibel-Palade bodies of endothelial cells. After tissue injury, it is exposed in the vascular lumen where it mediates the adhesion and activation of platelets and leukocytes[354]. In vFLIP chimera mice, p-selectin was strongly expressed on the luminal surface of inflamed vessels of large and small caliber, whereas it was not detectable in the lungs of WT mice (**Figure 20C**). We investigated further the alteration of immune system in splenic compartment of chimera mice. Notably, a marked accumulation of myeloid cells was identified also in the spleen of vFLIP chimera mice with an increase of NE^+ cells and mononuclear phagocytes (hereafter identified as $F4/80^+$ cells) compared to WT mice (**Figure 20D**). Finally, lymphocytic populations were subject to dramatic changes. Flow cytometry analysis revealed a profound decrease of $CD4^+$ and $CD8^+$ cells. Interestingly, T naïve ($CD4^+/CD8^+$ $CD62L^+$ $CD44^-$) and central memory T lymphocytes ($CD4^+/CD8^+$ $CD62L^+$ $CD44^+$) were heavily contracted, whereas effector T cells ($CD4^+/CD8^+$ $CD62L^-$ $CD44^+$) showed an increase in chimera spleens (**Figure 20E**). Moreover, T regulatory lymphocytes (Tregs), identified as $CD4^+$ $FoxP3^+$ cells through IF staining, significantly expanded in splenic context of vFLIP chimera mice (**Figure 20F**). Finally, taking account that soluble factors, such as growth factors and inflammatory cytokines, are directly involved in engaging, activating, and regulating innate immune cells in pathological conditions[355], we focused on assessing cytokines-producing cells isolated from the

spleen of chimera model. We analysed in detail by intracellular staining, the expression of TNF-α- and IL-6 cytokines in mononuclear phagocytes ($CD45.2^+Ly6C^+$ cells) and neutrophils ($CD45.2^+Ly6G^+$ cells). We could not isolate enough myeloid cells from WT mouse lungs. Inflammatory cytokine production was higher in monocytes than in neutrophils, but in both subpopulations the cytokines expression reported higher values in spleen of vFLIP chimera mice compared to WT mice (**Figure 20G**). Considering all data above, we speculated that vFLIP-induced immunological scenario might establish a multiple organ failure, an unfavorable environment for T cells leading to a pronounced systemic lymphopenia, an accumulation of immune-regulatory cells such as myeloid cells and Tregs and promoting an inflammatory context. This vFLIP-induced immune disfunction resembles the dysregulated immunological scenario which we observed in ROSA26.vFLIP Tg mice[66].

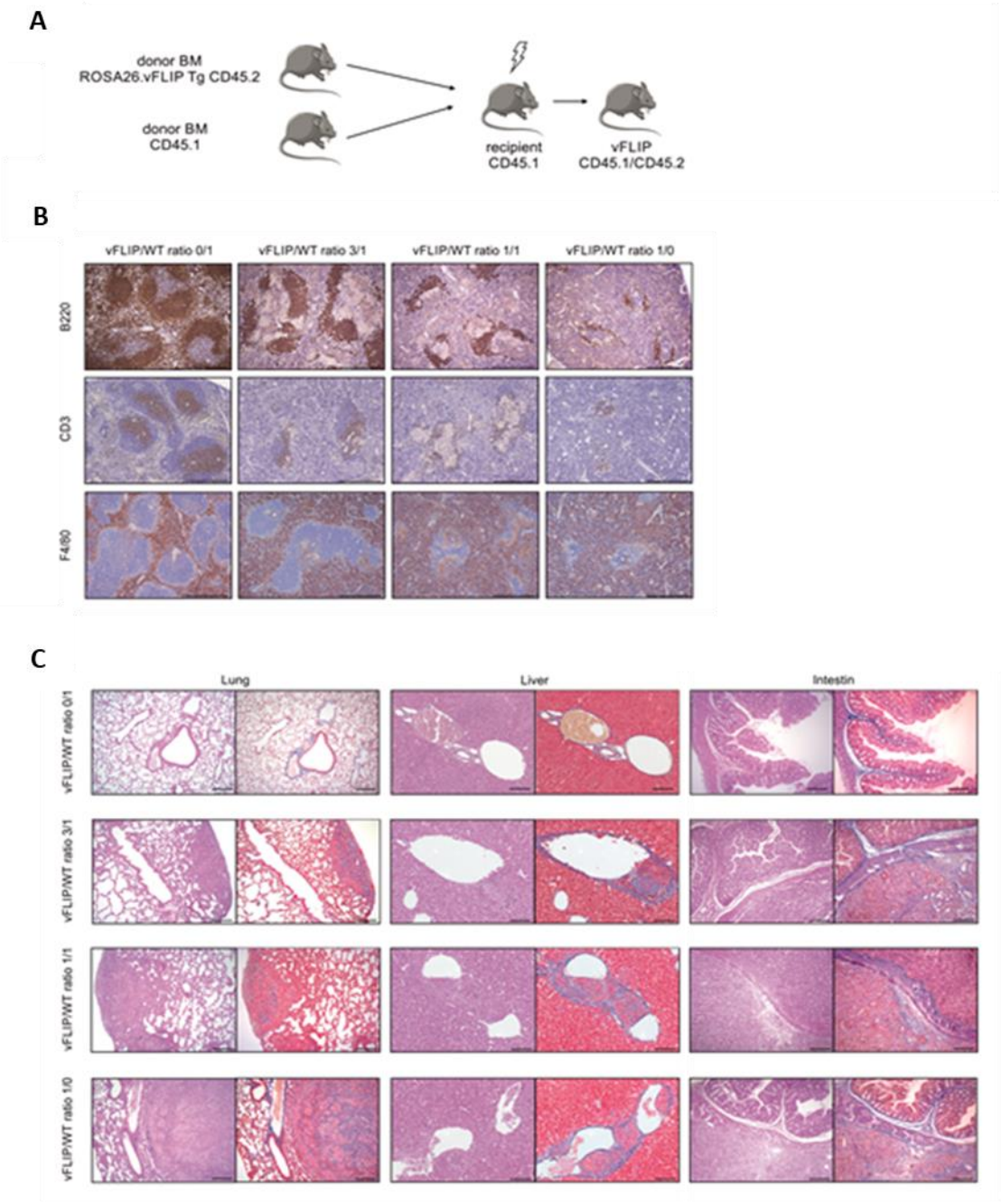

Figure 19. vFLIP chimera mice generation and FLIP-mediated multi-organ alterations. (A) Experimental layout of vFLIP chimera mice generation. **(B)** IHC analysis of spleen in vFLIP chimera mice generated at different ratio (vFLIP/WT ratio 0/1; 1/1; 3/1; 1/0): lymphocytes ($B220^+$ cells: B lymphocytes; $CD3^+$ cells: T lymphocytes) and mononuclear phagocytes ($F4/80^+$ cells). Scale bar, 400 μm. **(C)** Representative H&E-stained microscopy images and Masson's Trichrome of lung, liver, and intestine of vFLIP chimera mice generated at different ratio (vFLIP/WT ratio 0/1; 1/1; 3/1; 1/0). Scale bar, 100 μm.

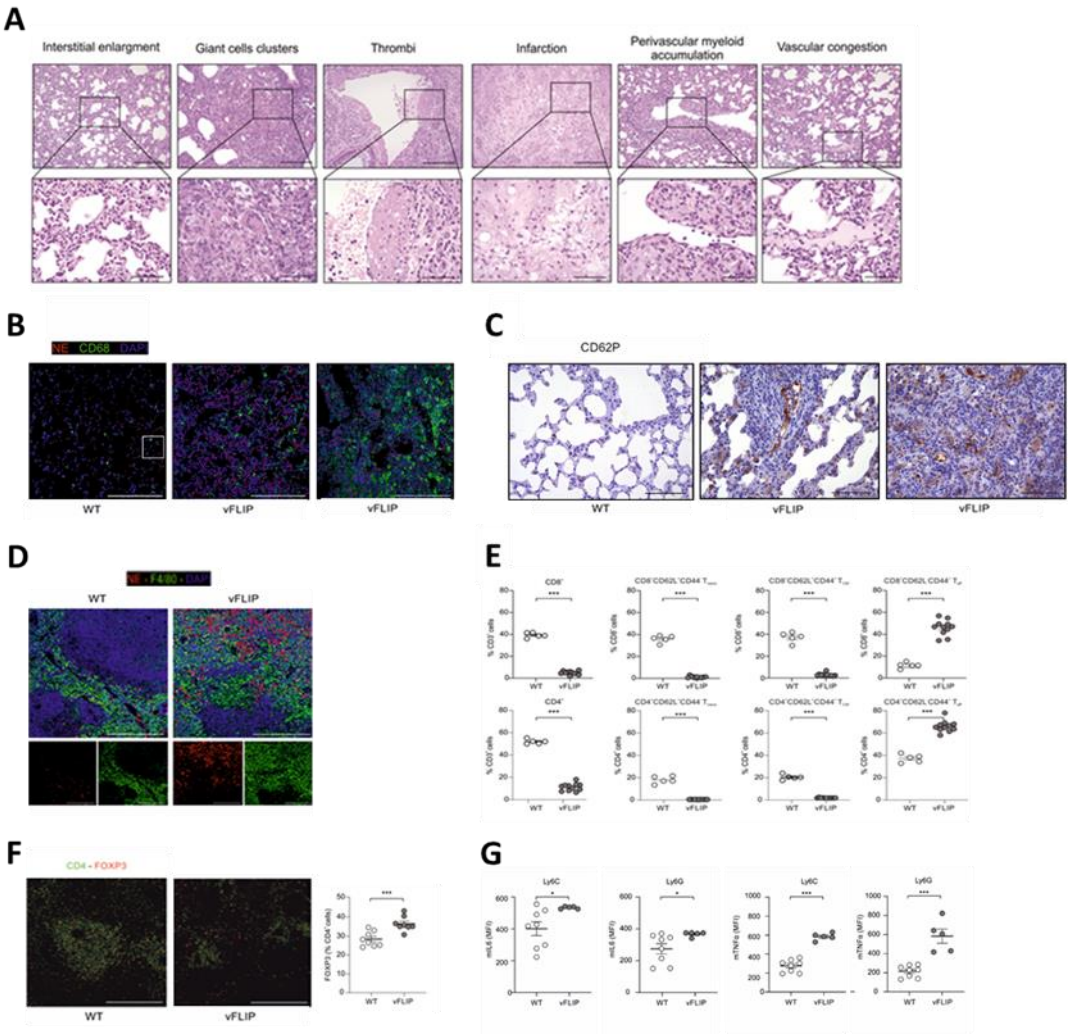

Figure 20. vFLIP-mediated multi-organ immune dysregulation in chimera mice resembles immunological scenario observed in ROSA26.vFLIP Tg mice (A) Representative H&E-stained microscopy images of pathological score: interstitial enlargement, giant cells clusters, thrombi, infarction, perivascular myeloid accumulation, vascular congestion, fibroplasia organization and peribronchiolar or perivascular infiltrate in lungs of vFLIP chimera mice. Scale bar, 200 μm (upper panel) and 50 μm (bottom panel). **(B)** Representative IF staining of lung-infiltrating neutrophils (NE^+ cells) and mononuclear phagocytes ($CD68^+$ cells) in WT and vFLIP chimera mice. Cells were stained for DAPI (blue), neutrophils elastase (NE) (red, middle panel), and CD68 (green, panel on the right). Scale bar, 200μm. **(C)** P-selectin (CD62P) presence in lung of WT (panel on the left) or vFLIP chimera mice by H&E staining. Scale bar, 100μm. **(D)** Representative IF staining of spleen-infiltrating neutrophils (NE^+ cells) and mononuclear phagocytes ($F4/80^+$ cells) in WT or vFLIP chimera mice. Cells were stained for DAPI (blue), NE (red, middle panel),

and F4/80 (green, bottom panel). Scale bar, 200µm. **(E)** Flow cytometry analysis of $CD3^+$ T cell subsets in the spleen of vFLIP chimera mice (n=11) and WT mice (n=5). Lymphocytes were segregated into $T_{effector}$ ($CD62L^-CD44^+$), T_{naive} ($CD62L^+CD44^-$) and $T_{central\ memory}$ ($CD62L^+CD44^+$). The analysis was performed on percentage of $CD4^+$ or $CD8^+$ cells. **(F)** Representative IF staining of $CD4^+$ $FoxP3^+$ cells in spleen of vFLIP chimera mice (n=8) and WT (n=8). **(G)** Dot plots of IL-6 and TNF-α expression (reported as mean fluorescence intensity, MFI) in mononuclear ($Ly6C^+$ cells) and polymorphonuclear ($Ly6G^+$ cells) myeloid cells in spleen of WT (n=8) or vFLIP chimera mice (n=9). Data are reported as mean ± S.E.M. *$p \leq 0.05$, **$p \leq 0.01$ and ***$p \leq 0.001$ by Mann–Whitney test **(E, F, G)**.

3. vFLIP chimera model promotes the activation of STAT3 pathway which distinguishes FLIP-over-expressing suppressive monocytes

We investigated further, in vFLIP chimera model, the pathways induced by vFLIP over-expression in myeloid compartment. We observed that in both lung and splenic tissues, pSTAT3 was mostly expressed in mononuclear phagocytes (identified as $CD68^+$ or $F4/80^+$ cells in lung and spleen respectively) and in neutrophils (NE^+ cells) compared to normal mice (**Figures 21A-B**). In detail, we firstly performed a single-cell RNA sequencing (scRNA-seq) on lung-infiltrating cells of 2 WT and 2 vFLIP chimera mice. After preprocessing, quality control steps, integration and cell annotation, a total of 31,274 mouse cell transcriptomes were obtained across WT and vFLIP mice. All the cells were visualized through t-distributed stochastic neighbor embedding (t-SNE) assessing the cell proportions across the different mouse samples to have a global overview of the cell composition. The cell identification was performed using multiple reference-based cell annotation and manual inspection. Only 2% of mouse cells were labeled as Unclassified. When we compared the percentage of each cell type across WT and vFLIP conditions, vFLIP mice showed a higher proportion of neutrophils (~65%) compared to WT mice (~23%) and a marked decrease in T (~5% vFLIP; ~17% WT) and B lymphocytes (~3% vFLIP; ~21% WT), confirming the data previously reported in **Figure 3**. Conversely, monocytes (~9% vFLIP; ~12% WT) and macrophages (~13% vFLIP; ~16% WT) were comparable between the two groups

(**Figure 21C**). Secondly, to picture a global overview about biological pathways activated in vFLIP chimera mice, we performed GSEA comparing vFLIP and WT cells. The analysis was performed in lung tissues. The 50 hallmark gene sets from MSigDB[351] were used as input for GSEA. We noticed a significant up-regulation in inflammatory responses, TNF-α signaling via NF-κB and JAK-STAT3 signaling (**Figure 21D**). Notably, these processes were related to the over-expression of several pro-inflammatory mediators such as Il1b, Ccrl2, Il1a and Tnf (**Figure 21E**). All these results are in line with previous data about FLIP-mediated controlling of NF-κB and STAT3 signaling activation reported in FLIP-enforced myeloid cells[66, 356]. We demonstrated that even *in vivo* vFLIP chimera model, the over-expression of FLIP could be associated with a dysfunctional activity of immune cells, with a suppressive myeloid cell's involvement in damaged tissues, and an inflammatory scenario as reported in ROSA26.vFLIP Tg mice[66]. Therefore, to confirm our previous *in vitro* data, obtained from STAT3 targeting in myeloid cells, we investigated in *in vivo* model the impact of STAT3 pathway inhibition on FLIP-mediated uncontrolled immune dysregulation.

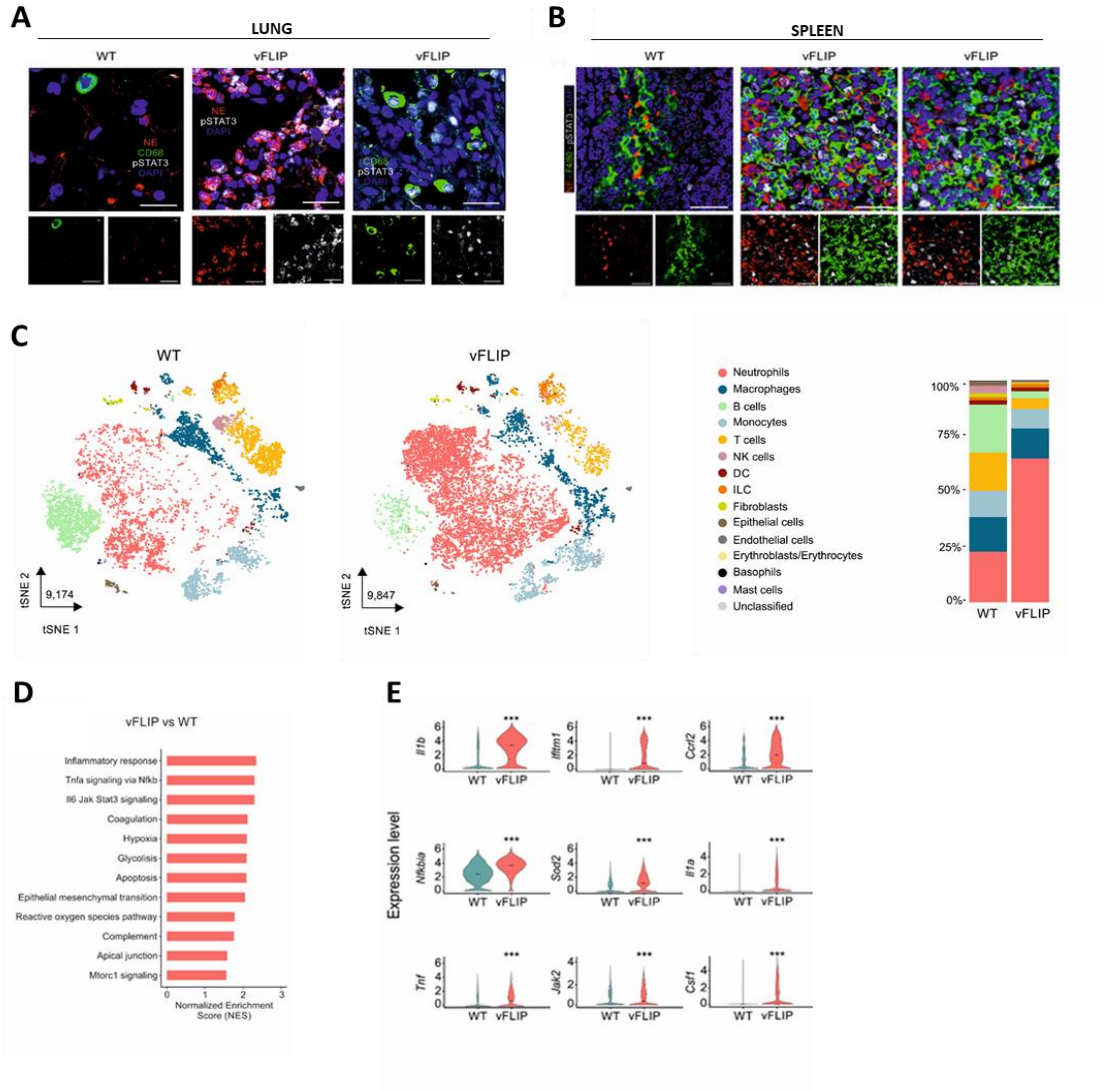

Figure 21. STAT3-dependent inflammation in vFLIP chimera mice. (A, B) Representative IF staining of lung **(A)** and spleen **(B)**-infiltrating neutrophils and mononuclear phagocytes in WT or vFLIP chimera mice. Scale bar, 20 µm. Cells were stained for DAPI (blue), NE (red, middle panel), CD68 **(A)** or F4/80 **(B)** (green, bottom panel), and pSTAT3 Tyr705 (grey). **(C)** tSNE representation of scRNA-seq from 2 WT and 2 v-FLIP chimera mice lungs (WT: 9174; vFLIP: 9874) colored according to cell type. Stacked bar plots representing cell-type proportions across WT and vFLIP conditions. **(D)** Bar plot representing the upregulated (NES > 0, adjusted p-value <0.05) hallmark gene sets in the analysis of vFLIP chimera mice vs WT cells obtained through GSEA analysis. **(E)** Violin plots showing the expression of key genes that drive the upregulation of inflammatory response, TNF-α signaling via NF-κB and JAK-STAT3 signaling pathway in the lung of vFLIP chimera mice. The asterisks denote statistically significant

upregulation in the comparison between vFLIP and WT conditions (*p < 0.05, **p < 0.01, ***p < 0.001).

4. STAT3 targeting restrains immunopathology and inflammatory conditions in vFLIP chimera mice

In order to dampen the FLIP-mediated uncontrolled immune dysregulation in chimera model we investigated the efficacy of two STAT3 inhibitors, silibinin and baricitinib. Four weeks post bone-marrow transplantation, peripheral blood of recipient mice was analyzed for the establishment of BM chimerism in recipients (T0) and chimera mice that displayed at least 20% of donor-derived cells were randomized before beginning treatment. Then, mice were treated every two days by using 8 intraperitoneal administrations of baricitinib (10 mg/Kg) or silibinin (100 mg/Kg). IHC analysis of spleen demonstrated a reduction in systemic lymphopenia of treated vFLIP chimera mice. Especially, we observed that baricitinib treatment was able to induce a raise in both $CD3^+$ (T lymphocytes) and $B220^+$ (B lymphocytes) cells, whereas silibinin affected only T lymphocyte frequency. $F4/80^+$ cells reported a decrease after both treatments in splenic tissues of chimera compared to WT mice (**Figure 22A**). Moreover, by analyzing eight different parameters in lungs of vFLIP chimera mice (i.e. interstitial enlargement, vascular congestion, perivascular neutrophils, presence of thrombi, presence of infarction, fibroplasia, foam cell clusters and perivascular infiltrate), we confirmed a reduction in the pathological score of inflammatory pneumonia in treated mice (**Figure 22B**). Furthermore, consistent with involvement of inflammatory cytokines in pathological conditions such as vFLIP-mediated immune dysregulation, the treatments with STAT3 inhibitors revealed a strong reduction of plasma concentration of several pro-inflammatory cytokines. Indeed, IL-6, TNF-α, IL-1β and IL-10 peripheral levels significantly decreased in treated chimera compared to untreated ones that produced abnormal cytokines levels. For the analysis, peripheral cytokines levels at T0 (before starting the treatment) were reported as control (**Figure 22C**).

To explore further the molecular underpinnings of the inflammatory shutdown induced by treatments, we evaluated the lung-infiltrating leukocyte profile of

treated and untreated vFLIP chimera mice by scRNA-seq to assess the effect of pharmacological treatments on the proportions of the main cellular subsets. Lung pooled from 3 untreated-chimera, 3 silibinin-treated and 3 baricitinib-treated chimeras were used for the analyses. 10^4 cells of cell suspension were loaded on GemCode Single Cell instrument to generate single cell GEMs. The quality control steps were performed individually for each sample using R package "Seurat"[337, 338, 339] and "Scrublet"[340] and the data integration was carried out by using the standard Seurat v3 integration procedure[339]. Principal component analysis (PCA) was performed on the top 2,000 most variable features obtained using the 'vst' procedure of Seurat. The top 20 principal components were used to execute t-distributed stochastic neighbor embedding (tSNE) algorithm and to project the cells into a 2-dimensional space. SingleR[341] with gene expression profiles from Immunological Genome Project[342] and Mouse RNA-seq[343] were used in combination with scMCA[344] for cell type identification. Ultra-rare (<20 cells) cell annotations were discarded, and final cell identify was obtained taking the classification determined by reference datasets. Cells were annotated as "Unclassified" if differently labelled with reference datasets. The analysis showed that both treatments reduced the neutrophil proportion (~82% UT; ~76% silibinin; ~66% baricitinib), with a compensatory increase in other cells, such as T and B lymphocytes, indicating a trend towards rebalancing the lung-infiltrating leukocyte frequency (**Figure 22D**). Moreover, GSEA analysis, which was performed on the same samples, reported an up-regulation of IFN-α/-γ pathways in both STAT3-based treatments compared to controls, and, simultaneously, the down-regulation of gene signatures associated to inflammatory response, JAK-STAT3-dependent signaling and TNF-α signaling via NF-κB (**Figure 22E**). Consistent with this effect, several inflammatory genes, such as *Il1b, Clec5a, Ccrl2* and *Ifitm1* were down-regulated while *Ifitm3*, *Stat1* and *Isg15* genes, which are associated to IFN response pathways, were up-regulated in baricitinib-treated vFLIP mice (**Figure 22F**). These data demonstrated that STAT3-targeting approaches can alter not only the tissue immune cell composition of vFLIP-over-expressing murine model, by prevent T cell dysregulation and reducing the myeloid cells infiltration, but also the treatments are able to mitigate the inflammatory pathology, both locally and

systemically, by affecting the aberrant FLIPs-STAT3 feedforward loop while keeping the antiviral response active.

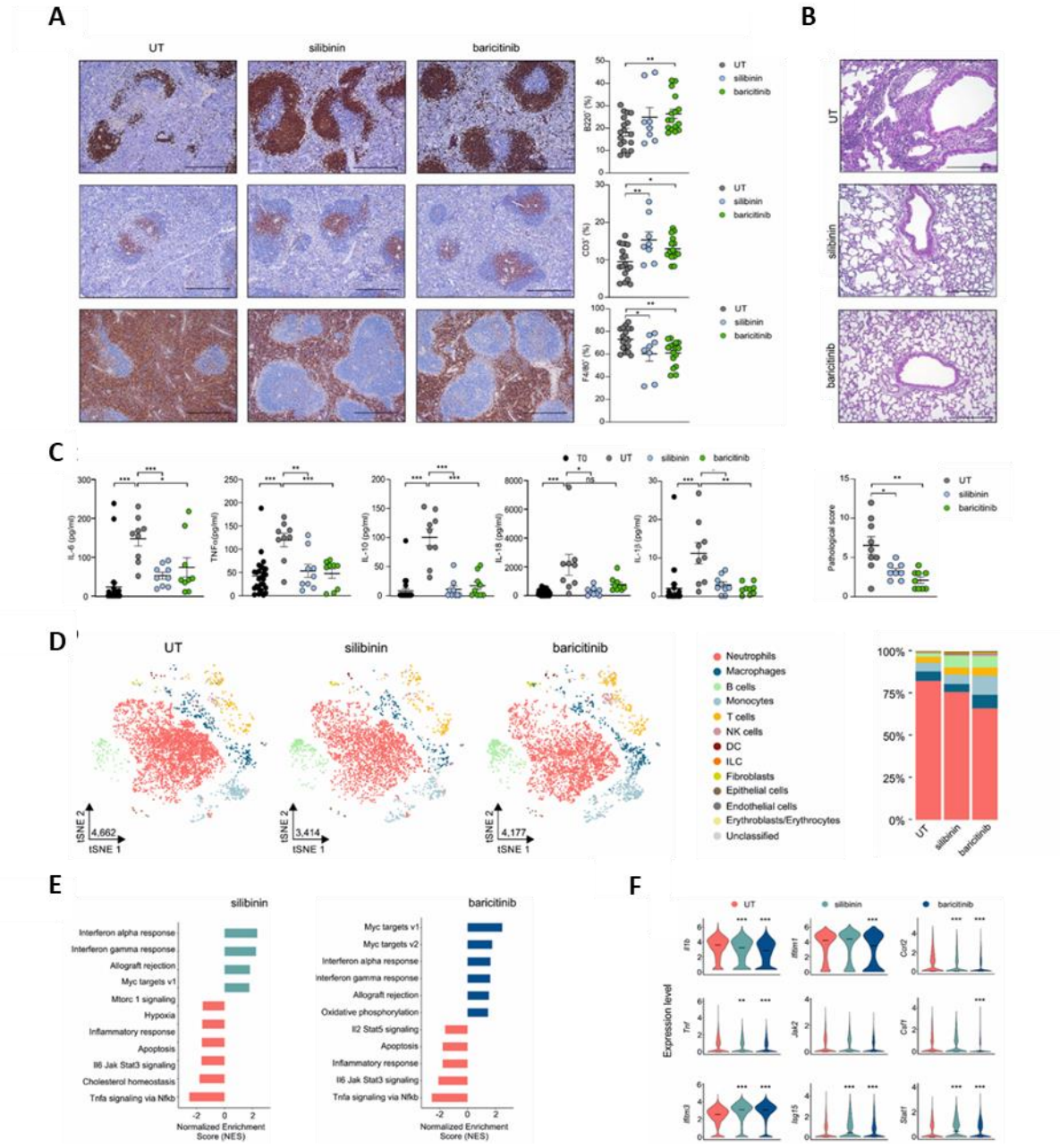

Figure 22. STAT3 targeting reduces lung damage and both multi-organ and systemic immune dysfunctions in vFLIP chimera mice. (A) Lymphocytes (B cells: $B220^+$ cells; T cells: $CD3^+$ cells) and macrophages ($F4/80^+$ cells) quantification in spleens of untreated (n = 14), silibinin (n = 8), and baricitinib (n = 16) vFLIP chimera mice by H&E staining. Scale bar, 200 μm. **(B)** Pathological score of lungs of untreated (n = 14), silibinin (n = 8),

and baricitinib (n = 16) vFLIP chimera mice by H&E staining. Scale bar, 200 μm. **(C)** Analysis of cytokines levels in serum of vFLIP chimera mice before treatment (T0) or at the end of treatment (untreated n= 9, n = 9; silibinin, n = 9; baricitinib). **(D)** tSNE representation of scRNA-seq from lung tissue of untreated (4662) mice and treated with silibinin (3414) and baricitinib (4177) colored according to cell type. Stacked bar plots representing cell-type proportions across conditions. **(E)** Bar plot representing some of the up- and down-regulated (adjusted p-value <0.05) hallmark gene sets of treated compared to untreated vFLIP chimera lung cells obtained through GSEA analysis. **(F)** Violin plots showing the expression of genes involved in inflammatory response, JAK-STAT3 signaling pathway, and interferon response in the lung of treated or untreated vFLIP chimera mice (*p < 0.05, **p <0.01, ***p < 0.001). Data are reported as mean ± S.E.M. *p ≤ 0.05, **p ≤ 0.01, and ***p ≤ 0.001 by Student's t-test, Mann-Whitney test.

5. SARS-CoV-2 infection in COVID-19 patients induces c-FLIP over-expression and c-FLIP-correlated immunosuppressive properties in myeloid cells, and displays a dysregulated immunological landscape similar to vFLIP chimera model

Viruses have evolved a myriad of ways to escape host apoptotic process and thereby preserve infected cells from early death[218]. A mechanism of immune evasion implemented by viruses is the induction of c-FLIP or proteins with high homology to c-FLIP to block caspase-mediated cell death[132]. As already explained, ROSA26.vFLIP Tg mice was used by our laboratory as murine model for our experiments given the homology between virus-induced FLIP (v-FLIP), from Kaposi's sarcoma virus, and c-FLIP proteins. Thus, FLIP expression is not only linked to oncology or inflammatory conditions but also to viral replication by favoring the suppression of host cell death.

For these reasons, we investigated the FLIP expression in SARS-CoV-2 infection of COVID-19 patients to determine the involvement of this protein in such pathology. We started analyzing the c-FLIP presence in lung tissue in 23 patients infected by SARS-CoV-2 (COVID-19). Patients affected by bacterial pneumonia (BP; n= 4) or other diseases (non-respiratory diseases (NRD)); n = 4) were used as control. Firstly, when we examined the lung structure by analysis of H&E-stained

microscopy images, the respiratory tract of COVID-19 patients reported a massive lung infiltration compared to control groups (**Figure 23A, first line**) which is in keeping with heterogeneous inflammation and tissue damage reported in literature for COVID-19 patients[357, 358]. These data mirror the pathological immune features of our mouse model (**Figure 19C**). Then, we evaluated the number of FLIP-expressing $CD68^+$ myeloid cells (which encompass alveolar macrophages, monocytes/interstitial macrophages and histiocytes[358, 359, 360]). We noticed that COVID-19 samples displayed a variable number of FLIP-expressing $CD68^+$ cells (**Figure 23A, second line**) suggesting an accumulation of $FLIP^+$ myeloid cells during COVID-19 progression which does not characterize BP and NRD conditions. Conversely, COVID-19 samples displayed also a moderate and heterogeneous infiltration of neutrophils, identified as NE positive cells, which were not positive also for FLIP (data not reported). When we moved to peripheral compartment, the data reported that not only the percentage of c-FLIP-expressing $CD14^+$ cells were increased in COVID-19 patients, as showed by immunofluorescence analysis (**Figure 23B**), but also that circulating monocytes of COVID-19 patients revealed a significant raise in c-FLIP expression compared to HDs, as showed by FACS analysis (**Figure 23C**). The up-regulation of c-FLIP expression and a linear correlation between c-FLIP expression in monocytes and their immunosuppressive properties (**Figure 23D**), were in agreement with our previous findings in PDAC patients[66]. Moreover, a linear correlation between the surface expression of CD274 marker (PD-L1) and c-FLIP was reported in COVID-19 circulating monocytes (**Figure 23E**), hinting common mechanisms of innate immunity modulation in COVID-19 and cancer. Finally, in order to compare the pulmonary immune landscape of v-FLIP chimera mice and COVID-19 patients, we evaluated the lung-infiltrating leukocytes in bronchoalveolar lavage fluids (BALB) of severe COVID-19 patients (n=7; WHO= ordinal score 7). The patients were admitted to ICU of Verona Hospital. A procedure similar to mouse cell integration and annotation was performed in order to assess cell composition in human BAL samples. Human scRNA-seq data from BALs was obtained from the Gene Expression Omnibus (GEO) under accession GSE157344. SingleR was executed using reference gene signatures from Blueprint/ENCODE[345, 346], Human primary

cell atlas[361] and Monaco immune data[347]. tSNE and stacked bar plots representations of scRNA-seq from fatal COVID-19 BALs patients (19,996) showed patient-specific leucocyte infiltration. The most representative immune component is represented by neutrophils. Moreover, a low percentage of T lymphocytes distinguishes COVID-19 patients' BAL samples (**Figure 23F**). This immunological landscape resembles the v-FLIP mediated immune dysregulation observed in lung tissue of vFLIP chimera model.

Considering all data above, we could suppose that c-FLIP could steer the immune dysregulation and inflammation damage which characterizes COVID-19 patients. c-FLIP could also determine the suppressive activity of peripheral monocytes in infected patients. The immune dysfunction, in both local and peripheral compartments, which distinguishes SARS-CoV-2 infection, resembles the vFLIP-induced immunological scenario observed in chimera mice. Therefore, these data suggest that FLIP expression might be crucial in the progression of COVID-19 infection.

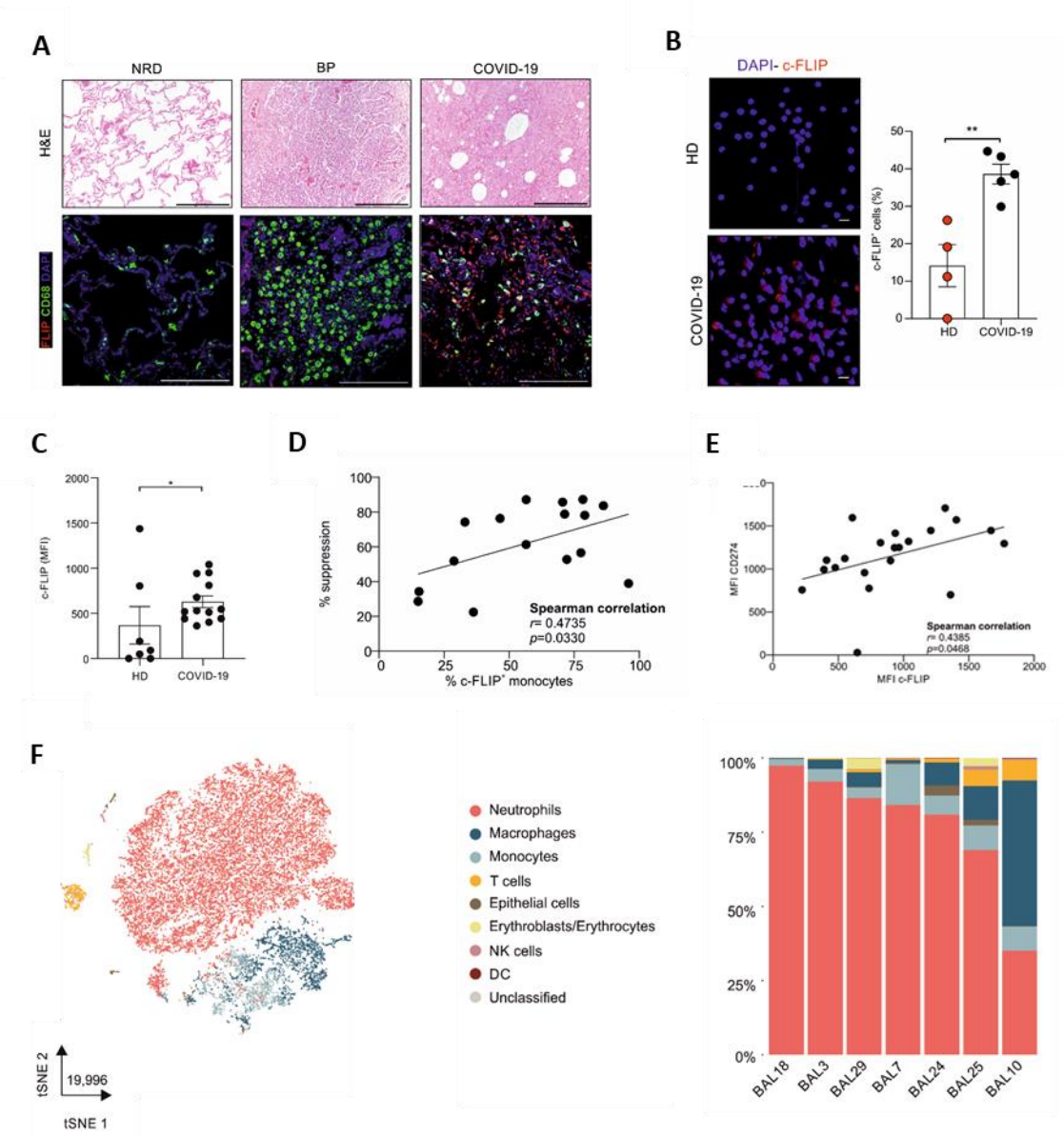

Figure 23. c-FLIP expression and c-FLIP-correlated suppressive properties in COVID-19 infection-derived monocytes. (A) Representative H&E-stained microscopy images of lung tissue of non-respiratory disease (NRD), bacterial pneumonia (BP), and COVID-19 patients (upper panel). Scale bar, 200µm. Representative IF staining of $CD68^+$ myeloid cells. Cells were stained for CD68 (green), c-FLIP (red), and DAPI (blue) (second line). Scale bar, 20 µm. **(B)** Quantification and representative IF staining of c-FLIP in circulating monocytes ($CD14^+$ cells) purified from HDs (HD, n=4) or COVID-19 patients (n=5). Cells were stained for DAPI (blue) and c-FLIP (red). Scale bar, 10µm. Data are reported as percentage of $c\text{-}FLIP^+$ cells. **(C)** FLIP expression in circulating $CD14^+$ cells purified from health donor (HD, n=7) or COVID-19 patients (n=13). Data are reported as

mean fluorescence intensity (MFI) of c-FLIP on $CD14^+$ cells. **(D)** Correlation between percentage of monocytes suppression and percentage of circulating c-FLIP-expressing monocytes isolated from COVID-19 patients (n=16). **(E)** Correlation between CD274 (PD-L1) and c-FLIP expression in COVID-19 circulating $CD14^+$ cells (n=19). **(F)** tSNE representation of scRNA-seq from 7 fatal COVID-19 BALs patients (19,996) colored according to cell type. Stacked bar plots representing cell type proportions across all the human BAL samples. Correlation analysis was performed by Spearman's rank correlation **(D, E)**. Data are reported as mean ± S.E.M. **(B, C**).

6. pSTAT3 over-expression in both COVID-19 patients and virus-infected, HFH4-hACE2 transgenic mice and the efficacy of STAT3 targeting to mitigate the suppressive activity of COVID-19-derived monocytes

Previously, we found that the enforced c-FLIP expression was able to induce the upregulation of genes typical of MDSCs signatures and responsible for their immunosuppressive activity, such as STAT3[66]. Moreover, it has already been reported in this thesis that FLIP over-expression could be associated not only with a dysfunctional activity of immune cells, but also with an inflammatory scenario, as demonstrated by the activation of pro-inflammatory STAT3 pathway in vFLIP chimera mice. Furthermore, since STAT3 hyperactivation was advanced as the orchestrator of most commonly COVID-19-associated features, such as rapid coagulopathy, thrombosis, tissue fibrosis, production of inflammatory cytokines and chemokines, as well as T cell lymphopenia[362], we next evaluated the expression of pSTAT3 in the selected pathological lung fields. We detected a weak pSTAT3 expression in NRD samples, while a limited pSTAT3 pattern was restricted to stromal cells in bacterial pneumonia sections. However, consistent and diffuse expression of pSTAT3 was shared in COVID-19 samples by numerous cell types; among them, several $CD68^+FLIP^+$ alveolar macrophages (**Figure 24A, first line**), and histiocytic cells (**Figure 24A, second line**). Interestingly, $CD68^+FLIP^+pSTAT3^+$ cells were present in 56.5% (13/23) of analyzed cases and their presence significantly correlated with a shorter time to fatal evolution, expressed as number of hospitalization days (i.e. absence of $CD68^+FLIP^+pSTAT3^+$ cells (n=10) 25 ± 14.4 days *vs*. presence of $CD68^+FLIP^+pSTAT3^+$ cells (n=13) 18

± 9.3 days; p=0.0223). Then, we assessed the pSTAT3 expression in fresh circulating monocytes ($CD14^+$ cells) isolated from SARS-CoV-2 infected individuals. We observed a significant direct correlation between pSTAT3 and c-FLIP expression in circulating $CD14^+$ cells of COVID-19 patients (**Figure 24B**), hinting to the aberrant activation of FLIP/STAT3 axis in myeloid cells not only at pulmonary site but also in periphery. The STAT3 pathway in myeloid cells is relevant for acquiring immunosuppressive functions[54, 55, 363] and for driving production of cytokines during immune disorders[364], two conditions jointly cooperating to establish a severe lymphopenia, one the signs of clinical severity in COVID-19 patients. Indeed, when we evaluated the cytokine levels (especially IL-6 and TNF-α), we noticed that greater amount of cytokines secreted by COVID-19 patients monocytes correlated directly with pSTAT3 expression (**Figure 24C**), consistent with published data about the monocyte contribution to the cytokine storm[323, 365].

To establish a direct link between FLIP and pSTAT3 dysregulation following SARS-Cov-2 infection, we analyzed the lung of mice transgenic for hACE2 (HFH4-hACE2 mice) that were intranasally infected with either SARS-CoV-2 or mock virus, as previously described[333]. Examination of lung tissues 7 days after virus challenge demonstrated that SARS-CoV-2 infection induced severe pneumonia characterized by increased $CD11b^+$ myeloid cell accumulation in perivascular and alveolar locations. More interestingly, lung-infiltrating myeloid cells in SARS-CoV-2-infected mice expressed higher pSTAT3 levels than the control group. We also observed an increase of c-$FLIP^+$ cells in the lung of SARS-CoV-2-infected mice and a raise of pSTAT3 expression in c-$FLIP^+$ cells (**Figure 24D**).

Moreover, the presence of p-$STAT3^+$c-$FLIP^+CD68^+$ lung-infiltrating cells was observed exclusively in SARS-CoV-2-infected mice (**Figure 24E**). The phenotype of myeloid cells in infected murine model resembles as observed not only in vFLIP chimera mice but also in COVID-19 infected lung tissue where the myeloid subsets are converted into FLIP- and pSTAT3-expressing elements characterized by pro-inflammatory and immunosuppressive features. These results confirm a link between STAT3 and FLIP in SARS-CoV-2 infection.

In order to confirm further the FLIP-STAT3 axis and the FLIP-induced inflammation pathways in COVID-19 infection, as observed in vFLIP chimera mice with inflammation landscape induced by FLIP over-expression, we matched GSEA results obtained from chimera model with GSEA analysis of bulk RNA-seq data of lung from hACE2 transgenic mouse infected with Sars-CoV-2[366]. Comparing v-FLIP up-regulated pathways with those enriched following infection of hACE2 mice (day 7 post infection *vs* day 0), we found that SARS-CoV-2-induced inflammatory pathways were shared with vFLIP chimera mice. Indeed, we noticed a significant up-regulation in inflammatory responses, TNF-α signaling via NF-κB and JAK-STAT3 signaling pathways (**Figure 24F**). Interestingly, these data are in line with transcriptomic analysis using additional animal models of SARS-CoV-2 infection[367]. In summary, a conserved landscape of myeloid cells enriched for transcriptional signatures associated with the inflammatory response was detailed in the lung environment of both vFLIP chimera mice and severe COVID-19 patients, in line with the concept that FLIP-expressing myeloid cells drive lung pathology. Considering all data above, STAT3 targeting could represent a viable approach to mitigate the FLIP-mediated inflammatory pathology not only in vFLIP chimera model, as already reported, but also in COVID-19 patients. Treatments with baricitinib and silibinin on circulating monocytes of patients reported a significant preservation of T cell proliferation compared to untreated controls (**Figure 24G**). These results indicated that STAT3 targeting may prevent T cell dysregulation by limiting FLIP-associated immunosuppressive features of SARS-CoV-2-eductaed myeloid cells, endorsing the clinical results about baricitinib efficacy in altering immunoregulatory properties of myeloid cells in COVID-19 patients[323].

Taken together, these data indicate that the STAT3-targeting might be effective in tempering immunopathological disorders triggered by the accumulation of FLIP-expressing cells such as in infection and inflammatory contexts, and supposedly even in oncology conditions.

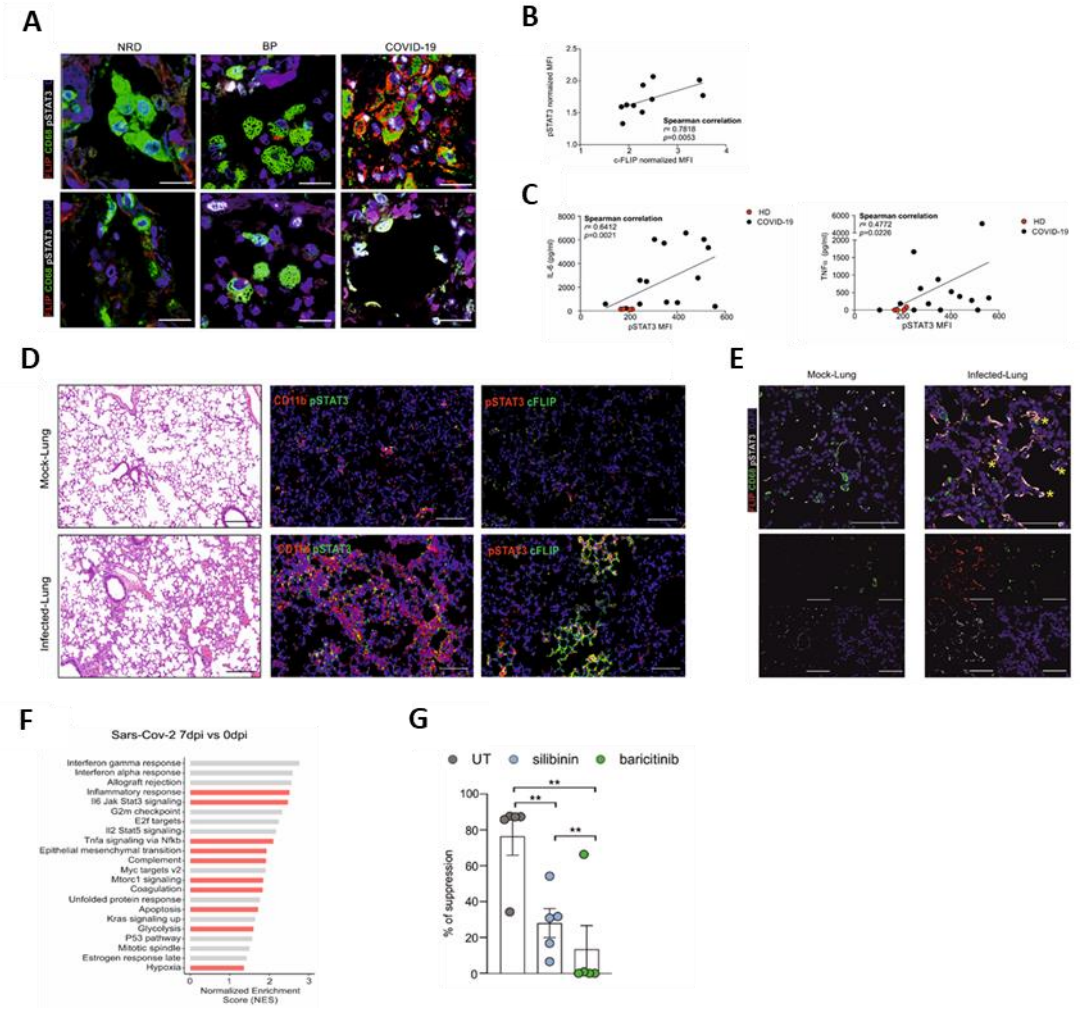

Figure 24. pSTAT3 expression in SARS-CoV-2-infected hosts and the efficacy of STAT3 targeting in mitigating the immunological disorder in COVID-19 patients. (A) Representative IF staining of alveolar macrophages (first line) and histiocytic cells (second line) in lung tissue of non-respiratory disease (NRD), bacterial pneumonia (BP), and COVID-19 patients (upper panel). Cells were stained for CD68 (green), c-FLIP (red), pSTAT3 (white), and DAPI (blue). Scale bar, 20 µm. **(B)** Correlation between pSTAT3 and c-FLIP normalized expression in circulating monocytes ($CD14^+$ cells) isolated from COVID-19 patients (n = 10). **(C)** Correlation between the release of IL-6 or TNF-α cytokines and pSTAT3 expression in monocytes ($CD14^+$ cells) from HD (red, n = 4) and COVID-19 patients (black, n = 13). **(D)** Representative H&E-stained microscopy images of lung tissue of HFH4-hACE2 transgenic mice SARS-CoV-2-infected or mock-infected mice. Scale bar, 200 µm. pSTAT3, c-FLIP, and CD11b expression levels were detected by indirect immunofluorescence (IFA) staining. Scale bar, 100 µm. **(E)** Representative IFA staining of FLIP (red), CD68 (green), pSTAT3 (white) and DAPI (blue) in lungs of HFH4-

hACE2 transgenic mice SARS-CoV-2-infected or mock-infected. Scale bar, 60μm. **(F)** Bar plot representing the upregulated (NES > 0, adjusted p-value <0.05) hallmark gene sets in bulk RNA-seq data obtained through GSEA analysis of ACE2-transgenic mice infected with Sars-CoV-2[57] comparing day 7 post infection (dpi) with mock-infected (0 dpi). Red bars refer to the gene sets enriched in both v-FLIP chimera mice and ACE2-transgenic mice. **(G)** Functional assay performed at 1:3 ratio of PBMCs:$CD14^+$ cells using purified monocytes from COVID-19 patients (n = 5) treated for 30 minutes with silibinin (200μM), baricitinib (200μM) or left untreated. Correlation analysis was performed by Spearman's rank correlation **(B, C)**. Data are reported as mean ± S.E.M. *p ≤ 0.05, **p ≤ 0.01 and ***p ≤ 0.001 by Mann–Whitney test **(B, C, G)**.

7. ICIs treatments restrain the normal c-FLIP expression levels and consequently mitigate the suppressive activity of NSCLC's cohort monocytes

In this thesis, we also investigated the role of c-FLIP in oncology. Our laboratory has already demonstrated that percentage of $CD14^+$ $c\text{-}FLIP^+$ cells significantly increased in cancer condition and especially in PDAC patients[66]. In this thesis, we analyzed the c-FLIP involvement in lung cancer cohort and c-FLIP expression trend over clinical treatments. 32 patients with stage IIIC/IV NSCLC were enrolled in the study from January 2019 to June 2020. According to the current guidelines[208], Pembrolizumab was used as first line treatment in patients with PD-L1≥50%, whereas Nivolumab, Atezolizumab or Durvalumab (for PD-L1≥1%) were chosen as second or further line treatment after chemotherapy. RECIST 1.1 criteria were used to assess clinical tumor response. NSCLC cohort's peripheral blood samples were collected before treatment initiation (T0) and at different time points during the treatment, to evaluate the c-FLIP expression over time. More specifically, to reduce the variability among different administered immunotherapies, blood samples were clustered in two time points, 1-2 months (time point 1, T1) from the immunotherapy administration, and 3-6 months after therapy initiation (time point 2, T2). According to RECIST criteria and clinical evaluation, patients were classified as Responders (R) and Non-Responders (NR) at T2. When we evaluated the c-FLIP presence in PBMC of NSCLC's cohort, we observed that the percentage of $CD14^+$ $c\text{-}FLIP^+$ cells remarkably decreased in the R sub-group after first ICIs

administration, while it remained high or increased in the NR sub-group. The data obtained allowed to discriminate R and NR already at the first time point (**Figure 25A** first and second lines**, 25B** upper panel). Interestingly, the percentage of c-FLIP$^+$ cells reached by R group after treatment equaled the values reported for HDs[66]. We also noticed that c-FLIP expression on the CD14$^+$ cells noticeably decreased in the R sub-group after T0, while it reached higher levels in the NR one (**Figure 25A** first and third lines**, 25B** lower panel). Hence, clinical response to ICIs treatment in patients suffered from advanced NSCLC, seems to progress at the same pace with percentage of c-FLIP$^+$ circulating monocytes and their c-FLIP expression. More intriguingly, both parameters might represent promising predictive biomarkers, easily measurable by FACS analysis, for predicting the clinical outcome of NSCLC subjects. As already reported by this laboratory[66], c-FLIP expression is constitutively required for the development and survival of the monocytic subset of MDSCs and cancer-induced FLIP expression promotes immune suppressive functions in mature monocytes. For this reason, we decided to evaluate the suppressive activity of this population in NSCLC cohort and to analyze changes in monocytes function over ICIs immunotherapy. Data showed that CD3$^+$ cells proliferative potential kept increasing during the treatment in the R group, whereas a strong reduction of lymphocytes proliferation was reported after T1 in NR group (**Figure 25C**). These data confirm that monocytes in R lose their suppressive potential along the treatment, while in NR monocytes a recover of suppressive properties after T1 can be observed, consistent with previous data reported for c-FLIP percentage or expression in CD14$^+$ cells. These results suggest for the first time that immunotherapy with ICIs can impact the suppressive function of tumor-derived monocytes in NSCLC R patients, presumably through c-FLIP modulation. Moreover, a linear correlation was observed between the immunosuppressive activity of circulating CD14$^+$ cells and their c-FLIP expression at T0 in advanced NSCLS patients (**Figure 25D**), in agreement with previous findings of our research group PDAC patients[66]. This further assesses the c-FLIP involvement in immunosuppression of lung tumor-derived monocytes.

Taking all the above into account, these results highlight, for the first time, the critical role of c-FLIP in the mechanisms of immunosuppression in lung cancer

setting. Therefore, the c-FLIP-related mechanisms of innate immunity modulation are involved not only in the inflammatory process, or in the SARS-CoV-2 mediated infection processes, but also in the different cancer contexts.

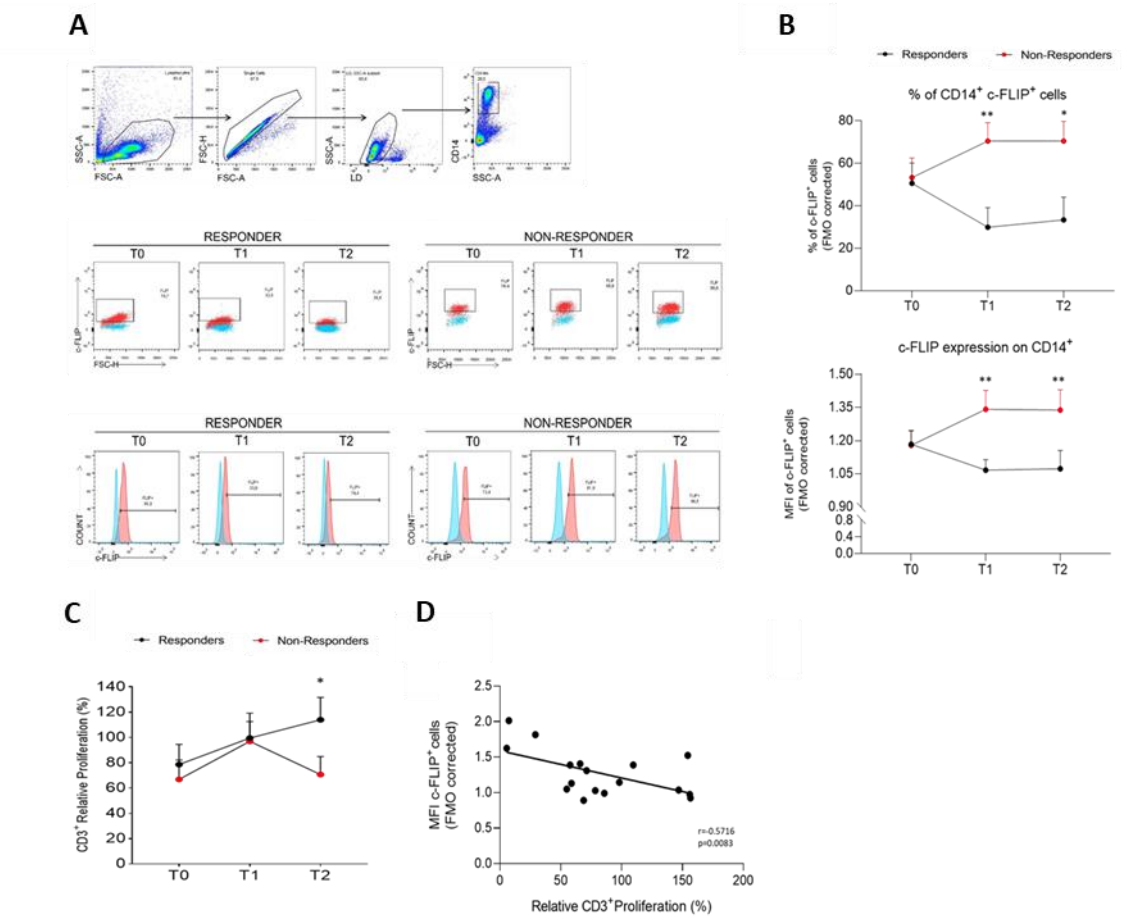

Figure 25. c-FLIP expression and immunosuppressive capacity of NSCLC patients 'monocytes. (A) FACS gating strategy for $CD14^+$ cells selection (first line) and representative dot plots of c-$FLIP^+$ cells percentage (second line), and histograms of c-FLIP fluorescence intensity (FI) (third line), at different time points in responder (R) and non-responder (NR) monocytes. The % of $CD14^+$ c-$FLIP^+$ cells (red, second line) or the FI of c-$FLIP^+$ cells (red, third line) for each time point were normalized for its corresponding FMO (blue). **(B)** Percentages of $CD14^+$ c-$FLIP^+$ cells (upper panel) and c-FLIP expression in $CD14^+$ monocytes (lower panel) in the NSCLC cohort at each time point of treatment. Data about c-FLIP expression is reported as c-FLIP mean fluorescence intensity (MFI) on $CD14^+$ cells. **(C)** Immunosuppressive assay on peripheral NSCLC-derived monocytes during immunotherapy. Data are reported as percentage of $CD3^+$ relative proliferation. **(D)** Spearman correlation between $CD3^+$ relative proliferation and c-FLIP expression in

NSCLC-derived monocytes at T0. Data are reported as mean ± SEM. Statistical analyses were performed by Mann-Whitney test **(B,C,D)**.

8. c-FLIP as transcriptional regulator of immune responses-involved genes through p50 physical interaction in c-FLIP over-expressing monocytic cells

Finally, given the c-FLIP involvement in immunosuppressive phenotype in several cancer settings, such as PDAC, as already demonstrated by our laboratory[66], but also in NSCLC-derived monocytes, we investigated further the molecular role of c-FLIP behind the mechanisms of immunomodulation in this myeloid cell subset. As already reported by Fiore *et al*.[66], c-FLIP over-expression promoted the nuclear translocation of the NF-κB subunits p65 and p50, mediators of the canonical NF-κB activation pathway, while no difference in the p52 subunit translocation was detected. More interestingly, nuclear co-localization between c-FLIP and p50 was observed. Therefore, we hypothesized that c-FLIP could play unexpected and key epigenetic role by regulating directly or indirectly, by binding NF-κB subunits, the transcription of suppression-involved genes. To explore the c-FLIP molecular role in gene transcription, we analyzed the physical interactions between this target and NF-κB subunits in c-FLIP-over-expression conditions. $CD14^+$ human monocytes isolated from HDs were transiently transfected with c-FLIP-encoding mRNA to push the c-FLIP over-expression. Considering the target protein's over-expression in tumor context[158-165], we decided to maximize *in vitro* the protein expression, through transfection technique, in order to study the underlying mechanisms of c-FLIP in overexpression conditions and to define potential partners/co-factors that participate in the signaling network c-FLIP-induced.

The transfection was performed by using mRNA encoding for both long and short splice forms of c-FLIP (50% $c\text{-}FLIP_L$ + 50% $c\text{-}FLIP_S$ mRNAs). GFP-encoding mRNA was used as control to estimate the transfection efficiency by FACS analysis. Our experiments reported a transfection efficiency of 50% (**Figure 26A,** upper panel). c-FLIP detection was performed on nuclear and cytoplasmatic extracts of transfected cells. Western blot analysis allowed to detect 2 c-FLIP splicing forms ($c\text{-}FLIP_L$, $c\text{-}FLIP_S$) and $c\text{-}FLIP_L$ fragment after cleavage in the

caspase8-cleavage site, c-FLIP(p43). More importantly, these isoforms were detected not only in the cytoplasmic but also in the nuclear fraction (**Figure 26B**). The presence of the protein in the nuclear compartment visibly confirms that c-FLIP over-expression favors its translocation inside the nucleus. We decided to move on to another *in vitro* human model that our laboratory has already developed and standardized. This model, THP1 immortalized cell line, is easier to handle than HDs-derived $CD14^+$ monocytes, and allowed us to comprehend the key role of c-FLIP before translating all the information into human samples. THP1 cell line was transiently transfected with c-FLIP-encoding mRNA for inducing enforced c-FLIP expression, and with GFP-encoding mRNA as control. The transfection efficiency reached levels similar to $CD14^+$ cells transfection (**Figure 26A,** lower panel). Moreover, to assess the suitability of immortalized *in vitro* human model as suppressive monocytic cell line, we evaluated the expression through Real Time qPCR of some immunosuppression-correlated genes such as *CD274*, *IDO1*, *PTGS2* and *IL6* which were reported to be upregulated in c-FLIP over-expressing human monocytes isolated from HDs[65]. *IDO1*, *IL6* and *CD274* genes appeared to be significantly upregulated in c-FLIP-over-expressing THP1 cells after transfection compared to GFP-transfected control (**Figure 26C**). These results confirm c-FLIP transfected THP1 cell lines as *in vitro* human suppressive monocytic model for our experiment. Finally, we carried out the c-FLIP detection, through western blot analysis, on nuclear and cytoplasmatic extracts of transfected THP1 cell line. As reported for $CD14^+$ cells, even in THP1 cells, c-FLIP splicing forms ($c\text{-}FLIP_L$, $c\text{-}FLIP_S$) and c-FLIP(p43) fragment were detected in both compartments (**Figure 26D**) strengthening our hypothesis that c-FLIP over-expression might promote directly or indirectly the transcriptional regulation by its nuclear translocation. To quantify the nuclear c-FLIP we availed of the IF staining. The co-localization study was performed by analyzing c-FLIP fluorescence signal inside the nucleus in transfected THP1 cells with Imaris software. Approximatively 100% of GFP^+ cells reported c-FLP fluorescence signal. Moreover, we observed a wide range of intensity signal of protein target. $c\text{-}FLIP^+$ cells, on average, presented 30% of maximum fluorescence intensity of c-FLIP protein (**Figure 26E**, panels on the right), hypothesizing a correlation with different transfection efficacy. Looking at

nuclear localization of c-FLIP (**Figure 26F**), we observed that the percentage of volume of c-FLIP signal localized inside the nucleus was on average 25% of total observed c-FLIP signal. The quantification of nuclear c-FLIP allowed us to continue our study aimed at understanding the protein partners and the epigenetic role of c-FLIP at transcriptional level.

To investigate the biological mechanisms with which c-FLIP translocates inside the nucleus, we focused on examining the physical interactions between c-FLIP and canonical NF-κB subunits. For this purpose, we performed a p105/50 IP from c-FLIP transfected THP1 cell lines. Non-immunoprecipitated lysates were used as control. On the total lysate we observed the presence of not only NF-κB1 complex (p105) and its p50 subunit, but also the presence of another protein, above p50 detection, which we supposed to be a post translational modification of p50 induced by c-FLIP overexpression. Moreover, all the 3 isoforms of c-FLIP (c-$FLIP_L$, c-$FLIP_S$, and c-FLIP(p43)) were observed in c-FLIP immunoprecipitated sample (even if the c-$FLIP_L$ isoform was not detected appropriately because of noise signal caused by the unspecific detection of the α-p105/50 antibody heavy chain) (**Figure 27A**). This data demonstrates that in total lysate p50 is physically bound to c-FLIP. Looking separately at cytoplasmic and nuclear fractions, we observed the presence of both NF-κB1 complex (p105) and p50 subunit in cytoplasmic compartments, and only the p50 in the nuclear one. Much more intriguing, all the 3 c-FLIP isoforms were detected in both fractions in the c-FLIP over-expressing THP1 cells (**Figure 27B**). Collectively these results highlight the generation of a c-FLIP/p50 complex in the cytoplasm able to translocate in the nucleus, where it could act as a transcriptional regulator of immunosuppression-associated gene expression.

Therefore, these results encouraged us to investigate deeply the c-FLIP activity inside the nucleus. We focused on researching the specific c-FLIP-binding DNA sequences of which c-FLIP could regulate the transcription. We performed a ChIP-seq on c-FLIP-associated DNA sequences in THP1 cell line transiently transfected with c-FLIP encoding mRNA after c-FLIP IP. Firstly, DNA sequences significantly enriched in c-FLIP transfected THP1 cells compared to GFP transfected ones, were selected for the analysis. ChIP-Seq analysis allowed to identify more than 4000 c-FLIP-associated DNA sequences. 776 of them were located within “upstream 10

Kb sequences" of annotated transcriptional starting sites of specific genes; 2654 sequences were overlapping known genes ("overlapping sequences"); 1024 were inside an intergenic region ("intergenic sequences"). Moreover, genes belonging to these DNA sequences included not only protein coding genes, but also several other gene biotypes such as miRNA, lincRNA and snoRNA coding genes. Downstream sequencing analysis focused on the selection of protein coding genes and "upstream 10 Kb sequences". Genes obtained from the selection were further filtered by gene ontology (GO) annotation in order to screen only the genes involved in the immune system processes. Finally, downstream analysis turned out in a list of 27 genes: MUC4, SLAMF6, TSPn14, SERINC3, FCG, CCT2, SIRT1, DYN, MMP12, ST6GAL1, OPRD1, SIX4, HDAC4, PIP, IL9, SLAMF7, ACKR3, LGALS7B, CALML5, ADGRG3, FZD9, MERTK, DPEP1, DEFA1, ENPP2, COTL1, TNF. The expression of these genes was later assessed by real time qPCR in c-FLIP transfected THP1 cells. Results pointed out the upregulation of 2 genes over the others, IL9 and TNF, and the down-regulation of 9 genes, SLAMF6, CCT2, SIRT1, SIX4, HDAC4, SLAMF7, MERTK, DPEP1, and DEFA1. Moreover, MUC4 and ACKR3 genes report a slight upregulation, even though not statistically significant (**Figure 27C**).

Among these putative targets the most intriguing ones are:

IL9: it encodes interleukin-9 (IL-9). IL-9 was reported to contribute to immunosuppression mediated by Tregs and mast cells (MCs) in B-cell non-hodgkin's lymphoma[368]. Moreover, IL-9 transcriptional upregulation was associated with an increase in DNA binding activity of NF-κB subunit p50[369], regulating negatively the immune responses in inflammatory conditions.

TNF: it encodes TNF-α involved in a range of pathologies[370]. Upon binding to TRAF, TNF-α is able to activate NF-κB signaling pathway, one of the transcriptional regulators of IL-9 promoter[371]. c-FLIP over-expressing $CD14^+$ cells were reported to upregulate genes, such as TNF, associated to MDSC-related molecular programs[66]. In the tumor context, this suggests that TNF-α over-expression in circulating monocytes could trigger a positive feedback mechanism to increase NF-κB signaling and IL-9 and c-FLIP transcription.

SLAMF6-7: these proteins encoded by these genes, belong to Signaling Lymphocyte Activation Molecules (SLAM) receptors family. They are expressed on NK cells, a subset of $CD8^+$ T lymphocytes, mature DCs, and activated B cells[372]. SLAMF6 functions as a coreceptor in the process of NK cell activation as reported in X-linked lymphoproliferative patients[373]. SLAMF6 is an important regulator of T cell activation by increasing T cell adhesiveness[374]. In NK, SLAMF7 (known also as CS1) acts to activate the Phosphoinositide 3-kinases PI3K and phospholipase Cγ signaling pathways resulting in activation of NK cell function[375]. Studies demonstrated that CS1 plays an inhibitory role in human monocytes to control proinflammatory immune responses[376].

HDAC4: it encodes histone deacetylase 4, an important enzyme involved in epigenetic cell control, leading DNA to be less accessible to transcription[377]. In c-FLIP expressing monocytic cell line, HDAC4 down-expression could be critical for promoting the transcription of genes involved in immunosuppression.

SIRT1: it encodes for a member of the sirtuin protein family, homologs to the yeast Sir2 protein. The functions of human sirtuins have not yet been determined; however, yeast sirtuin proteins are known to regulate epigenetic gene silencing and suppress recombination of rDNA[378]. It has reported that the expression of SIRT1 is involved in inhibiting tumor growth and invasion, and decreased levels of this protein are showed in patients suffering from gastric cancer[379].

MUC4: it encodes for mucin 4. Mucins are transmembrane glycoproteins expressed by the epithelial cells and are involved mainly in preventing infection at mucosal surfaces[380]. Mucins contribute to the development, progression, and metastasis of tumor cells and an aberrant expression of MUC4 has also been associated to a variety of carcinomas, including PDAC and NSCLC[380].

ACKR3: it encodes for atypical chemokine receptor 3 (ACKR3), also known as C-X-C chemokine receptor type 7 (CXCR-7). It is a member of the G protein-coupled receptor family and indirectly participates to chemotaxis events mediating chemokine internalization and degradation. CXCR-7 has been reported to be over-expressed in numerous cancer types, including lung cancer, and increasing evidence suggests that it positively affects tumor cell proliferation and migration, and tumor

angiogenesis[381]. ACKR3 is considered not only as a potential therapeutic target, but also as a new prognostic factor[382].

This data supports further the hypothesis that c-FLIP could be able to act as a transcriptional regulator translocating inside the nucleus as complex with p50 NF-κB subunit and to bind directly DNA sequences involved in both inflammation and tumor progression processes. Although these are preliminary data, the obtained results suggest new putative therapeutic strategies aimed at interfering with the transcriptional role of c-FLIP for the treatment of diseases characterized by FLIP-associated immune dysregulation.

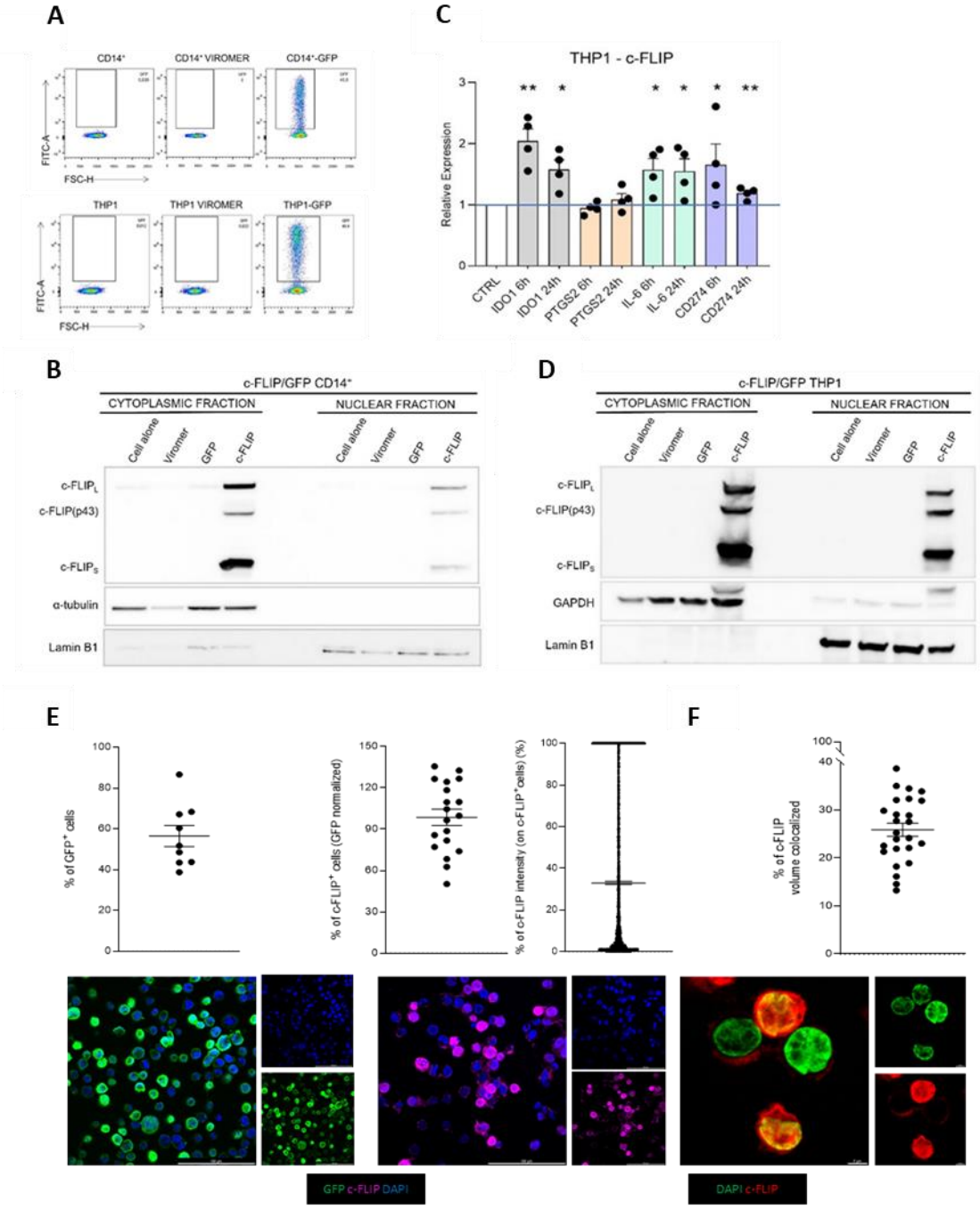

Figure 26. c-FLIP-over-expression in monocytic cells promotes the nuclear translocation of protein target. (A) Representative plots showing GFP signal detected by flow cytometry in HDs isolated $CD14^+$ cells (above panels) and in THP1 cell line (lower panels) transfected with GFP-encoding mRNA. $CD14^+$ cells and THP1 cell line alone and with viromer (transfection reagent) only, were used as control. **(B,D)** Cytoplasmic and nuclear c-FLIP protein expression assessed by western blot in $CD14^+$ cells (**B**) and THP1 cell line (**D**) transfected with c-FLIP mRNAs. $CD14^+$ cells and THP1 cell line alone, with

viromer (transfection reagent) only and transfected with GFP-encoding mRNA were used as control. GAPDH or α-tubulin and Lamin B1 housekeeping proteins were used as controls of the cytoplasmic and nuclear compartment respectively. **(C)** Relative expression of immunosuppressive genes at different time points (6 hours, and 24 hours) in THP1 cells transfected with c-FLIP mRNAs, measured by real-time qPCR. GAPDH was used as housekeeping gene and the analysis was performed by normalizing with THP1 cell line transfected with GFP-encoding mRNAs. **(E)** Quantification and representative IF staining of GFP (panels on the left), and c-FLIP (panels on the right) in GFP- or c-FLIP-, respectively, transfected THP1 cell lines in three independent experiments. Cells were stained for c-FLIP (magenta), and DAPI (blue). GFP signal is showed in green. Scale bar, 100 μm. Data are reported as percentage of GFP^+ cells, and c-$FLIP^+$ cells. Data about c-FLIP were normalized with percentage of GFP^+ cells of each experiment. **(F)** Quantification and representative IF staining of c-FLIP in c-FLIP-transfected THP1 cell lines in three independent experiments. Cells were stained for c-FLIP (red), and DAPI (green). Scale bar, 5 μm. Data are reported as percentage of c-FLIP colocalized volume. Data are reported as mean ± SEM. Statistical analyses were performed by Mann-Whitney test **(C,E,F)**.

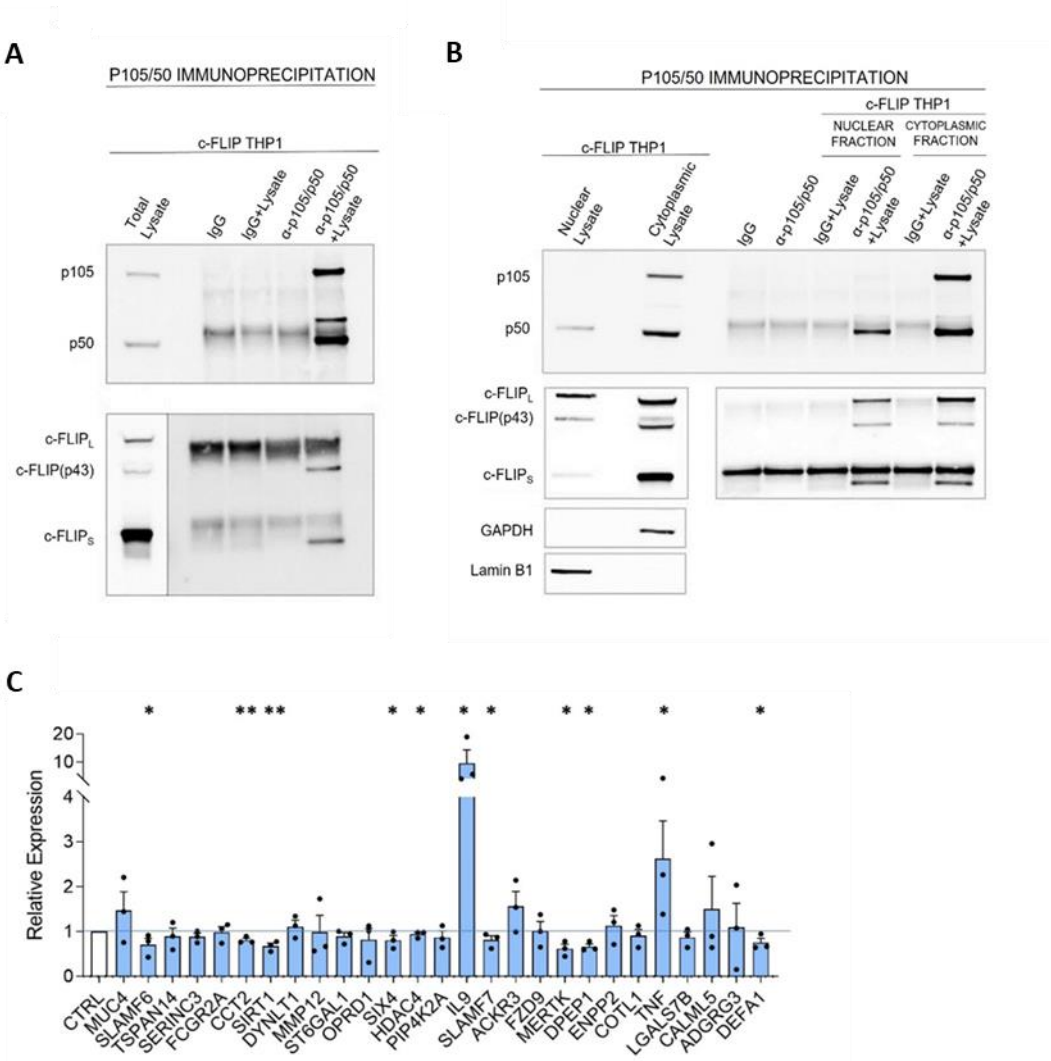

Figure 27. Physical interaction between p50 NF-κB subunit and c-FLIP in nuclear compartment in c-FLIP over-expressing cells, and ChIP-seq analysis on c-FLIP-linked genes. (A, B) Western blot analysis of p50/p105 and c-FLIP performed after p105/p50 IP on total lysate **(A)** and on cytoplasmic and nuclear fractions **(B)** in c-FLIP-over-expressing THP1 cells. GAPDH and Lamin B1 were used respectively as cytoplasmatic and nuclear housekeeping proteins. Non-immunoprecipitated lysates (total, cytoplasmatic and nuclear) were used as control. IgG, α-p105/50 antibodies only and total/nuclear/cytoplasmatic protein lysates of c-FLIP over-expressing THP1 cells after IgG IP were used as further technical controls for IP. **(C)** Relative expression of c-FLIP-linked genes in THP1 cells transfected with c-FLIP-encoding mRNAs, measured by real-time qPCR. Genes used for this analysis were revealed by ChIP-seq analysis in c-FLIP-encoding mRNAs transfected THP1 cell line. Data were normalized by using GFP-encoding mRNA transfected THP1 cells. GAPDH was used as housekeeping gene. Data are represented as mean ± SEM. Statistical analysis was performed by paired Student's *t* test.

DISCUSSION

The role of MDSCs in altering the immune response was described in several pathological contexts such as cancer, inflammation disorders and infectious diseases[4, 7, 8,329]. High number of circulating MDSCs in cancer patients is associated with poorer prognosis and a weaker response to treatment[83]. It has been reported that the main mediator of tumor-induced immunosuppression is represented by M-MDSCs subset[96]. c-FLIP has been shown to be over-expressed in several cancer settings[158, 330], and its up-regulation in tumor-derived monocytes has been reported[66]. Our laboratory demonstrated a direct role of c-FLIP in triggering immunosuppressive properties in human monocytes under over-expression conditions. c-FLIP in these cells led to the upregulation of many genes associated to the MDSCs' immunosuppressive activity, such as STAT3, IL-6, IDO1 and PD-L1[65]. STAT3 is required to prevent the normal differentiation of myeloid progenitor cells, promoting their conversion in functional MDSCs[56]. It promotes the suppressive activity of MDSCs by binding different sites on the ARG-1 promoter to favor its transcription[54] and by inducing the transcription of IDO through NF-κB activation[64]. Therefore, strategies based on neutralizing STAT3 might be promising in order to restrain the FLIP-mediated immune dysregulation not only in oncology context but also in other disease in which MDSCs can play a pathogenic role.

In vFLIP chimera mice, that over-express v-FLIP in the myeloid lineage and present systemic lymphopenia, systemic cytokine storm, massive infiltration of myeloid cells in several organs, and an inflammatory scenario, it was observed an over-expression of pSTAT3 in both lung and splenic myeloid cells. Moreover, we registered an upregulation of inflammatory response characterized by JAK-STAT3 signaling in lung tissue. The pro-inflammatory STAT3 pathway activation in vFLIP chimera mice confirms that the FLIP over-expression confers both immunosuppressive and pro-inflammatory properties. Treatments with silibinin[331] and baricitinib[120, 121, 343] were previously tested in *in vitro* differentiated MDSCs to evaluate their efficacy of modulating the MDSCs' suppressive activity. The administration of these drugs in *in vivo* model demonstrated a reduction in systemic lymphopenia, a decrease of $F4/80^+$ cells and neutrophils in splenic and lung tissue

respectively, a profound reduction in the pathological score of inflammatory pneumonia, and an impairment of plasma concentration of several pro-inflammatory cytokines (IL-6, TNF-α, IL-1β and IL-10) in treated mice. Moreover, an up-regulation of IFN-α/-γ pathways and simultaneously a down-regulation of gene signatures associated to inflammatory response, JAK-STAT3-dependent signaling, were reported in both STAT3-based treatments compared to controls. These data demonstrate that STAT3-targeting can mitigate the FLIP-mediated inflammatory pathology, both locally and systemically, and it can dampen FLIP-associated uncontrolled immune dysregulation. Moreover, our results demonstrated that this targeting provides a significant disease control in mice with CRS by affecting the aberrant FLIPs-STAT3 feedforward loop. Although, in the last decades, mouse models have been developed to replicate clinical stage and outcomes of CRS[383, 384], no suitable and appropriate experimental *in vivo* models have been developed to identify alterations in molecular and cellular processes that might highlight the triggers of CRS. Our study based on a tissue-specific Tg conditional knock-in mouse model offer a novel tool for defining the mechanisms that fuel inflammation and CRS-associated immune dysfunctions.

FLIP expression was observed to be also linked to viral replication by favoring the suppression of host cell death[218, 219, 220, 221, 222, 223, 224]. We wondered whether FLIP expression could be involved in the progression of COVID-19 infection caused by SARS-CoV-2 virus. In this work, studying the immune infiltration in respiratory tract of COVID-19 patients, we demonstrated an accumulation of c-FLIP-expressing $CD68^+$ myeloid cells compared to control conditions. We also reported an increase of c-FLIP expression in COVID-19-derived peripheral monocytes and a correlation between the immunosuppressive activity of this population and the percentage of circulating c-$FLIP^+$ $CD14^+$ cells, as previously reported in PDAC patients[66]. The massive accumulation of neutrophils in BALF of severe COVID-19 patients, and the over-expression of STAT3 in lung myeloid cells of infected hosts, mirror the landscape observed in lung tissue of vFLIP chimera mice. Moreover, a direct correlation between STAT3 expression in circulating monocytes and peripheral levels of pro-inflammatory cytokines (IL-6, TNF-α) was reported in COVID-19 patients. These data, which correlated with a shorter time to fatal

evolution of COVID-19 cohort, confirmed the aberrant activation of FLIP/STAT3 axis in myeloid cells. The STAT3 pathway in myeloid cells is relevant for acquiring immunosuppressive functions[54, 323, 363] and for driving production of cytokines during immune disorders[364], two conditions jointly cooperating to establish a severe lymphopenia and to determine clinical severity in COVID-19 patients[253, 303, 355]. Our data suggest that FLIP expression might be crucial in the progression of COVID-19 infection and it is determinant to exacerbate inflammation in these patients. To dampen the viral replication and immune dysregulation SARS-CoV-2 virus-induced, we hypothesized to target STAT3 pathway, by using silibinin and baricitinib. We demonstrated that immunosuppression in circulating monocytes isolated from COVID-19 patients can be reverted by STAT3 inhibitors. Data presented here are in line with recent clinical results about baricitinib efficacy in controlling SARS-CoV-2-mediated immune dysregulation[323] and with the decision of FDA to approve this drug as monotherapy in hospitalized adults and pediatric patients 2 years of age older[385], as well as in combination with remdesivir for the treatment of sever COVID-19 patients. These results sustain the therapeutic effectiveness of STAT3 on-target strategy to mitigate immune disorders triggered by the accumulation of FLIP-expressing cells such as in infection and inflammatory contexts, and supposedly even in oncology conditions, which serve as a foundation for the development of more accurate and evidence-based therapies.

Given the c-FLIP involvement in the LC progression[169], and the MDSCs role in driving angiogenesis and metastasis in this tumor[80,386], it could be intriguing to elucidate better the implication of c-FLIP in determining the immunosuppressive activity of monocytes in NSCLC. Our data reported that both percentage of c-FLIP^{+} circulating monocytes and c-FLIP expression in the same population, were in keeping with the clinical response to ICIs treatment. We also reported that the ICIs immunotherapy promoted recovery of T-cell proliferation in the responder group of patients, by impacting the suppression of the monocytic subset, probably as consequence of dampening c-FLIP expression. Therefore, our data highlight the critical role of c-FLIP in the mechanisms of immunosuppression in lung cancer. Furthermore, the assessment of c-FLIP expression revealed to anticipate the clinical evaluation of patients to immunotherapies. Therefore, c-FLIP evaluation might

represent a promising predictive biomarker, easily measurable by FACS analysis, to optimize the current oncology treatments for this or other cancer setting. A longer follow-up and a larger number of enrolled patients could permit to discriminate better and comprehend the significant differences between responder and non-responder patients.

Several evidence demonstrate that the aberrant expression of FLIP in immature progenitors drives development of a massive and rapid myeloproliferative disease characterized by accumulation of immunosuppressive cells and release of high number of inflammatory cytokines mirroring a cytokine release syndrome[387], as observed in vFLIP Tg mice and vFLIP chimera mice. Therefore, in the future we plan to evaluate the expression of c-FLIP and c-FLIP-regulated genes in myeloid cells from myelodysplastic patients and to perform transcriptome analysis to depict molecular pathway involved in these syndromes. The milestone achievement will allow us to investigate FLIP in other cancer setting not only in solid tumor. Moreover, we plan to test therapeutic efficacy of STAT3 inhibitors used in this work to control the progression of myelodysplastic disease in pre-clinical models by blocking the unveiled targets.

Our laboratory showed that canonical NF-κB pathway was mainly up-regulated in the c-FLIP-induced suppressive phenotype[66]. Our work allowed to demonstrate that in over-expression conditions, as reported in the literature in cancer settings, c-FLIP is able to translocate into the nucleus compartment as complex with p50 NF-κB subunit. We hypothesized that c-FLIP, as a "moonlighting" protein, is able to play a key role as transcriptional regulator, unrelated with its original anti-apoptotic function. The ChIP-seq analysis revealed that several DNA sequences, that are involved in different immune system processes, were physically c-FLIP-linked, supporting the hypothesis that c-FLIP can act as transcriptional regulator of genes involved in both inflammation and tumor progression processes.

For the future, we plan to investigate further the FLIP/p50 interaction in monocytic subset isolated from tumor-bearing, as well as in human monocytes freshly isolated from cancer patients. In these human samples, we will perform the ChIP-Seq analysis in order to validate the c-FLIP-linked genes in cancer setting. We will focus on IL-9 and TNF-α encoding genes, the most upregulated genes observed in ChIP-

Seq analysis performed in the c-FLIP transfected THP1 cell line. At moment, we are also studying the c-FLIP-linked protein after c-FLIP immunoprecipitation. In this way, we could have a complete mapping of functional mechanisms induced by up-regulation of c-FLIP. To decode properly the biological role of FLIP/p50 complex during inflammation or immune disorders and translate these studies *in vivo,* we will generate a conditional Tg mouse model with $vFLIP^{+}p50^{-/-}$ myeloid cells. The milestone achievement will confirm the role of FLIP as a new transcriptional regulator able to drive MDSC-associated immunosuppression, and it will allow us to define the potential partners/co-factors that participate in the signaling network c-FLIP-induced. Moreover, the obtained data will allow us to discover new therapeutic targets to inhibit MDSC functions aimed at interfering with the transcriptional role of c-FLIP for the treatment of diseases characterized by FLIP-associated immune dysregulation.

REFERENCES

1. Paul, F. *et al.* Transcriptional Heterogeneity and Lineage Commitment in Myeloid Progenitors. *Cell* 163, 1663-1677 (2015).
2. Turkistany, S.A. & DeKoter, R.P. The transcription factor PU.1 is a critical regulator of cellular communication in the immune system. *Arch Immunol Ther Exp (Warsz)* 59, 431-440 (2011).
3. Bronte, V. *et al.* Recommendations for myeloid-derived suppressor cell nomenclature and characterization standards. *Nat Commun* 7, 12150 (2016).
4. Gabrilovich, D.I. Myeloid-Derived Suppressor Cells. *Cancer Immunology Research* 5, 3-8 (2017).
5. Ueda, Y., Cain, D.W., Kuraoka, M., Kondo, M. & Kelsoe, G. IL-1R Type I-Dependent Hemopoietic Stem Cell Proliferation Is Necessary for Inflammatory Granulopoiesis and Reactive Neutrophilia. *The Journal of Immunology* 182, 6477-6484 (2009).
6. Jordan, K.R. *et al.* Immunosuppressive myeloid-derived suppressor cells are increased in splenocytes from cancer patients. *Cancer Immunology, Immunotherapy* 66, 503-513 (2017).
7. Gabrilovich, D.I. *et al.* The Terminology Issue for Myeloid-Derived Suppressor Cells. *Cancer Research* 67, 425-425 (2007).
8. Veglia, F., Perego, M. & Gabrilovich, D. Myeloid-derived suppressor cells coming of age. *Nature Immunology* 19, 108-119 (2018).
9. Groth, C. *et al.* Immunosuppression mediated by myeloid-derived suppressor cells (MDSCs) during tumour progression. *British Journal of Cancer* 120, 16-25 (2019).
10. Youn, J.I., Nagaraj, S., Collazo, M. & Gabrilovich, D.I. Subsets of myeloid-derived suppressor cells in tumor-bearing mice. *J Immunol* 181, 5791-5802 (2008).
11. Dolcetti, L. *et al.* Hierarchy of immunosuppressive strength among myeloid-derived suppressor cell subsets is determined by GM-CSF. *European Journal of Immunology* 40, 22-35 (2009).
12. Bronte, V. *et al.* Identification of a CD11b(+)/Gr-1(+)/CD31(+) myeloid progenitor capable of activating or suppressing CD8(+) T cells. *Blood* 96, 3838-3846 (2000).
13. Youn, J.I. *et al.* Epigenetic silencing of retinoblastoma gene regulates pathologic differentiation of myeloid cells in cancer. *Nat Immunol* 14, 211-220 (2013).
14. Ugel, S. *et al.* Immune Tolerance to Tumor Antigens Occurs in a Specialized Environment of the Spleen. *Cell Reports* 2, 628-639 (2012).
15. Haverkamp, J.M. *et al.* Myeloid-derived suppressor activity is mediated by monocytic lineages maintained by continuous inhibition of extrinsic and intrinsic death pathways. *Immunity* 41, 947-959 (2014).

16. Solito, S. *et al.* Myeloid-derived suppressor cell heterogeneity in human cancers. *Ann N Y Acad Sci* 1319, 47-65 (2014).
17. Filipazzi, P. *et al.* Identification of a new subset of myeloid suppressor cells in peripheral blood of melanoma patients with modulation by a granulocyte-macrophage colony-stimulation factor-based antitumor vaccine. *J Clin Oncol* 25, 2546-2553 (2007).
18. Mandruzzato, S. *et al.* IL4Ralpha+ myeloid-derived suppressor cell expansion in cancer patients. *J Immunol* 182, 6562-6568 (2009).
19. Schmielau, J. & Finn, O.J. Activated granulocytes and granulocyte-derived hydrogen peroxide are the underlying mechanism of suppression of t-cell function in advanced cancer patients. *Cancer Res* 61, 4756-4760 (2001).
20. Rodriguez, P.C. *et al.* Arginase I-producing myeloid-derived suppressor cells in renal cell carcinoma are a subpopulation of activated granulocytes. *Cancer Res* 69, 1553-1560 (2009).
21. Brandau, S. *et al.* Myeloid-derived suppressor cells in the peripheral blood of cancer patients contain a subset of immature neutrophils with impaired migratory properties. *J Leukoc Biol* 89, 311-317 (2011).
22. Condamine, T. *et al.* Lectin-type oxidized LDL receptor-1 distinguishes population of human polymorphonuclear myeloid-derived suppressor cells in cancer patients. *Science Immunology* 1, aaf8943-aaf8943 (2016).
23. Nan, J. *et al.* Endoplasmic reticulum stress induced LOX-1 $^{+}$ CD15 $^{+}$ polymorphonuclear myeloid-derived suppressor cells in hepatocellular carcinoma. *Immunology* 154, 144-155 (2018).
24. Lewinsky, H. *et al.* CD84 is a regulator of the immunosuppressive microenvironment in Multiple Myeloma. *JCI Insight* (2021).
25. Alshetaiwi, H. *et al.* Defining the emergence of myeloid-derived suppressor cells in breast cancer using single-cell transcriptomics. *Science Immunology* 5, eaay6017 (2020).
26. Vanhaver, C., van der Bruggen, P. & Bruger, A.M. MDSC in Mice and Men: Mechanisms of Immunosuppression in Cancer. *Journal of Clinical Medicine* 10, 2872 (2021).
27. Zhao, F., Korangy, F. & Greten, T.F. Cellular Immune Suppressor Mechanisms in Patients with Hepatocellular Carcinoma. *Digestive Diseases* 30, 477-482 (2012).
28. Tavukcuoglu, E. *et al.* Human splenic polymorphonuclear myeloid-derived suppressor cells (PMN-MDSC) are strategically located immune regulatory cells in cancer. *European Journal of Immunology* 50, 2067-2074 (2020).

29. Diaz-Montero, C.M. *et al.* Increased circulating myeloid-derived suppressor cells correlate with clinical cancer stage, metastatic tumor burden, and doxorubicin-cyclophosphamide chemotherapy. *Cancer Immunol Immunother* 58, 49-59 (2009).
30. Solito, S. *et al.* A human promyelocytic-like population is responsible for the immune suppression mediated by myeloid-derived suppressor cells. *Blood* 118, 2254-2265 (2011).
31. Serafini, P., Mgebroff, S., Noonan, K. & Borrello, I. Myeloid-derived suppressor cells promote cross-tolerance in B-cell lymphoma by expanding regulatory T cells. *Cancer Res* 68, 5439-5449 (2008).
32. Huang, B. *et al.* Gr-1 $^{+}$ CD115 $^{+}$ Immature Myeloid Suppressor Cells Mediate the Development of Tumor-Induced T Regulatory Cells and T-Cell Anergy in Tumor-Bearing Host. *Cancer Research* 66, 1123-1131 (2006).
33. Otsuji, M., Kimura, Y., Aoe, T., Okamoto, Y. & Saito, T. Oxidative stress by tumor-derived macrophages suppresses the expression of CD3 zeta chain of T-cell receptor complex and antigen-specific T-cell responses. *Proc Natl Acad Sci U S A* 93, 13119-13124 (1996).
34. Nagaraj, S., Schrum, A.G., Cho, H.-I., Celis, E. & Gabrilovich, D.I. Mechanism of T Cell Tolerance Induced by Myeloid-Derived Suppressor Cells. *The Journal of Immunology* 184, 3106-3116 (2010).
35. Molon, B. *et al.* Chemokine nitration prevents intratumoral infiltration of antigen-specific T cells. *J Exp Med* 208, 1949-1962 (2011).
36. De Sanctis, F. *et al.* The emerging immunological role of post-translational modifications by reactive nitrogen species in cancer microenvironment. *Front Immunol* 5, 69 (2014).
37. Liu, Y., Wei, J., Guo, G. & Zhou, J. Norepinephrine-induced myeloid-derived suppressor cells block T-cell responses *via* generation of reactive oxygen species. *Immunopharmacology and Immunotoxicology* 37, 359-365 (2015).
38. Munn, D.H. *et al.* GCN2 kinase in T cells mediates proliferative arrest and anergy induction in response to indoleamine 2,3-dioxygenase. *Immunity* 22, 633-642 (2005).
39. Munn, D.H. & Mellor, A.L. Indoleamine 2,3 dioxygenase and metabolic control of immune responses. *Trends Immunol* 34, 137-143 (2013).
40. Mondanelli, G. *et al.* A Relay Pathway between Arginine and Tryptophan Metabolism Confers Immunosuppressive Properties on Dendritic Cells. *Immunity* 46, 233-244 (2017).
41. Rolinski, J. & Hus, I. Breaking immunotolerance of tumors: a new perspective for dendritic cell therapy. *J Immunotoxicol* 11, 311-318 (2014).

42. Li, J. *et al.* CD39/CD73 upregulation on myeloid-derived suppressor cells via TGF-β-mTOR-HIF-1 signaling in patients with non-small cell lung cancer. *OncoImmunology* 6, e1320011 (2017).
43. Hoskin, D.W., Mader, J.S., Furlong, S.J., Conrad, D.M. & Blay, J. Inhibition of T cell and natural killer cell function by adenosine and its contribution to immune evasion by tumor cells (Review). *Int J Oncol* 32, 527-535 (2008).
44. Lu, C., Redd, P.S., Lee, J.R., Savage, N. & Liu, K. The expression profiles and regulation of PD-L1 in tumor-induced myeloid-derived suppressor cells. *Oncoimmunology* 5, e1247135 (2016).
45. Juneja, V.R. *et al.* PD-L1 on tumor cells is sufficient for immune evasion in immunogenic tumors and inhibits CD8 T cell cytotoxicity. *Journal of Experimental Medicine* 214, 895-904 (2017).
46. Iwata, T. *et al.* PD-L1+MDSCs are increased in HCC patients and induced by soluble factor in the tumor microenvironment. *Scientific Reports* 6, 39296 (2016).
47. Morales, J.K., Kmieciak, M., Knutson, K.L., Bear, H.D. & Manjili, M.H. GM-CSF is one of the main breast tumor-derived soluble factors involved in the differentiation of CD11b-Gr1- bone marrow progenitor cells into myeloid-derived suppressor cells. *Breast Cancer Research and Treatment* 123, 39-49 (2010).
48. Elkabets, M. *et al.* IL-1β regulates a novel myeloid-derived suppressor cell subset that impairs NK cell development and function. *European Journal of Immunology* 40, 3347-3357 (2010).
49. Zhao, X. *et al.* TNF signaling drives myeloid-derived suppressor cell accumulation. *The Journal of Clinical Investigation* 122, 4094-4104 (2012).
50. Condamine, T. & Gabrilovich, D.I. Molecular mechanisms regulating myeloid-derived suppressor cell differentiation and function. *Trends in Immunology* 32, 19-25 (2011).
51. Kortylewski, M. *et al.* Inhibiting Stat3 signaling in the hematopoietic system elicits multicomponent antitumor immunity. *Nat Med* 11, 1314-1321 (2005).
52. Canè, S. *et al.* The Endless Saga of Monocyte Diversity. *Frontiers in Immunology* 10, 1786 (2019).
53. Corzo, C.A. *et al.* Mechanism Regulating Reactive Oxygen Species in Tumor-Induced Myeloid-Derived Suppressor Cells. *The Journal of Immunology* 182, 5693-5701 (2009).
54. Vasquez-Dunddel, D. *et al.* STAT3 regulates arginase-I in myeloid-derived suppressor cells from cancer patients. *J Clin Invest* 123, 1580-1589 (2013).

55. Trovato, R. *et al.* Immunosuppression by monocytic myeloid-derived suppressor cells in patients with pancreatic ductal carcinoma is orchestrated by STAT3. *Journal for ImmunoTherapy of Cancer* 7, 255 (2019).
56. Sinha, P. *et al.* Proinflammatory S100 proteins regulate the accumulation of myeloid-derived suppressor cells. *J Immunol* 181, 4666-4675 (2008).
57. Schouppe, E. *et al.* Tumor-induced myeloid-derived suppressor cell subsets exert either inhibitory or stimulatory effects on distinct CD8+ T-cell activation events. *Eur J Immunol* 43, 2930-2942 (2013).
58. Karin, M. NF- B as a Critical Link Between Inflammation and Cancer. *Cold Spring Harbor Perspectives in Biology* 1, a000141-a000141 (2009).
59. Khongthong, P., Roseweir, A.K. & Edwards, J. The NF-KB pathway and endocrine therapy resistance in breast cancer. *Endocrine-Related Cancer* 26, R369-R380 (2019).
60. Ghosh, S. & Karin, M. Missing Pieces in the NF-κB Puzzle. *Cell* 109, S81-S96 (2002).
61. Srivastava, M.K., Sinha, P., Clements, V.K., Rodriguez, P. & Ostrand-Rosenberg, S. Myeloid-Derived Suppressor Cells Inhibit T-Cell Activation by Depleting Cystine and Cysteine. *Cancer Research* 70, 68-77 (2010).
62. Liu, Y. *et al.* Contribution of MyD88 to the Tumor Exosome-Mediated Induction of Myeloid Derived Suppressor Cells. *The American Journal of Pathology* 176, 2490-2499 (2010).
63. Diao, J. *et al.* Exosomal Hsp70 mediates immunosuppressive activity of the myeloid-derived suppressor cells via phosphorylation of Stat3. *Medical Oncology* 32, 35 (2015).
64. Yu, J. *et al.* Noncanonical NF-κB Activation Mediates STAT3-Stimulated IDO Upregulation in Myeloid-Derived Suppressor Cells in Breast Cancer. *The Journal of Immunology* 193, 2574-2586 (2014).
65. Hu, X. *et al.* Transmembrane TNF-α promotes suppressive activities of myeloid-derived suppressor cells via TNFR2. *Journal of Immunology (Baltimore, Md.: 1950)* 192, 1320-1331 (2014).
66. Fiore, A. *et al.* Induction of immunosuppressive functions and NF-κB by FLIP in monocytes. *Nature Communications* 9, 5193 (2018).
67. Nefedova, Y. *et al.* Activation of Dendritic Cells via Inhibition of Jak2/STAT3 Signaling. *The Journal of Immunology* 175, 4338-4346 (2005).
68. Lee, H. *et al.* Persistently Activated Stat3 Maintains Constitutive NF-κB Activity in Tumors. *Cancer Cell* 15, 283-293 (2009).
69. Karin, N. The Development and Homing of Myeloid-Derived Suppressor Cells: From a Two-Stage Model to a Multistep Narrative. *Frontiers in Immunology* 11, 557586 (2020).

70. Zhang, J. *et al.* CCL2 expression correlates with Snail expression and affects the prognosis of patients with gastric cancer. *Pathol Res Pract* 213, 217-221 (2017).
71. Shan, J. *et al.* Genetic Variation in CCL5 Signaling Genes and Triple Negative Breast Cancer: Susceptibility and Prognosis Implications. *Front Oncol* 9, 1328 (2019).
72. Qian, B.-Z. *et al.* CCL2 recruits inflammatory monocytes to facilitate breast-tumour metastasis. *Nature* 475, 222-225 (2011).
73. Fridlender, Z.G. *et al.* CCL2 blockade augments cancer immunotherapy. *Cancer Res* 70, 109-118 (2010).
74. Fridlender, Z.G. *et al.* Monocyte chemoattractant protein-1 blockade inhibits lung cancer tumor growth by altering macrophage phenotype and activating CD8+ cells. *Am J Respir Cell Mol Biol* 44, 230-237 (2011).
75. Treffers, L.W., Hiemstra, I.H., Kuijpers, T.W., van den Berg, T.K. & Matlung, H.L. Neutrophils in cancer. *Immunological Reviews* 273, 312-328 (2016).
76. Ostrand-Rosenberg, S. Myeloid derived-suppressor cells: their role in cancer and obesity. *Current Opinion in Immunology* 51, 68-75 (2018).
77. Ostrand-Rosenberg, S., Beury, D.W., Parker, K.H. & Horn, L.A. Survival of the fittest: how myeloid-derived suppressor cells survive in the inhospitable tumor microenvironment. *Cancer Immunology, Immunotherapy* 69, 215-221 (2020).
78. Gabrilovich, D.I., Ostrand-Rosenberg, S. & Bronte, V. Coordinated regulation of myeloid cells by tumours. *Nature Reviews Immunology* 12, 253-268 (2012).
79. Ostrand-Rosenberg, S. & Fenselau, C. Myeloid-Derived Suppressor Cells: Immune-Suppressive Cells That Impair Antitumor Immunity and Are Sculpted by Their Environment. *Journal of Immunology (Baltimore, Md.: 1950)* 200, 422-431 (2018).
80. Veglia, F., Sanseviero, E. & Gabrilovich, D.I. Myeloid-derived suppressor cells in the era of increasing myeloid cell diversity. *Nature Reviews Immunology* 21, 485-498 (2021).
81. Trovato, R. *et al.* The Engagement Between MDSCs and Metastases: Partners in Crime. *Frontiers in Oncology* 10, 165 (2020).
82. Wang, Y., Ding, Y., Guo, N. & Wang, S. MDSCs: Key Criminals of Tumor Pre-metastatic Niche Formation. *Frontiers in Immunology* 10, 172 (2019).
83. Kumar, V., Patel, S., Tcyganov, E. & Gabrilovich, D.I. The Nature of Myeloid-Derived Suppressor Cells in the Tumor Microenvironment. *Trends in Immunology* 37, 208-220 (2016).
84. Keller, L. & Pantel, K. Unravelling tumour heterogeneity by single-cell profiling of circulating tumour cells. *Nature Reviews. Cancer* 19, 553-567 (2019).
85. Szczerba, B.M. *et al.* Neutrophils escort circulating tumour cells to enable cell cycle progression. *Nature* 566, 553-557 (2019).

86. Lopez-Soto, A., Gonzalez, S., Smyth, M.J. & Galluzzi, L. Control of Metastasis by NK Cells. *Cancer Cell* 32, 135-154 (2017).
87. Spiegel, A. *et al.* Neutrophils Suppress Intraluminal NK Cell-Mediated Tumor Cell Clearance and Enhance Extravasation of Disseminated Carcinoma Cells. *Cancer Discovery* 6, 630-649 (2016).
88. Wang, J. & Yang, J. Identification of CD4+CD25+CD127− regulatory T cells and CD14+HLA−DR−/low myeloid-derived suppressor cells and their roles in the prognosis of breast cancer. *Biomedical Reports* 5, 208-212 (2016).
89. Wang, P.-F. *et al.* Prognostic role of pretreatment circulating MDSCs in patients with solid malignancies: A meta-analysis of 40 studies. *OncoImmunology* 7, e1494113 (2018).
90. Zhang, S. *et al.* The Role of Myeloid-Derived Suppressor Cells in Patients with Solid Tumors: A Meta-Analysis. *PLOS ONE* 11, e0164514 (2016).
91. Gunes, E.G., Rosen, S.T. & Querfeld, C. The role of myeloid-derived suppressor cells in hematologic malignancies. *Current Opinion in Oncology* 32, 518-526 (2020).
92. Almand, B. *et al.* Increased production of immature myeloid cells in cancer patients: a mechanism of immunosuppression in cancer. *J Immunol* 166, 678-689 (2001).
93. Gabitass, R.F., Annels, N.E., Stocken, D.D., Pandha, H.A. & Middleton, G.W. Elevated myeloid-derived suppressor cells in pancreatic, esophageal and gastric cancer are an independent prognostic factor and are associated with significant elevation of the Th2 cytokine interleukin-13. *Cancer Immunol Immunother* 60, 1419-1430 (2011).
94. Eruslanov, E. *et al.* Circulating and tumor-infiltrating myeloid cell subsets in patients with bladder cancer. *Int J Cancer* 130, 1109-1119 (2012).
95. Yuan, X.K., Zhao, X.K., Xia, Y.C., Zhu, X. & Xiao, P. Increased circulating immunosuppressive CD14(+)HLA-DR(-/low) cells correlate with clinical cancer stage and pathological grade in patients with bladder carcinoma. *J Int Med Res* 39, 1381-1391 (2011).
96. Xie, Z., Ikegami, T., Ago, Y., Okada, N. & Tachibana, M. Valproic acid attenuates CCR2-dependent tumor infiltration of monocytic myeloid-derived suppressor cells, limiting tumor progression. *Oncoimmunology* 9, 1734268 (2020).
97. Ziegler-Heitbrock, L. *et al.* Nomenclature of monocytes and dendritic cells in blood. *Blood* 116, e74-80 (2010).
98. Burke, M.C., Oei, M.S., Edwards, N.J., Ostrand-Rosenberg, S. & Fenselau, C. Ubiquitinated proteins in exosomes secreted by myeloid-derived suppressor cells. *J Proteome Res* 13, 5965-5972 (2014).

99. Guilliams, M., Mildner, A. & Yona, S. Developmental and Functional Heterogeneity of Monocytes. *Immunity* 49, 595-613 (2018).
100. Mildner, A. *et al.* Genomic Characterization of Murine Monocytes Reveals C/EBPβ Transcription Factor Dependence of Ly6C- Cells. *Immunity* 46, 849-862.e847 (2017).
101. Marigo, I. *et al.* Tumor-Induced Tolerance and Immune Suppression Depend on the C/EBPβ Transcription Factor. *Immunity* 32, 790-802 (2010).
102. Lesokhin, A.M. *et al.* Monocytic CCR2(+) myeloid-derived suppressor cells promote immune escape by limiting activated CD8 T-cell infiltration into the tumor microenvironment. *Cancer Research* 72, 876-886 (2012).
103. Chen, Q., Zhang, X.H.-F. & Massagué, J. Macrophage binding to receptor VCAM-1 transmits survival signals in breast cancer cells that invade the lungs. *Cancer Cell* 20, 538-549 (2011).
104. Zhang, H. *et al.* Circulating Tumor Microparticles Promote Lung Metastasis by Reprogramming Inflammatory and Mechanical Niches via a Macrophage-Dependent Pathway. *Cancer Immunology Research* 6, 1046-1056 (2018).
105. Serafini, P., Borrello, I. & Bronte, V. Myeloid suppressor cells in cancer: recruitment, phenotype, properties, and mechanisms of immune suppression. *Semin Cancer Biol* 16, 53-65 (2006).
106. Califano, J.A. *et al.* Tadalafil augments tumor specific immunity in patients with head and neck squamous cell carcinoma. *Clin Cancer Res* 21, 30-38 (2015).
107. Grzywa, T.M. *et al.* Myeloid Cell-Derived Arginase in Cancer Immune Response. *Front Immunol* 11, 938 (2020).
108. Le Naour, J., Galluzzi, L., Zitvogel, L., Kroemer, G. & Vacchelli, E. Trial watch: IDO inhibitors in cancer therapy. *Oncoimmunology* 9, 1777625 (2020).
109. Veltman, J.D. *et al.* COX-2 inhibition improves immunotherapy and is associated with decreased numbers of myeloid-derived suppressor cells in mesothelioma. Celecoxib influences MDSC function. *BMC Cancer* 10, 464 (2010).
110. Bracci, L., Schiavoni, G., Sistigu, A. & Belardelli, F. Immune-based mechanisms of cytotoxic chemotherapy: implications for the design of novel and rationale-based combined treatments against cancer. *Cell Death Differ* 21, 15-25 (2014).
111. Suzuki, E., Kapoor, V., Jassar, A.S., Kaiser, L.R. & Albelda, S.M. Gemcitabine selectively eliminates splenic Gr-1+/CD11b+ myeloid suppressor cells in tumor-bearing animals and enhances antitumor immune activity. *Clin Cancer Res* 11, 6713-6721 (2005).

112. Le, H.K. *et al.* Gemcitabine directly inhibits myeloid derived suppressor cells in BALB/c mice bearing 4T1 mammary carcinoma and augments expansion of T cells from tumor-bearing mice. *Int Immunopharmacol* 9, 900-909 (2009).
113. Tomihara, K. *et al.* Gemcitabine chemotherapy induces phenotypic alterations of tumor cells that facilitate antitumor T cell responses in a mouse model of oral cancer. *Oral Oncol* 50, 457-467 (2014).
114. Vincent, J. *et al.* 5-Fluorouracil selectively kills tumor-associated myeloid-derived suppressor cells resulting in enhanced T cell-dependent antitumor immunity. *Cancer Res* 70, 3052-3061 (2010).
115. Blaskovich, M.A. *et al.* Discovery of JSI-124 (cucurbitacin I), a selective Janus kinase/signal transducer and activator of transcription 3 signaling pathway inhibitor with potent antitumor activity against human and murine cancer cells in mice. *Cancer Res* 63, 1270-1279 (2003).
116. Ko, J.S. *et al.* Sunitinib mediates reversal of myeloid-derived suppressor cell accumulation in renal cell carcinoma patients. *Clin Cancer Res* 15, 2148-2157 (2009).
117. Ugel, S. *et al.* Therapeutic targeting of myeloid-derived suppressor cells. *Curr Opin Pharmacol* 9, 470-481 (2009).
118. Singh, R.P., Raina, K., Deep, G., Chan, D. & Agarwal, R. Silibinin suppresses growth of human prostate carcinoma PC-3 orthotopic xenograft via activation of extracellular signal-regulated kinase 1/2 and inhibition of signal transducers and activators of transcription signaling. *Clin Cancer Res* 15, 613-621 (2009).
119. Priego, N. *et al.* STAT3 labels a subpopulation of reactive astrocytes required for brain metastasis. *Nat Med* 24, 1024-1035 (2018).
120. Fridman, J.S. *et al.* Selective inhibition of JAK1 and JAK2 is efficacious in rodent models of arthritis: preclinical characterization of INCB028050. *J Immunol* 184, 5298-5307 (2010).
121. Taylor, P.C. *et al.* Baricitinib versus Placebo or Adalimumab in Rheumatoid Arthritis. *N Engl J Med* 376, 652-662 (2017).
122. Cheng, P. *et al.* Inhibition of dendritic cell differentiation and accumulation of myeloid-derived suppressor cells in cancer is regulated by S100A9 protein. *J Exp Med* 205, 2235-2249 (2008).
123. Priceman, S.J. *et al.* Targeting distinct tumor-infiltrating myeloid cells by inhibiting CSF-1 receptor: combating tumor evasion of antiangiogenic therapy. *Blood* 115, 1461-1471 (2010).
124. Swierczak, A. *et al.* The promotion of breast cancer metastasis caused by inhibition of CSF-1R/CSF-1 signaling is blocked by targeting the G-CSF receptor. *Cancer Immunol Res* 2, 765-776 (2014).

125. Ries, C.H. *et al.* Targeting tumor-associated macrophages with anti-CSF-1R antibody reveals a strategy for cancer therapy. *Cancer Cell* 25, 846-859 (2014).
126. Kusmartsev, S. *et al.* Oxidative stress regulates expression of VEGFR1 in myeloid cells: link to tumor-induced immune suppression in renal cell carcinoma. *J Immunol* 181, 346-353 (2008).
127. Kusmartsev, S. & Gabrilovich, D.I. STAT1 signaling regulates tumor-associated macrophage-mediated T cell deletion. *J Immunol* 174, 4880-4891 (2005).
128. Mirza, N. *et al.* All-trans-retinoic acid improves differentiation of myeloid cells and immune response in cancer patients. *Cancer Res* 66, 9299-9307 (2006).
129. Iclozan, C., Antonia, S., Chiappori, A., Chen, D.T. & Gabrilovich, D. Therapeutic regulation of myeloid-derived suppressor cells and immune response to cancer vaccine in patients with extensive stage small cell lung cancer. *Cancer Immunol Immunother* 62, 909-918 (2013).
130. De Sanctis, F. *et al.* MDSCs in cancer: Conceiving new prognostic and therapeutic targets. *Biochim Biophys Acta* 1865, 35-48 (2016).
131. Humphreys, L., Espona-Fiedler, M. & Longley, D.B. FLIP as a therapeutic target in cancer. *The FEBS journal* 285, 4104-4123 (2018).
32. Safa, A.R. c-FLIP, a master anti-apoptotic regulator. *Experimental Oncology* 34, 176-184 (2012).
133. Yu, J.W., Jeffrey, P.D. & Shi, Y. Mechanism of procaspase-8 activation by c-FLIPL. *Proc Natl Acad Sci U S A* 106, 8169-8174 (2009).
134. Vetsika, E.-K. *et al.* A circulating subpopulation of monocytic myeloid-derived suppressor cells as an independent prognostic/predictive factor in untreated non-small lung cancer patients. *Journal of Immunology Research* 2014, 659294 (2014).
135. Hughes, M.A. *et al.* Co-operative and Hierarchical Binding of c-FLIP and Caspase-8: A Unified Model Defines How c-FLIP Isoforms Differentially Control Cell Fate. *Molecular Cell* 61, 834-849 (2016).
136. Smyth, P., Sessler, T., Scott, C.J. & Longley, D.B. FLIP(L): the pseudo-caspase. *FEBS J* 287, 4246-4260 (2020).
137. Malik, A. & Kanneganti, T.-D. Inflammasome activation and assembly at a glance. *Journal of Cell Science* 130, 3955-3963 (2017).
138. Sharma, D. & Kanneganti, T.-D. The cell biology of inflammasomes: Mechanisms of inflammasome activation and regulation. *The Journal of Cell Biology* 213, 617-629 (2016).
139. Wu, Y.H. *et al.* Participation of c-FLIP in NLRP3 and AIM2 inflammasome activation. *Cell Death Differ* 21, 451-461 (2014).

140. Li, Y. & Bu, G. LRP5/6 in Wnt signaling and tumorigenesis. *Future Oncology (London, England)* 1, 673-681 (2005).
141. Cadigan, K.M. & Waterman, M.L. TCF/LEFs and Wnt signaling in the nucleus. *Cold Spring Harbor Perspectives in Biology* 4, a007906 (2012).
142. Naito, M. *et al.* Cellular FLIP inhibits beta-catenin ubiquitylation and enhances Wnt signaling. *Molecular and Cellular Biology* 24, 8418-8427 (2004).
143. Zhang, J. *et al.* C-FLIPL Modulated Wnt/β-Catenin Activation via Association with TIP49 Protein. *The Journal of Biological Chemistry* 292, 2132-2142 (2017).
144. Dikic, I. & Elazar, Z. Mechanism and medical implications of mammalian autophagy. *Nat Rev Mol Cell Biol* 19, 349-364 (2018).
145. Lamy, L. *et al.* Control of autophagic cell death by caspase-10 in multiple myeloma. *Cancer Cell* 23, 435-449 (2013).
146. Lee, J.-S. *et al.* FLIP-mediated autophagy regulation in cell death control. *Nature Cell Biology* 11, 1355-1362 (2009).
147. Kataoka, T. *et al.* The caspase-8 inhibitor FLIP promotes activation of NF-kappaB and Erk signaling pathways. *Current biology: CB* 10, 640-648 (2000).
148. Nakajima, A. *et al.* An antiapoptotic protein, c-FLIPL, directly binds to MKK7 and inhibits the JNK pathway. *The EMBO journal* 25, 5549-5559 (2006).
149. Marini, E.S. *et al.* The endogenous caspase-8 inhibitor c-FLIPL regulates ER morphology and crosstalk with mitochondria. *Cell Death and Differentiation* 22, 1131-1143 (2015).
150. Conti, S. *et al.* A novel role of c-FLIP protein in regulation of ER stress response. *Cellular Signalling* 28, 1262-1269 (2016).
151. Lei, S. *et al.* FLIP(L) is critical for aerobic glycolysis in hepatocellular carcinoma. *Journal of experimental & clinical cancer research: CR* 35, 79 (2016).
152. Park, D. *et al.* C-FLIP promotes the motility of cancer cells by activating FAK and ERK, and increasing MMP-9 expression. *Molecules and Cells* 25, 184-195 (2008).
153. Honda, K., Takaoka, A. & Taniguchi, T. Type I Inteferon Gene Induction by the Interferon Regulatory Factor Family of Transcription Factors. *Immunity* 25, 349-360 (2006).
154. Gates, L.T. & Shisler, J.L. cFLIP $_{L}$ Interrupts IRF3–CBP–DNA Interactions To Inhibit IRF3-Driven Transcription. *The Journal of Immunology* 197, 923-933 (2016).
155. Micheau, O., Lens, S., Gaide, O., Alevizopoulos, K. & Tschopp, J. NF-kappaB signals induce the expression of c-FLIP. *Molecular and Cellular Biology* 21, 5299-5305 (2001).

156. Ricci, M.S. *et al.* Direct repression of FLIP expression by c-myc is a major determinant of TRAIL sensitivity. *Molecular and Cellular Biology* 24, 8541-8555 (2004).
157. Chang, L. *et al.* The E3 ubiquitin ligase itch couples JNK activation to TNFalpha-induced cell death by inducing c-FLIP(L) turnover. *Cell* 124, 601-613 (2006).
158. Riley, J.S. *et al.* Prognostic and therapeutic relevance of FLIP and procaspase-8 overexpression in non-small cell lung cancer. *Cell Death & Disease* 4, e951-e951 (2013).
159. Korkolopoulou, P. *et al.* c-FLIP expression in colorectal carcinomas: association with Fas/FasL expression and prognostic implications. *Histopathology* 51, 150-156 (2007).
160. Haag, C. *et al.* Identification of c-FLIP(L) and c-FLIP(S) as critical regulators of death receptor-induced apoptosis in pancreatic cancer cells. *Gut* 60, 225-237 (2011).
161. Zhou, X.-D. *et al.* Overexpression of cellular FLICE-inhibitory protein (FLIP) in gastric adenocarcinoma. *Clinical Science (London, England: 1979)* 106, 397-405 (2004).
162. Korkolopoulou, P. *et al.* c-FLIP expression in bladder urothelial carcinomas: its role in resistance to Fas-mediated apoptosis and clinicopathologic correlations. *Urology* 63, 1198-1204 (2004).
163. McCourt, C. *et al.* Elevation of c-FLIP in castrate-resistant prostate cancer antagonizes therapeutic response to androgen receptor-targeted therapy. *Clinical Cancer Research: An Official Journal of the American Association for Cancer Research* 18, 3822-3833 (2012).
164. McLornan, D. *et al.* Prognostic and therapeutic relevance of c-FLIP in acute myeloid leukaemia. *British Journal of Haematology* 160, 188-198 (2013).
165. Yao, Q. *et al.* Prognostic significance of TRAIL signalling molecules in cervical squamous cell carcinoma. *Journal of Clinical Pathology* 69, 122-127 (2016).
166. Djerbi, M. *et al.* The inhibitor of death receptor signaling, FLICE-inhibitory protein defines a new class of tumor progression factors. *The Journal of Experimental Medicine* 190, 1025-1032 (1999).
167. Shirley, S. & Micheau, O. Targeting c-FLIP in cancer. *Cancer Letters* 332, 141-150 (2013).
168. Nam, S.Y. *et al.* Upregulation of FLIP(S) by Akt, a possible inhibition mechanism of TRAIL-induced apoptosis in human gastric cancers. *Cancer Science* 94, 1066-1073 (2003).
169. Salon, C. *et al.* E2F1 induces apoptosis and sensitizes human lung adenocarcinoma cells to death-receptor-mediated apoptosis through specific downregulation of c-FLIPshort. *Cell Death & Differentiation* 13, 260-272 (2006).

170. Longley, D.B. *et al.* c-FLIP inhibits chemotherapy-induced colorectal cancer cell death. *Oncogene* 25, 838-848 (2006).
171. Carson, R. *et al.* HDAC Inhibition Overcomes Acute Resistance to MEK Inhibition in BRAF-Mutant Colorectal Cancer by Downregulation of c-FLIPL. *Clinical Cancer Research: An Official Journal of the American Association for Cancer Research* 21, 3230-3240 (2015).
172. Mathas, S. *et al.* c-FLIP mediates resistance of Hodgkin/Reed-Sternberg cells to death receptor-induced apoptosis. *J Exp Med* 199, 1041-1052 (2004).
173. Thorburn, A., Behbakht, K. & Ford, H. TRAIL receptor-targeted therapeutics: resistance mechanisms and strategies to avoid them. *Drug Resist Updat* 11, 17-24 (2008).
174. Micheau, O., Solary, E., Hammann, A. & Dimanche-Boitrel, M.T. Fas ligand-independent, FADD-mediated activation of the Fas death pathway by anticancer drugs. *The Journal of Biological Chemistry* 274, 7987-7992 (1999).
175. Kinoshita, H. *et al.* Cisplatin (CDDP) sensitizes human osteosarcoma cell to Fas/CD95-mediated apoptosis by down-regulating FLIP-L expression. *Int J Cancer* 88, 986-991 (2000).
176. Abedini, M.R. *et al.* Cisplatin induces p53-dependent FLICE-like inhibitory protein ubiquitination in ovarian cancer cells. *Cancer Res* 68, 4511-4517 (2008).
177. Yerbes, R. & Lopez-Rivas, A. Itch/AIP4-independent proteasomal degradation of cFLIP induced by the histone deacetylase inhibitor SAHA sensitizes breast tumour cells to TRAIL. *Invest New Drugs* 30, 541-547 (2012).
178. Jani, T.S., DeVecchio, J., Mazumdar, T., Agyeman, A. & Houghton, J.A. Inhibition of NF-kappaB signaling by quinacrine is cytotoxic to human colon carcinoma cell lines and is synergistic in combination with tumor necrosis factor-related apoptosis-inducing ligand (TRAIL) or oxaliplatin. *J Biol Chem* 285, 19162-19172 (2010).
179. Plaza-Sirvent, C. *et al.* c-FLIP Expression in Foxp3-Expressing Cells Is Essential for Survival of Regulatory T Cells and Prevention of Autoimmunity. *Cell Reports* 18, 12-22 (2017).
180. Wu, Y.-J. *et al.* Cellular FLIP Inhibits Myeloid Cell Activation by Suppressing Selective Innate Signaling. *The Journal of Immunology* 195, 2612-2623 (2015).
181. Travis, W.D. *et al.* The 2015 World Health Organization Classification of Lung Tumors: Impact of Genetic, Clinical and Radiologic Advances Since the 2004 Classification. *J Thorac Oncol* 10, 1243-1260 (2015).
182. Travis, W.D. Pathology of lung cancer. *Clin Chest Med* 32, 669-692 (2011).

183. Travis, W.D., Brambilla, E., Burke, A.P., Marx, A. & Nicholson, A.G. Introduction to The 2015 World Health Organization Classification of Tumors of the Lung, Pleura, Thymus, and Heart. *Journal of Thoracic Oncology* 10, 1240-1242 (2015).
184. Huang, A. *et al.* Increased CD14(+)HLA-DR (-/low) myeloid-derived suppressor cells correlate with extrathoracic metastasis and poor response to chemotherapy in non-small cell lung cancer patients. *Cancer immunology, immunotherapy: CII* 62, 1439-1451 (2013).
185. Detterbeck, F.C., Boffa, D.J., Kim, A.W. & Tanoue, L.T. The Eighth Edition Lung Cancer Stage Classification. *Chest* 151, 193-203 (2017).
186. Detterbeck, F.C. The eighth edition TNM stage classification for lung cancer: What does it mean on main street? *J Thorac Cardiovasc Surg* 155, 356-359 (2018).
187. Beadsmoore, C.J. & Screaton, N.J. Classification, staging and prognosis of lung cancer. *Eur J Radiol* 45, 8-17 (2003).
188. Li, Y.D. *et al.* Tumor-induced peripheral immunosuppression promotes brain metastasis in patients with non-small cell lung cancer. *Cancer immunology, immunotherapy: CII* 68, 1501-1513 (2019).
189. Lee, J.W. *et al.* The Combination of MEK Inhibitor With Immunomodulatory Antibodies Targeting Programmed Death 1 and Programmed Death Ligand 1 Results in Prolonged Survival in Kras/p53-Driven Lung Cancer. *Journal of Thoracic Oncology: Official Publication of the International Association for the Study of Lung Cancer* 14, 1046-1060 (2019).
190. Ridder, K. *et al.* Extracellular vesicle-mediated transfer of functional RNA in the tumor microenvironment. *Oncoimmunology* 4, e1008371 (2015).
191. Yamauchi, Y. *et al.* Circulating and Tumor Myeloid-derived Suppressor Cells in Resectable Non-Small Cell Lung Cancer. *Am J Respir Crit Care Med* 198, 777-787 (2018).
192. Yang, Z. *et al.* Myeloid-derived suppressor cells—new and exciting players in lung cancer. *Journal of Hematology & Oncology* 13, 10 (2020).
193. Kim, H.R. *et al.* The Ratio of Peripheral Regulatory T Cells to Lox-1 $^{+}$ Polymorphonuclear Myeloid-derived Suppressor Cells Predicts the Early Response to Anti–PD-1 Therapy in Patients with Non–Small Cell Lung Cancer. *American Journal of Respiratory and Critical Care Medicine* 199, 243-246 (2019).
194. Limagne, E. *et al.* Tim-3/galectin-9 pathway and mMDSC control primary and secondary resistances to PD-1 blockade in lung cancer patients. *Oncoimmunology* 8, e1564505 (2019).

195. Li, A. *et al.* Indoleamine 2,3-dioxygenase 1 inhibition targets anti-PD1-resistant lung tumors by blocking myeloid-derived suppressor cells. *Cancer Letters* 431, 54-63 (2018).
196. de Goeje, P.L. *et al.* Immunoglobulin-like transcript 3 is expressed by myeloid-derived suppressor cells and correlates with survival in patients with non-small cell lung cancer. *Oncoimmunology* 4, e1014242 (2015).
197. Fois, S.S. *et al.* Molecular Epidemiology of the Main Druggable Genetic Alterations in Non-Small Cell Lung Cancer. *Int J Mol Sci* 22 (2021).
198. Yu, H., Boyle, T.A., Zhou, C., Rimm, D.L. & Hirsch, F.R. PD-L1 Expression in Lung Cancer. *J Thorac Oncol* 11, 964-975 (2016).
199. Hirsch, F.R. *et al.* Lung cancer: current therapies and new targeted treatments. *The Lancet* 389, 299-311 (2017).
200. Thai, A.A., Solomon, B.J., Sequist, L.V., Gainor, J.F. & Heist, R.S. Lung cancer. *The Lancet* 398, 535-554 (2021).
201. Sanaei, M.-J. *et al.* Recent advances in immune checkpoint therapy in non-small cell lung cancer and opportunities for nanoparticle-based therapy. *European Journal of Pharmacology* 909, 174404 (2021).
202. Zhang, M. *et al.* PD-L1 expression in lung cancer and its correlation with driver mutations: a meta-analysis. *Scientific Reports* 7, 10255 (2017).
203. Bodor, J.N., Boumber, Y. & Borghaei, H. Biomarkers for immune checkpoint inhibition in non-small cell lung cancer (NSCLC). *Cancer* 126, 260-270 (2020).
204. Spigel, D. *et al.* IMpower110: Interim overall survival (OS) analysis of a phase III study of atezolizumab (atezo) vs platinum-based chemotherapy (chemo) as first-line (1L) treatment (tx) in PD-L1-selected NSCLC. *Annals of Oncology* 30, 915-915 (2019).
205. Mok, T.S.K. *et al.* Pembrolizumab versus chemotherapy for previously untreated, PD-L1-expressing, locally advanced or metastatic non-small-cell lung cancer (KEYNOTE-042): a randomised, open-label, controlled, phase 3 trial. *Lancet (London, England)* 393, 1819-1830 (2019).
206. Carbone, D.P. *et al.* First-Line Nivolumab in Stage IV or Recurrent Non-Small-Cell Lung Cancer. *N Engl J Med* 376, 2415-2426 (2017).
207. Hellmann, M.D. *et al.* Nivolumab plus Ipilimumab in Advanced Non–Small-Cell Lung Cancer. *New England Journal of Medicine* 381, 2020-2031 (2019).
208. Guida, L. NEOPLASIE DEL POLMONE. *AIOM*, 296 (2019).
209. Reck, M. *et al.* Updated Analysis of KEYNOTE-024: Pembrolizumab Versus Platinum-Based Chemotherapy for Advanced Non-Small-Cell Lung Cancer With PD-

L1 Tumor Proportion Score of 50% or Greater. *Journal of Clinical Oncology: Official Journal of the American Society of Clinical Oncology* 37, 537-546 (2019).

210. Gadgeel, S. *et al.* Updated Analysis From KEYNOTE-189: Pembrolizumab or Placebo Plus Pemetrexed and Platinum for Previously Untreated Metastatic Nonsquamous Non-Small-Cell Lung Cancer. *Journal of Clinical Oncology: Official Journal of the American Society of Clinical Oncology* 38, 1505-1517 (2020).
211. Rodriguez-Abreu, D. *et al.* Final analysis of KEYNOTE-189: Pemetrexed-platinum chemotherapy (chemo) with or without pembrolizumab (pembro) in patients (pts) with previously untreated metastatic nonsquamous non-small cell lung cancer (NSCLC). *Journal of Clinical Oncology* 38 (2020).
212. Paz-Ares, L. *et al.* Pembrolizumab (pembro) 1 chemotherapy (chemo) in metastatic squamous NSCLC: Final analysis and progression after the next line of therapy (PFS2) in KEYNOTE-407. *Annals of Oncology* 30 (2019).
213. Reck, M. *et al.* Nivolumab (NIVO) + ipilimumab (IPI) + 2 cycles of platinum-doublet chemotherapy (chemo) vs 4 cycles chemo as first-line (1L) treatment (tx) for stage IV/recurrent non-small cell lung cancer (NSCLC): CheckMate 9LA. *Journal of Clinical Oncology* 38, 9501-9501 (2020).
214. Volaric, A. *et al.* Indoleamine-2,3-Dioxygenase in Non-Small Cell Lung Cancer: A Targetable Mechanism of Immune Resistance Frequently Coexpressed With PD-L1. *Am J Surg Pathol* 42, 1216-1223 (2018).
215. Lamberti, G. *et al.* The Mechanisms of PD-L1 Regulation in Non-Small-Cell Lung Cancer (NSCLC): Which Are the Involved Players? *Cancers (Basel)* 12 (2020).
216. Chen, J., Jiang, C.C., Jin, L. & Zhang, X.D. Regulation of PD-L1: a novel role of pro-survival signalling in cancer. *Ann Oncol* 27, 409-416 (2016).
217. Sakai, H. *et al.* Impact of cytotoxic chemotherapy on PD-L1 expression in patients with non-small cell lung cancer negative for EGFR mutation and ALK fusion. *Lung Cancer* 127, 59-65 (2019).
218. Roulston, A., Marcellus, R.C. & Branton, P.E. Viruses and apoptosis. *Annual Review of Microbiology* 53, 577-628 (1999).
219. Saito, K. *et al.* Hepatitis C virus core protein inhibits tumor necrosis factor alpha-mediated apoptosis by a protective effect involving cellular FLICE inhibitory protein. *Journal of Virology* 80, 4372-4379 (2006).
220. Lee, A.R. *et al.* Multiple Functions of Cellular FLIP Are Essential for Replication of Hepatitis B Virus. *Journal of Virology* 92, e00339-00318 (2018).
221. Krueger, A. *et al.* HTLV-1 Tax protects against CD95-mediated apoptosis by induction of the cellular FLICE-inhibitory protein (c-FLIP). *Blood* 107, 3933-3939 (2006).

222. Gibellini, D. *et al.* HIV-1 Tat protein concomitantly down-regulates apical caspase-10 and up-regulates c-FLIP in lymphoid T cells: a potential molecular mechanism to escape TRAIL cytotoxicity. *Journal of Cellular Physiology* 203, 547-556 (2005).
223. Tepper, C.G. & Seldin, M.F. Modulation of caspase-8 and FLICE-inhibitory protein expression as a potential mechanism of Epstein-Barr virus tumorigenesis in Burkitt's lymphoma. *Blood* 94, 1727-1737 (1999).
224. Rodrigue-Gervais, I.G. *et al.* Cellular inhibitor of apoptosis protein cIAP2 protects against pulmonary tissue necrosis during influenza virus infection to promote host survival. *Cell Host & Microbe* 15, 23-35 (2014).
225. Thome, M. *et al.* Viral FLICE-inhibitory proteins (FLIPs) prevent apoptosis induced by death receptors. *Nature* 386, 517-521 (1997).
226. Viruses, C.S.G.o.t.I.C.o.T.o. The species Severe acute respiratory syndrome-related coronavirus: classifying 2019-nCoV and naming it SARS-CoV-2. *Nature Microbiology* 5, 536-544 (2020).
227. Coronavirus disease (COVID-19) – World Health Organization. World Health Organisation [cited]Available from: https://www.who.int/emergencies/diseases/novel-coronavirus-2019
228. International Locations with Confirmed COVID-19 Cases. European Centre for Disease Prevention and Control [cited]Available from: https://www.ecdc.europa.eu/en/geographical-distribution-2019-ncov-cases
229. COVID Live Update: coronavirus cases and deaths. Worldometer [cited]Available from: https://www.worldometers.info/coronavirus/
230. CDC Weekly, C. & Team, T.N.C.P.E.R.E. The Epidemiological Characteristics of an Outbreak of 2019 Novel Coronavirus Diseases (COVID-19) — China, 2020. *China CDC Weekly* 2, 113-122 (2020).
231. Wang, C. *et al.* The establishment of reference sequence for SARS-CoV-2 and variation analysis. *Journal of Medical Virology* 92, 667-674 (2020).
232. Andersen, K.G., Rambaut, A., Lipkin, W.I., Holmes, E.C. & Garry, R.F. The proximal origin of SARS-CoV-2. *Nature Medicine* 26, 450-452 (2020).
233. Cui, J., Li, F. & Shi, Z.-L. Origin and evolution of pathogenic coronaviruses. *Nature Reviews. Microbiology* 17, 181-192 (2019).
234. Zhou, P. *et al.* A pneumonia outbreak associated with a new coronavirus of probable bat origin. *Nature* 579, 270-273 (2020).
235. Zhu, N. *et al.* A Novel Coronavirus from Patients with Pneumonia in China, 2019. *The New England Journal of Medicine* 382, 727-733 (2020).

236. Garg, S. *et al.* Hospitalization Rates and Characteristics of Patients Hospitalized with Laboratory-Confirmed Coronavirus Disease 2019 — COVID-NET, 14 States, March 1–30, 2020. *MMWR. Morbidity and Mortality Weekly Report* 69, 458-464 (2020).
237. Michelens, M., Jones, N. & Stavropoulou, C. In patients of COVID-19, what are the symptoms and clinical features of mild and moderate cases? The Centre for Evidence-Based Medicine 2020 2020 [cited]Available from: https://www.cebm.net/covid-19/in-patients-of-covid-19-what-are-the-symptoms-and-clinical-features-of-mild-and-moderate-case/
238. Qiu, Y. *et al.* Predicting the angiotensin converting enzyme 2 (ACE2) utilizing capability as the receptor of SARS-CoV-2. *Microbes and Infection* 22, 221-225 (2020).
239. Huang, C. *et al.* Clinical features of patients infected with 2019 novel coronavirus in Wuhan, China. *Lancet (London, England)* 395, 497-506 (2020).
240. Wang, Y. *et al.* Clinical Outcomes in 55 Patients With Severe Acute Respiratory Syndrome Coronavirus 2 Who Were Asymptomatic at Hospital Admission in Shenzhen, China. *The Journal of Infectious Diseases* 221, 1770-1774 (2020).
241. Mizumoto, K., Kagaya, K., Zarebski, A. & Chowell, G. Estimating the asymptomatic proportion of coronavirus disease 2019 (COVID-19) cases on board the Diamond Princess cruise ship, Yokohama, Japan, 2020. *Euro Surveillance: Bulletin Europeen Sur Les Maladies Transmissibles = European Communicable Disease Bulletin* 25 (2020).
242. Wang, D. *et al.* Clinical Characteristics of 138 Hospitalized Patients With 2019 Novel Coronavirus–Infected Pneumonia in Wuhan, China. *JAMA* 323, 1061 (2020).
243. Velavan, T.P. & Meyer, C.G. The COVID-19 epidemic. *Tropical medicine & international health: TM & IH* 25, 278-280 (2020).
244. Mossel, E.C. *et al.* SARS-CoV replicates in primary human alveolar type II cell cultures but not in type I-like cells. *Virology* 372, 127-135 (2008).
245. Masters, P.S. The molecular biology of coronaviruses. *Advances in Virus Research* 66, 193-292 (2006).
246. Organization, W.H. Modes of transmission of virus causing COVID-19: implications for IPC precaution recommendations: scientific brief, 27 March 2020. Geneva: World Health Organization; 2020 2020.
247. Arons, M.M. *et al.* Presymptomatic SARS-CoV-2 Infections and Transmission in a Skilled Nursing Facility. *The New England Journal of Medicine* 382, 2081-2090 (2020).

248. Liu, Y., Gayle, A.A., Wilder-Smith, A. & Rocklöv, J. The reproductive number of COVID-19 is higher compared to SARS coronavirus. *Journal of Travel Medicine* 27, taaa021 (2020).
249. Mason, R.J. Pathogenesis of COVID-19 from a cell biology perspective. *The European Respiratory Journal* 55, 2000607 (2020).
250. Chams, N. *et al.* COVID-19: A Multidisciplinary Review. *Frontiers in Public Health* 8, 383 (2020).
251. Hamming, I. *et al.* Tissue distribution of ACE2 protein, the functional receptor for SARS coronavirus. A first step in understanding SARS pathogenesis. *The Journal of Pathology* 203, 631-637 (2004).
252. Shereen, M.A., Khan, S., Kazmi, A., Bashir, N. & Siddique, R. COVID-19 infection: Origin, transmission, and characteristics of human coronaviruses. *Journal of Advanced Research* 24, 91-98 (2020).
253. Li, X., Geng, M., Peng, Y., Meng, L. & Lu, S. Molecular immune pathogenesis and diagnosis of COVID-19. *Journal of Pharmaceutical Analysis* 10, 102-108 (2020).
254. Li, G. *et al.* Coronavirus infections and immune responses. *Journal of Medical Virology* 92, 424-432 (2020).
255. Sette, A. & Crotty, S. Adaptive immunity to SARS-CoV-2 and COVID-19. *Cell* 184, 861-880 (2021).
256. Grifoni, A. *et al.* Targets of T Cell Responses to SARS-CoV-2 Coronavirus in Humans with COVID-19 Disease and Unexposed Individuals. *Cell* 181, 1489-1501.e1415 (2020).
257. Sekine, T. *et al.* Robust T Cell Immunity in Convalescent Individuals with Asymptomatic or Mild COVID-19. *Cell* 183, 158-168.e114 (2020).
258. Lee, J.S. *et al.* Immunophenotyping of COVID-19 and influenza highlights the role of type I interferons in development of severe COVID-19. *Science Immunology* 5, eabd1554 (2020).
259. Bost, P. *et al.* Deciphering the state of immune silence in fatal COVID-19 patients. *Nature Communications* 12, 1428 (2021).
260. Schulte-Schrepping, J. *et al.* Severe COVID-19 Is Marked by a Dysregulated Myeloid Cell Compartment. *Cell* 182, 1419-1440.e1423 (2020).
261. Zhang, D. *et al.* COVID-19 infection induces readily detectable morphological and inflammation-related phenotypic changes in peripheral blood monocytes, the severity of which correlate with patient outcome. preprint: Infectious Diseases (except HIV/AIDS); 2020 2020-03-26.
262. Grant, R.A. *et al.* Circuits between infected macrophages and T cells in SARS-CoV-2 pneumonia. *Nature* 590, 635-641 (2021).

263. Aschenbrenner, A.C. *et al.* Disease severity-specific neutrophil signatures in blood transcriptomes stratify COVID-19 patients. *Genome Medicine* 13, 7 (2021).
264. Schultze, J.L. & Aschenbrenner, A.C. COVID-19 and the human innate immune system. *Cell* 184, 1671-1692 (2021).
265. Liu, L. *et al.* Anti-spike IgG causes severe acute lung injury by skewing macrophage responses during acute SARS-CoV infection. *JCI insight* 4, 123158 (2019).
266. Zhou, Y. *et al.* Pathogenic T-cells and inflammatory monocytes incite inflammatory storms in severe COVID-19 patients. *National Science Review* 7, 998-1002 (2020).
267. Cavalcante-Silva, L.H.A. *et al.* Neutrophils and COVID-19: The road so far. *International Immunopharmacology* 90, 107233 (2021).
268. Abraham, E. Neutrophils and acute lung injury. *Critical Care Medicine* 31, S195-199 (2003).
269. Sacchi, A. *et al.* Early expansion of myeloid-derived suppressor cells inhibits SARS-CoV-2 specific T-cell response and may predict fatal COVID-19 outcome. *Cell Death & Disease* 11, 921 (2020).
270. Mathew, D. *et al.* Deep immune profiling of COVID-19 patients reveals distinct immunotypes with therapeutic implications. *Science (New York, N.Y.)* 369, eabc8511 (2020).
271. Adamo, S. *et al.* Profound dysregulation of T cell homeostasis and function in patients with severe COVID-19. *Allergy* 76, 2866-2881 (2021).
272. Galvan-Pena, S. *et al.* Profound Treg perturbations correlate with COVID-19 severity. *bioRxiv: The Preprint Server for Biology*, 2020.2012.2011.416180 (2020).
273. To, K.K.-W. *et al.* Temporal profiles of viral load in posterior oropharyngeal saliva samples and serum antibody responses during infection by SARS-CoV-2: an observational cohort study. *The Lancet Infectious Diseases* 20, 565-574 (2020).
274. Li, S. *et al.* Clinical and pathological investigation of patients with severe COVID-19. *JCI insight* 5, 138070 (2020).
275. Kaneko, N. *et al.* Loss of Bcl-6-Expressing T Follicular Helper Cells and Germinal Centers in COVID-19. *Cell* 183, 143-157.e113 (2020).
276. Zhao, J. *et al.* Antibody Responses to SARS-CoV-2 in Patients With Novel Coronavirus Disease 2019. *Clinical Infectious Diseases: An Official Publication of the Infectious Diseases Society of America* 71, 2027-2034 (2020).
277. Fajgenbaum, D.C. & June, C.H. Cytokine Storm. *New England Journal of Medicine* 383, 2255-2273 (2020).

278. Avau, A. *et al.* Systemic juvenile idiopathic arthritis-like syndrome in mice following stimulation of the immune system with Freund's complete adjuvant: regulation by interferon-γ. *Arthritis & Rheumatology (Hoboken, N.J.)* 66, 1340-1351 (2014).
279. van der Stegen, S.J.C. *et al.* Preclinical in vivo modeling of cytokine release syndrome induced by ErbB-retargeted human T cells: identifying a window of therapeutic opportunity? *Journal of Immunology (Baltimore, Md.: 1950)* 191, 4589-4598 (2013).
280. Kang, S., Tanaka, T., Narazaki, M. & Kishimoto, T. Targeting Interleukin-6 Signaling in Clinic. *Immunity* 50, 1007-1023 (2019).
281. Faulkner, L., Cooper, A., Fantino, C., Altmann, D.M. & Sriskandan, S. The mechanism of superantigen-mediated toxic shock: not a simple Th1 cytokine storm. *Journal of Immunology (Baltimore, Md.: 1950)* 175, 6870-6877 (2005).
282. Mazodier, K. *et al.* Severe imbalance of IL-18/IL-18BP in patients with secondary hemophagocytic syndrome. *Blood* 106, 3483-3489 (2005).
283. Netea, M.G., Kullberg, B.J., Verschueren, I. & Van Der Meer, J.W. Interleukin-18 induces production of proinflammatory cytokines in mice: no intermediate role for the cytokines of the tumor necrosis factor family and interleukin-1beta. *European Journal of Immunology* 30, 3057-3060 (2000).
284. Behrens, E.M. *et al.* Repeated TLR9 stimulation results in macrophage activation syndrome-like disease in mice. *The Journal of Clinical Investigation* 121, 2264-2277 (2011).
285. Del Valle, D.M. *et al.* An inflammatory cytokine signature predicts COVID-19 severity and survival. *Nature Medicine* 26, 1636-1643 (2020).
286. Angioni, R. *et al.* Age-severity matched cytokine profiling reveals specific signatures in Covid-19 patients. *Cell Death & Disease* 11, 957 (2020).
287. Xiong, Y. *et al.* Transcriptomic characteristics of bronchoalveolar lavage fluid and peripheral blood mononuclear cells in COVID-19 patients. *Emerging Microbes & Infections* 9, 761-770 (2020).
288. Tjan, L.H. *et al.* Early Differences in Cytokine Production by Severity of Coronavirus Disease 2019. *The Journal of Infectious Diseases* 223, 1145-1149 (2021).
289. Schneider, W.M., Chevillotte, M.D. & Rice, C.M. Interferon-stimulated genes: a complex web of host defenses. *Annu Rev Immunol* 32, 513-545 (2014).
290. Blanco-Melo, D. *et al.* Imbalanced Host Response to SARS-CoV-2 Drives Development of COVID-19. *Cell* 181, 1036-1045 e1039 (2020).
291. Stanifer, M.L. *et al.* Critical Role of Type III Interferon in Controlling SARS-CoV-2 Infection in Human Intestinal Epithelial Cells. *Cell Rep* 32, 107863 (2020).
292. Mantlo, E., Bukreyeva, N., Maruyama, J., Paessler, S. & Huang, C. Potent Antiviral Activities of Type I Interferons to SARS-CoV-2 Infection. *bioRxiv* (2020).

293. Channappanavar, R. *et al.* IFN-I response timing relative to virus replication determines MERS coronavirus infection outcomes. *J Clin Invest* 129, 3625-3639 (2019).
294. Cervantes-Barragan, L. *et al.* Control of coronavirus infection through plasmacytoid dendritic-cell-derived type I interferon. *Blood* 109, 1131-1137 (2007).
295. Lokugamage, K.G. *et al.* Type I Interferon Susceptibility Distinguishes SARS-CoV-2 from SARS-CoV. *J Virol* 94 (2020).
296. Bastard, P. *et al.* Autoantibodies against type I IFNs in patients with life-threatening COVID-19. *Science* 370 (2020).
297. Hemann, E.A., Gale, M., Jr. & Savan, R. Interferon Lambda Genetics and Biology in Regulation of Viral Control. *Front Immunol* 8, 1707 (2017).
298. Rugwizangoga, B. *et al.* IFNL4 Genotypes Predict Clearance of RNA Viruses in Rwandan Children With Upper Respiratory Tract Infections. *Front Cell Infect Microbiol* 9, 340 (2019).
299. Jordan, S.C. *et al.* Interleukin-6, A Cytokine Critical to Mediation of Inflammation, Autoimmunity and Allograft Rejection: Therapeutic Implications of IL-6 Receptor Blockade. *Transplantation* 101, 32-44 (2017).
300. García Roche, A., Díaz Lagares, C., Élez, E. & Ferrer Roca, R. Cytokine release syndrome. Reviewing a new entity in the intensive care unit. *Medicina Intensiva* 43, 480-488 (2019).
301. Siegel, A.M. *et al.* A critical role for STAT3 transcription factor signaling in the development and maintenance of human T cell memory. *Immunity* 35, 806-818 (2011).
302. Lipworth, B., Chan, R., Lipworth, S. & RuiWen Kuo, C. Weathering the Cytokine Storm in Susceptible Patients with Severe SARS-CoV-2 Infection. *The Journal of Allergy and Clinical Immunology. In Practice* 8, 1798-1801 (2020).
303. Doglioni, C. *et al.* Covid-19 Interstitial Pneumonia: Histological and Immunohistochemical Features on Cryobiopsies. *Respiration; International Review of Thoracic Diseases* 100, 488-498 (2021).
304. Nie, X. *et al.* Multi-organ proteomic landscape of COVID-19 autopsies. *Cell* 184, 775-791.e714 (2021).
305. Thwaites, R.S. *et al.* Inflammatory profiles across the spectrum of disease reveal a distinct role for GM-CSF in severe COVID-19. *Science Immunology* 6, eabg9873 (2021).

306. Falck-Jones, S. *et al.* Functional monocytic myeloid-derived suppressor cells increase in blood but not airways and predict COVID-19 severity. *The Journal of Clinical Investigation* 131, 144734 (2021).
307. Ugel, S., De Sanctis, F., Mandruzzato, S. & Bronte, V. Tumor-induced myeloid deviation: when myeloid-derived suppressor cells meet tumor-associated macrophages. *The Journal of Clinical Investigation* 125, 3365-3376 (2015).
308. Musiu, C. *et al.* Fatal cytokine release syndrome by an aberrant FLIP/STAT3 axis. preprint: Allergy and Immunology; 2021 2021-05-04.
309. Reyes, M. *et al.* Induction of a regulatory myeloid program in bacterial sepsis and severe COVID-19. *bioRxiv: The Preprint Server for Biology*, 2020.2009.2002.280180 (2020).
310. Yang, X. *et al.* Clinical course and outcomes of critically ill patients with SARS-CoV-2 pneumonia in Wuhan, China: a single-centered, retrospective, observational study. *The Lancet Respiratory Medicine* 8, 475-481 (2020).
311. Diao, B. *et al.* Reduction and Functional Exhaustion of T Cells in Patients With Coronavirus Disease 2019 (COVID-19). *Frontiers in Immunology* 11, 827 (2020).
312. Chen, P. *et al.* SARS-CoV-2 Neutralizing Antibody LY-CoV555 in Outpatients with Covid-19. *New England Journal of Medicine* 384, 229-237 (2021).
313. Lilly. Lilly's neutralizing antibody bamlanivimab (LY-CoV555) receives FDA emergency use authorization for the treatment of recently diagnosed COVID-19 | Eli Lilly and Company. Lilly INVESTORS 2020 2020 [cited]Available from: https://investor.lilly.com/news-releases/news-release-details/lillys-neutralizing-antibody-bamlanivimab-ly-cov555-receives-fda
314. Tchesnokov, E.P., Feng, J.Y., Porter, D.P. & Götte, M. Mechanism of Inhibition of Ebola Virus RNA-Dependent RNA Polymerase by Remdesivir. *Viruses* 11, E326 (2019).
315. Sallard, E., Lescure, F.-X., Yazdanpanah, Y., Mentre, F. & Peiffer-Smadja, N. Type 1 interferons as a potential treatment against COVID-19. *Antiviral Research* 178, 104791 (2020).
316. Sheahan, T.P. *et al.* An orally bioavailable broad-spectrum antiviral inhibits SARS-CoV-2 in human airway epithelial cell cultures and multiple coronaviruses in mice. *Science Translational Medicine* 12, eabb5883 (2020).
317. Ridgeback Biotherapeutics, L. The safety of molnupiravir (EIDD-2801) and its effect on viral shedding of SARS-CoV-2 (END-COVID). ClinicalTrials.gov 2020 2021 [cited]Available from: https://clinicaltrials.gov/ct2/show/NCT04405739
318. Group, R.C. *et al.* Dexamethasone in Hospitalized Patients with Covid-19. *The New England Journal of Medicine* 384, 693-704 (2021).

319. Thevarajan, I. *et al.* Breadth of concomitant immune responses prior to patient recovery: a case report of non-severe COVID-19. *Nature Medicine* 26, 453-455 (2020).
320. Kuchipudi, S.V. The Complex Role of STAT3 in Viral Infections. *Journal of Immunology Research* 2015, 272359 (2015).
321. Gotthardt, D. *et al.* Loss of STAT3 in murine NK cells enhances NK cell-dependent tumor surveillance. *Blood* 124, 2370-2379 (2014).
322. Zhang, W. *et al.* The use of anti-inflammatory drugs in the treatment of people with severe coronavirus disease 2019 (COVID-19): The Perspectives of clinical immunologists from China. *Clinical Immunology (Orlando, Fla.)* 214, 108393 (2020).
323. Bronte, V. *et al.* Baricitinib restrains the immune dysregulation in patients with severe COVID-19. *The Journal of Clinical Investigation* 130, 6409-6416 (2020).
324. Oja, A.E. *et al.* Divergent SARS-CoV-2-specific T- and B-cell responses in severe but not mild COVID-19 patients. *European Journal of Immunology* 50, 1998-2012 (2020).
325. Marconi, V.C. *et al.* Efficacy and safety of baricitinib in patients with COVID-19 infection: Results from the randomised, double-blind, placebo-controlled, parallel-group COV-BARRIER phase 3 trial. preprint: Infectious Diseases (except HIV/AIDS); 2021 2021-05-03.
326. Narazaki, M. & Kishimoto, T. The Two-Faced Cytokine IL-6 in Host Defense and Diseases. *International Journal of Molecular Sciences* 19, E3528 (2018).
327. Gordon, A.C., Angus, D.C. & Derde, L.P.G. Interleukin-6 Receptor Antagonists in Critically Ill Patients with Covid-19. Reply. *The New England Journal of Medicine* 385, 1147-1149 (2021).
328. Group, R.C. Tocilizumab in patients admitted to hospital with COVID-19 (RECOVERY): a randomised, controlled, open-label, platform trial. *Lancet (London, England)* 397, 1637-1645 (2021).
329. Gabrilovich, D.I. & Nagaraj, S. Myeloid-derived suppressor cells as regulators of the immune system. *Nature Reviews Immunology* 9, 162-174 (2009).
330. McLaughlin, K.A. *et al.* FLIP: A Targetable Mediator of Resistance to Radiation in Non-Small Cell Lung Cancer. *Molecular Cancer Therapeutics* 15, 2432-2441 (2016).
331. Verdura, S. *et al.* Silibinin is a direct inhibitor of STAT3. *Food and Chemical Toxicology: An International Journal Published for the British Industrial Biological Research Association* 116, 161-172 (2018).
332. O'Shea, J.J., Holland, S.M. & Staudt, L.M. JAKs and STATs in immunity, immunodeficiency, and cancer. *The New England Journal of Medicine* 368, 161-170 (2013).

333. Jiang, R.-D. *et al.* Pathogenesis of SARS-CoV-2 in Transgenic Mice Expressing Human Angiotensin-Converting Enzyme 2. *Cell* 182, 50-58.e58 (2020).
334. Cooke, K.R. *et al.* An experimental model of idiopathic pneumonia syndrome after bone marrow transplantation: I. The roles of minor H antigens and endotoxin. *Blood* 88, 3230-3239 (1996).
335. Stadler, C.R. *et al.* Elimination of large tumors in mice by mRNA-encoded bispecific antibodies. *Nature Medicine* 23, 815-817 (2017).
336. Holtkamp, S. *et al.* Modification of antigen-encoding RNA increases stability, translational efficacy, and T-cell stimulatory capacity of dendritic cells. *Blood* 108, 4009-4017 (2006).
337. Butler, A., Hoffman, P., Smibert, P., Papalexi, E. & Satija, R. Integrating single-cell transcriptomic data across different conditions, technologies, and species. *Nature Biotechnology* 36, 411-420 (2018).
338. Hafemeister, C. & Satija, R. Normalization and variance stabilization of single-cell RNA-seq data using regularized negative binomial regression. *Genome Biology* 20, 296 (2019).
339. Stuart, T. *et al.* Comprehensive Integration of Single-Cell Data. *Cell* 177, 1888-1902.e1821 (2019).
340. Wolock, S.L., Lopez, R. & Klein, A.M. Scrublet: Computational Identification of Cell Doublets in Single-Cell Transcriptomic Data. *Cell Systems* 8, 281-291.e289 (2019).
341. Aran, D. *et al.* Reference-based analysis of lung single-cell sequencing reveals a transitional profibrotic macrophage. *Nature Immunology* 20, 163-172 (2019).
342. Heng, T.S.P., Painter, M.W. & Consortium, I.G.P. The Immunological Genome Project: networks of gene expression in immune cells. *Nature Immunology* 9, 1091-1094 (2008).
343. Benayoun, B.A. *et al.* Remodeling of epigenome and transcriptome landscapes with aging in mice reveals widespread induction of inflammatory responses. *Genome Research* 29, 697-709 (2019).
344. Han, X. *et al.* Mapping the Mouse Cell Atlas by Microwell-Seq. *Cell* 172, 1091-1107.e1017 (2018).
345. Martens, J.H.A. & Stunnenberg, H.G. BLUEPRINT: mapping human blood cell epigenomes. *Haematologica* 98, 1487-1489 (2013).
346. de Souza, N. The ENCODE project. *Nature Methods* 9, 1046 (2012).
347. Monaco, G. *et al.* RNA-Seq Signatures Normalized by mRNA Abundance Allow Absolute Deconvolution of Human Immune Cell Types. *Cell Reports* 26, 1627-1640.e1627 (2019).

348. Korotkevich, G. *et al.* Fast gene set enrichment analysis. preprint: Bioinformatics; 2016 2016-06-20.
349. Subramanian, A. *et al.* Gene set enrichment analysis: a knowledge-based approach for interpreting genome-wide expression profiles. *Proceedings of the National Academy of Sciences of the United States of America* 102, 15545-15550 (2005).
350. Love, M.I., Huber, W. & Anders, S. Moderated estimation of fold change and dispersion for RNA-seq data with DESeq2. preprint: Bioinformatics; 2014 2014-02-19.
351. Liberzon, A. *et al.* The Molecular Signatures Database (MSigDB) hallmark gene set collection. *Cell Systems* 1, 417-425 (2015).
352. Hadley, W. ggplot2: elegant graphics for data analysis. *Springer* (2016).
353. Murakami, M. *et al.* Disease-association analysis of an inflammation-related feedback loop. *Cell Reports* 3, 946-959 (2013).
354. Hallahan, D.E., Staba-Hogan, M.J., Virudachalam, S. & Kolchinsky, A. X-ray-induced P-selectin localization to the lumen of tumor blood vessels. *Cancer Research* 58, 5216-5220 (1998).
355. Griffith, J.W., Sokol, C.L. & Luster, A.D. Chemokines and chemokine receptors: positioning cells for host defense and immunity. *Annual Review of Immunology* 32, 659-702 (2014).
356. Thome, M. & Tschopp, J. Regulation of lymphocyte proliferation and death by FLIP. *Nature Reviews. Immunology* 1, 50-58 (2001).
357. Carsana, L. *et al.* Pulmonary post-mortem findings in a series of COVID-19 cases from northern Italy: a two-centre descriptive study. *The Lancet Infectious Diseases* 20, 1135-1140 (2020).
358. Nienhold, R. *et al.* Two distinct immunopathological profiles in autopsy lungs of COVID-19. *Nature Communications* 11, 5086 (2020).
359. Rossi, G. *et al.* The role of macrophages in interstitial lung diseases: Number 3 in the Series "Pathology for the clinician" Edited by Peter Dorfmüller and Alberto Cavazza. *European Respiratory Review: An Official Journal of the European Respiratory Society* 26, 170009 (2017).
360. Duan, M., Hibbs, M.L. & Chen, W. The contributions of lung macrophage and monocyte heterogeneity to influenza pathogenesis. *Immunology and Cell Biology* 95, 225-235 (2017).
361. Mabbott, N.A., Baillie, J.K., Brown, H., Freeman, T.C. & Hume, D.A. An expression atlas of human primary cells: inference of gene function from coexpression networks. *BMC genomics* 14, 632 (2013).

362. Matsuyama, T., Kubli, S.P., Yoshinaga, S.K., Pfeffer, K. & Mak, T.W. An aberrant STAT pathway is central to COVID-19. *Cell Death & Differentiation* 27, 3209-3225 (2020).
363. Ugel, S., Canè, S., De Sanctis, F. & Bronte, V. Monocytes in the Tumor Microenvironment. *Annual Review of Pathology* 16, 93-122 (2021).
364. Yu, H., Pardoll, D. & Jove, R. STATs in cancer inflammation and immunity: a leading role for STAT3. *Nature Reviews. Cancer* 9, 798-809 (2009).
365. Merad, M. & Martin, J.C. Pathological inflammation in patients with COVID-19: a key role for monocytes and macrophages. *Nature Reviews Immunology* 20, 355-362 (2020).
366. Winkler, E.S. *et al.* SARS-CoV-2 infection of human ACE2-transgenic mice causes severe lung inflammation and impaired function. *Nature Immunology* 21, 1327-1335 (2020).
367. Hoang, T.N. *et al.* Baricitinib treatment resolves lower-airway macrophage inflammation and neutrophil recruitment in SARS-CoV-2-infected rhesus macaques. *Cell* 184, 460-475.e421 (2021).
368. Feng, L.-L., Gao, J.-M., Li, P.-P. & Wang, X. IL-9 Contributes to Immunosuppression Mediated by Regulatory T Cells and Mast Cells in B-Cell Non-Hodgkin's Lymphoma. *Journal of Clinical Immunology* 31, 1084-1094 (2011).
369. Richard, M., Louahed, J., Demoulin, J.-B. & Renauld, J.-C. Interleukin-9 Regulates NF-κB Activity Through BCL3 Gene Induction. *Blood* 93, 4318-4327 (1999).
370. Aggarwal, B.B., Gupta, S.C. & Kim, J.H. Historical perspectives on tumor necrosis factor and its superfamily: 25 years later, a golden journey. *Blood* 119, 651-665 (2012).
371. Jash, A. *et al.* Nuclear Factor of Activated T Cells 1 (NFAT1)-induced Permissive Chromatin Modification Facilitates Nuclear Factor-κB (NF-κB)-mediated Interleukin-9 (IL-9) Transactivation. *Journal of Biological Chemistry* 287, 15445-15457 (2012).
372. Boles, K.S. & Mathew, P.A. Molecular cloning of CS1, a novel human natural killer cell receptor belonging to the CD2 subset of the immunoglobulin superfamily. *Immunogenetics* 52, 302-307 (2001).
373. SLAMF6 SLAM family member 6 [Homo sapiens (human)]. NCBI Gene Database [cited]Available from: https://www.ncbi.nlm.nih.gov/gene?Db=gene&Cmd=DetailsSearch&Term=114836
374. Dragovich, M.A. *et al.* SLAMF6 clustering is required to augment T cell activation. *PloS One* 14, e0218109 (2019).

375. Tassi, I. & Colonna, M. The cytotoxicity receptor CRACC (CS-1) recruits EAT-2 and activates the PI3K and phospholipase Cgamma signaling pathways in human NK cells. *Journal of Immunology (Baltimore, Md.: 1950)* 175, 7996-8002 (2005).
376. Kim, J.R., Horton, N.C., Mathew, S.O. & Mathew, P.A. CS1 (SLAMF7) inhibits production of proinflammatory cytokines by activated monocytes. *Inflammation Research: Official Journal of the European Histamine Research Society ... [et Al.]* 62, 765-772 (2013).
377. Liu, Q. *et al.* HDAC4 is expressed on multiple T cell lineages but dispensable for their development and function. *Oncotarget* 8, 17562-17572 (2017).
378. SIRT1 sirtuin 1 [Homo sapiens (human)]. NCBI Gene Database [cited]Available from: https://www.ncbi.nlm.nih.gov/gene?Db=gene&Cmd=DetailsSearch&Term=23411
379. Li, Q.-K. *et al.* Circ-sirt1 inhibits growth and invasion of gastric cancer by sponging miR-132-3p/miR-212-3p and upregulating sirt1 expression. *Neoplasma* 68, 780-787 (2021).
380. van Putten, J.P.M. & Strijbis, K. Transmembrane Mucins: Signaling Receptors at the Intersection of Inflammation and Cancer. *Journal of Innate Immunity* 9, 281-299 (2017).
381. Wang, C., Chen, W. & Shen, J. CXCR7 Targeting and Its Major Disease Relevance. *Frontiers in Pharmacology* 9, 641 (2018).
382. Fan, H., Wang, W., Yan, J., Xiao, L. & Yang, L. Prognostic significance of CXCR7 in cancer patients: a meta-analysis. *Cancer Cell International* 18, 212 (2018).
383. Norelli, M. *et al.* Monocyte-derived IL-1 and IL-6 are differentially required for cytokine-release syndrome and neurotoxicity due to CAR T cells. *Nature Medicine* 24, 739-748 (2018).
384. Karki, R. *et al.* Synergism of TNF-α and IFN-γ Triggers Inflammatory Cell Death, Tissue Damage, and Mortality in SARS-CoV-2 Infection and Cytokine Shock Syndromes. *Cell* 184, 149-168.e117 (2021).
385. Company, E.L.a. <Baricitinib LOA FINAL 07.28.21.pdf>. *FDA Food and Drug Aministration* (2021).
386. Ostrand-Rosenberg, S. Myeloid-derived suppressor cells: more mechanisms for inhibiting antitumor immunity. *Cancer Immunology, Immunotherapy* 59, 1593-1600 (2010).
387. Hay, K.A. *et al.* Kinetics and biomarkers of severe cytokine release syndrome after CD19 chimeric antigen receptor-modified T-cell therapy. *Blood* 130, 2295-2306 (2017).

ADKNOWLEDGMENTS

Few last words are needed to thank who made possible the achievement of this important goal. Many thanks are due to my tutor Prof. Vincenzo Bronte, who gave me the invaluable opportunity to challenge myself with this PhD project. To Prof. Stefano Ugel, who believed in me 4 years ago, allowed me to work in his project and gave me the opportunity to grow up as researcher. Thanks go to incredible lab team, with which I worked in these years, because nothing of this could have been possible without its daily help and collaboration. To my colleagues Silvia, Simone, Fang, Roza, Tian, , Luca, Giulio, Cristina, Ornella, Davide, whose support and comprehension never missed. Special thanks to my parents, my milestone for life, and to my brother, who believe in me and support me in every decision to make.

RINGRAZIAMENTI

Poche ultime parole sono necessarie per ringraziare chi ha reso possibile il raggiungimento di questo importante obiettivo. Ringrazio il mio tutor, il Prof. Vincenzo Bronte, che mi ha dato l'inestimabile opportunità di mettere alla prova me stessa con questo progetto di dottorato. Ringrazio il Prof. Stefano Ugel, che ha creduto in me 4 anni fa, mi ha permesso di lavorare nel suo progetto e mi ha dato l'opportunità di crescere come ricercatrice. Un grande ringraziamento va all'incredibile team di laboratorio con il quale ho lavorato in questi anni, perché niente di tutto ciò sarebbe stato possibile senza il suo quotidiano aiuto e collaborazione. Ringrazio i miei colleghi Silvia, Simone, Fang, Roza, Tian, Luca, Giulio, Cristina, Ornella, Davide, il cui supporto e comprensione non sono mai mancati. Uno speciale ringraziamento va ai miei genitori, la mia "pietra miliare" per la vita, e a mio fratello, che ha sempre creduto in me e mi supporta in ogni mia decisione.